Spring 2015

Modeling person-to-person contaminant transport in enclosed environments

Chun Chen
Purdue University

Graduate School Form 30
(Revised 08/14)

PURDUE UNIVERSITY
GRADUATE SCHOOL
Thesis/Dissertation Acceptance

This is to certify that the thesis/dissertation prepared

By Chun Chen

Entitled
Modeling Person-To-Person Contaminant Transport In Enclosed Environments

For the degree of Doctor of Philosophy

Is approved by the final examining committee:

Dr. Qingyan Chen

Dr. Athanassios Tzempelikos

Dr. Panagiota Karava

Dr. Chao-Hsin Lin

To the best of my knowledge and as understood by the student in the Thesis/Dissertation Agreement, Publication Delay, and Certification/Disclaimer (Graduate School Form 32), this thesis/dissertation adheres to the provisions of Purdue University's "Policy on Integrity in Research" and the use of copyrighted material.

Approved by Major Professor(s): Dr. Qingyan Chen

Approved by: Dr. Ganesh Subbarayan 04/09/2015

Head of the Department Graduate Program Date

MODELING PERSON-TO-PERSON CONTAMINANT TRANSPORT IN ENCLOSED ENVIRONMENTS

A Dissertation

Submitted to the Faculty

of

Purdue University

by

Chun Chen

In Partial Fulfillment of the

Requirements for the Degree

of

Doctor of Philosophy

May 2015

Purdue University

West Lafayette, Indiana

TO MY PARENTS, LONGXUAN CHEN AND LIZHEN ZENG.

TO MY GIRLFRIEND, RUOYU YOU.

FOR THEIR LOVE AND SUPPORT

ACKNOWLEDGEMENTS

First, I would like to express my deep gratitude to Dr. Qingyan (Yan) Chen for his time and effort on mentoring me as my advisor. He has shaped me in many ways during my graduate study at Purdue University. Without his guidance, completion of the research and this thesis would be impossible.

I am also grateful to Dr. Chao-Hsin Lin, Dr. Thanos (Athanasios) Tzempelikos, and Dr. Panagiota Karava for their serving on the exam committee, and generously offering their time and encouragement. I would also like to thank the former and current group members: Mingang Jin, Aakash Rai, Wei Liu, Dayi Lai, Haojie Wang, Yan Xue, and Zhu Shi for their help and support. Special thanks to the Herrick family for their assistance.

Finally, I would like to thank my parents, Longxuan Chen and Lizhen Zeng, and my girlfriend, Ruoyu You, for their love and support.

This study was partially funded by the Boeing Company and American Society of Heating, Refrigerating and Air-Conditioning Engineers (ASHRAE). They neither endorse nor reject the findings of this research. The presentation of this information is in the interest of invoking technical community comment on the results and conclusions of the research.

TABLE OF CONTENTS

Page

Page

LIST OF TABLES

LIST OF FIGURES

Figure Page

Figure Page

Figure Page

ABSTRACT

Chen, Chun. Ph.D., Purdue University, May 2015. Modeling Person-To-Person Contaminant Transport in Enclosed Environments. Major Professor: Dr. Qingyan (Yan) Chen, School of Mechanical Engineering.

It is essential to predict person-to-person contaminant transport in enclosed environments to improve air distribution design and reduce the infection risk from airborne infectious diseases. This study aims to improve and accelerate the simulation of person-to-person contaminant transport in enclosed environments.

This investigation first conducted experimental measurements of person-to-person contaminant transport in an office mockup and the first-class cabin of a functional MD-82 aircraft. The experimental data of steady-state airflow, temperature, and gas contaminant concentration fields obtained in the office were used to validate the steady-state computational fluid dynamics (CFD) models. In the aircraft cabin, the transient particle concentrations were measured at the breathing zones of each passenger. The experimental data were used for evaluating the transient particle models in this study.

When applying the CFD models, most of the existing studies assumed that the index person coughed or sneezed directly without covering the mouth. In reality, however, people usually cover their mouths with a hand or a tissue when they cough or sneeze. Currently, no simple method is available in the literature for predicting the exhaled airflow from a cough with the mouth covered. Therefore, this study developed simplified models for predicting the airflow on the basis of the smoke visualization experiment. This investigation then applied the developed simplified models to assess the influence of mouth coverings on the receptor's exposure to exhaled particles. It was found that

covering a cough with a tissue, a cupped hand, or an elbow can significantly reduce the horizontal transport of exhaled particles.

As a popular particle model, the Lagrangian model needs to track a large number of particles in the calculations in order to ensure accuracy. Traditionally, modelers have conducted an independence test in order to find a reasonable value for this particle number. However, the unguided process of an independence test can be highly time-consuming. Therefore, this investigation developed a method for estimating the necessary particle number in the Lagrangian model. The results show that the proposed method can estimate the necessary particle number with a reasonable magnitude and thus reduce the effort that is normally required for evaluating different numbers of particles in order to achieve statistically meaningful results. Moreover, the superimposition and time-averaging method was proposed, which can reduce the necessary particle number, and, as a result, the computing cost can be further reduced.

Although the traditional Eulerian and Lagrangian models can provide informative results of transient particle transport indoors, they are considerably time-consuming. Thus, this study further developed a new particle model on the basis of a Markov chain frame for quickly predicting transient particle transport indoors. When solving the particle transport equations, the Markov chain model does not require iterations in each time step, and thus it can significantly reduce the computing cost. The validation results show that, in general, the trends in the transient particle concentration distributions predicted by the Markov chain model agreed reasonably well with the experimental data. Furthermore, the Markov chain model produced similar results to those of the Lagrangian and Eulerian models, while the speed of calculation increased by at least 6 times in comparison to the latter two models for the studied case.

To further identify a suitable model for indoor transient particle transport simulations, this study systematically compared the Eulerian, Lagrangian, and Markov chain models in terms of performance, computing cost, and robustness. This investigation used four cases, including three cases with experimental data, for the comparison. The comparison shows that all the three models can predict transient particle transport in enclosed

environments with a similar accuracy. With the same time step size and grid number, the Markov chain model was the fastest among the three models. Unless super-find grid was used, the Eulerian model was faster than the Lagrangian model. The Eulerian and Lagrangian models were more robust than the Markov chain model, because the Markov chain model was sensitive to the time step size.

CHAPTER 1. INTRODUCTION

1.1 Background and Significance

Researchers from both the medical and engineering disciplines have been collectively addressing the issue of transmission of airborne infectious diseases (Mangili and Gendreau, 2005). Airborne infectious diseases include cold, influenza, avian flu, tuberculosis (TB) and Severe Acute Respiratory Syndrome (SARS). Viboud et al. (2004) reported that about 47,200 deaths were caused by influenza epidemics every year in the United States. The Spanish flu of 1918-19 (H1N1) was found as the most lethal flu pandemic of the 20th century, which infected about one-quarter of the global population and killed more than 40 million people (WHO, 2002). The World Bank (2005) concluded that a pandemic of avian flu among humans could cost the global economy $800 billion a year. The evaluation of the global burden of TB showed that TB infections were found in about 22 countries and cause a total of 1.87 million deaths (Dye et al., 1999). The World Health Organization (WHO) (2002) reported that there were 8098 people all over the world infected by SARS and 774 of them lost their lives. These airborne diseases cause endless social and economic disruptions. Thus, it is important to understand and control the transmission of airborne disease to reduce its influence on human health.

Enclosed spaces such as buildings and transport vehicles are more susceptible to the transmission of airborne infectious diseases than the outdoors due to the low air exchange rate (Mangili and Gendreau, 2005). For instance, among enclosed spaces, a greater risk of infection is possible in aircraft cabins due to the high occupant density and long exposure time. Some of the outbreaks of TB (Kenyon et al., 1996), influenza (Moser et al., 1979), SARS (Olsen et al., 2003), and norovirus transmission (Kirking et al., 2010) are alleged to have happened during air travel. The swine flu epidemic in 2009 also created a panic

among air travelers and caught the attention of researchers (Khan et al., 2010). These transmissions could have happened through direct contact, indirect contact, droplets or airborne route. The infection spread to rows away from the infected person indicated the transmission to these places may have happened through airborne route (Olsen et al., 2003; Li et al., 2005; Li et al., 2007; Kirking et al., 2010). Due to the rapidly growing number of air passengers (800 million air passengers in 2010, US DOT 2011), the transmission of airborne infectious diseases in aircraft cabins becomes more and more important. Furthermore, people spend roughly 90% of their life time indoors (Klepeis et al., 2001). Thus, it is essential to predict and control the transmission of airborne infectious disease in enclosed environments.

The airborne disease transmission process starts from droplets carrying the infectious agents. These droplets are exhaled by an infected person through various respiratory exhalations (Cole and Cook, 1998; Nicas et al., 2005). They then disperse in the enclosed environment and can be inhaled by susceptible fellow occupants (Morawska, 2006). The droplet dispersion depends on the airflow in the enclosed environment and the exhalation process. The airflow in enclosed environments is normally not uniform (Chen, 2009). The pulse release of infectious agents by the index passenger through coughing, breathing, or talking exhalations is transient (Gupta et al., 2009 and 2010). Therefore, the expiratory droplet distribution and the risk of infection in enclosed environments are inhomogeneous and temporal.

To predict such complex airborne infectious diseases transmission, one can use simple models such as well-mixed models (Walkinshaw, 2010), multi-zone models (Chen et al., 2011), and zonal models (Song et al., 2008). However, these models can provide only limited information with poor accuracy (Chen, 2009). In recent years, computational fluid dynamics (CFD) has been widely used in modeling person-to-person contaminant transport in enclosed environments, since it can provide more detailed and accurate information than the simple models. For particle modeling, the Eulerian (e.g. Li et al., 2011; Seepana and Lai, 2012) and Lagrangian (e.g. Chao and Wan, 2006; Zhang and Li, 2012) are two popular models. The Eulerian model treats the particle phase as a

continuum and solves the scalar transport equation. The Lagrangian model calculates the trajectories of numerous individual particles based on Newton's law. Both the Eulerian and Lagrangian models can provide detailed information about transient particle concentration distributions in enclosed environments (Wang et al., 2012).

However, there are some problems of the existing models for transient particle transport indoors. First, when applying the CFD models, most of the existing studies assumed that the index person coughed or breathed directly without covering the mouth (e.g. Seepana and Lai, 2012). In reality, however, people usually cover their mouths when they cough or sneeze. For instance, Tang et al. (2009) indicated that people might cover their cough or sneeze with a tissue, cupped hand, fist, sleeve, surgical mask or N95 mask. Therefore, the uncovered coughing/sneezing assumption would make the simulation of person-to-person particle transport become unrealistic. To overcome this problem, a model for predicting the exhaled airflow from a cough/sneeze with the mouth covered is desirable. However, no simple method is available in the literature for predicting such exhaled airflow. Thus, it is worthwhile to develop such a model to make the simulation more realistic.

Another major problem of the existing particle models is that they are considerably time-consuming (Wang et al., 2012). For the Lagrangian model, the discrete random walk (DRW) model is typically used to calculate the turbulence dispersion. Statistically speaking, a large number of particles are needed in the calculations in order to ensure accuracy. Traditionally, modelers have conducted an independence test in order to find a reasonable value for this particle number (Zhang and Chen, 2006). However, the unguided process of an independence test can be highly time-consuming. For the Eulerian model, the unsteady-state calculation with iterations in each time step is also very time-consuming. For instance, Wang et al. (2012) reported that the computing times of the Eulerian and Lagrangian models for calculating transient particle transport in a typical room were 62.2 and 84.9 hours, respectively, on an eight-core cluster with two 2.5 GHz AMD quad-core processors. Thus, it is necessary to accelerate the particle models for quickly predicting person-to-person contaminant transport in enclosed environments.

1.2 Outline of this Thesis

Chapter 2 presents a literature review on the models for predicting person-to-person contaminant transport in enclosed environments. The review identified two major problems of the existing particle models, which will be addressed in the following chapters.

Chapter 3 presents experimental measurements of person-to-person particle transport in an office mockup and the first-class cabin of an MD-82 aircraft cabin. The steady-state experimental data obtained in the office were used to validate the steady-state CFD model. The experimental data of transient particle transport obtained in the aircraft will be used for evaluating the transient particle models in the next chapters.

Chapter 4 develops simplified models for exhaled airflow from a cough with the mouth covered to make the simulation of person-to-person particle transport more realistic. The models were developed on the basis of smoke visualization of the exhaled airflow. Numerical simulations were then performed to assess the influence of mouth coverings on the receptor's exposure to exhaled particles.

Chapter 5 develops a method for estimating the necessary particle number in the Lagrangian model, in order to reduce the effort that is normally required for evaluating different numbers of particles in order to achieve statistically meaningful results. Moreover, this chapter proposes the superimposition and time-averaging method to reduce the necessary particle number, and so to reduce the computing cost.

Chapter 6 develops a new particle model on the basis of Markov chain model for quickly predicting person-to-person particle transport indoors. When solving the particle transport equations, the Markov chain model does not require iterations in each time step, and thus it can significantly reduce the computing cost. This chapter used three sets of experimental data for transient particle transport to validate the model.

Chapter 7 compares the Eulerian, Lagrangian, and Markov chain models in terms of performance, computing cost, and robustness, in order to identify a suitable model for indoor transient particle transport simulations. This chapter used four cases, including three cases with experimental data, for the comparison.

Chapter 8 summarizes the major findings of this investigation and discusses the directions for future work.

CHAPTER 2. LITERATURE REVIEW

To accurately and quickly obtain information about airborne infectious disease transmission in enclosed environments is critical in reducing the infection risk to the occupants. Therefore, it is worthwhile to improve and accelerate the computer models for predicting person-to-person contaminant transport in enclosed environments. This goal requires a good understanding of the existing models. Thus, this chapter conducts a literature review on the existing particle models in order to identify their major problems.

2.1 Models for Person-to-Person Contaminant Transport Indoors

The first part of this chapter reviews the existing models for predicting person-to-person particle transport in enclosed environments. These models were categorized into two groups. The first group is simple particle models, including well-mixed, multi-zone, and zonal models, which can provide only limited and inaccurate results. The second group is CFD-based models, including Eulerian and Lagrangian models, which can provide informative and accurate results.

2.1.1 Well-Mixed, Multi-Zone, and Zonal Models

The first group of particle models includes the well-mixed, multi-zone, and zonal models. The well-mixed model is traditionally used to predict the contaminant concentration in enclosed environments. For instance, Walkinshaw (2010) applied a well-mixed model to predict the number of virus inhaled by aircraft passenger and office worker groups exposed to the exhaled breath of an infected person, as shown in Figure 2-1. Bolster and

Linden (2009) used a well-mixed to predict the transient particle concentrations in a room with displacement ventilation. In the well-mixed model, the entire room is treated as a well mixed space, i.e. the contaminant concentration distribution is assumed to be uniform. However, in reality, the contaminant concentration distribution is not uniform in most of cases. Therefore, the applications of the well-mixed model are limited.

Figure 2-1. Number of influenza virus particles inhaled by office worker and aircraft passenger groups exposed to the exhaled breath of one infected person (Walkinshaw, 2010).

The well-mixed model is used for a single room, while the multi-zone models are applied for multiple rooms connected with openings such as doors and windows. Similar to the well-mixed model, the multi-zone models also assume each zone to be a well-mixed space. A comprehensive history and theory of multi-zone models can be found in Axley (2007). The multi-zone models have been used for predicting airborne infectious disease transmission indoors. For instance, Ko et al. (2004) and Jones et al. (2009) used multi-zone models to calculate the risks based on dose response models. Chen et al. (2011) applied an improved multi-zone model to investigate the influence of two-way airflow due to temperature difference on the transmission of SARS in the hospital Ward 8A in

Hong Kong, as shown in Figure 2-2. However, the assumption that air contaminant concentration in a zone is uniform may not be valid.

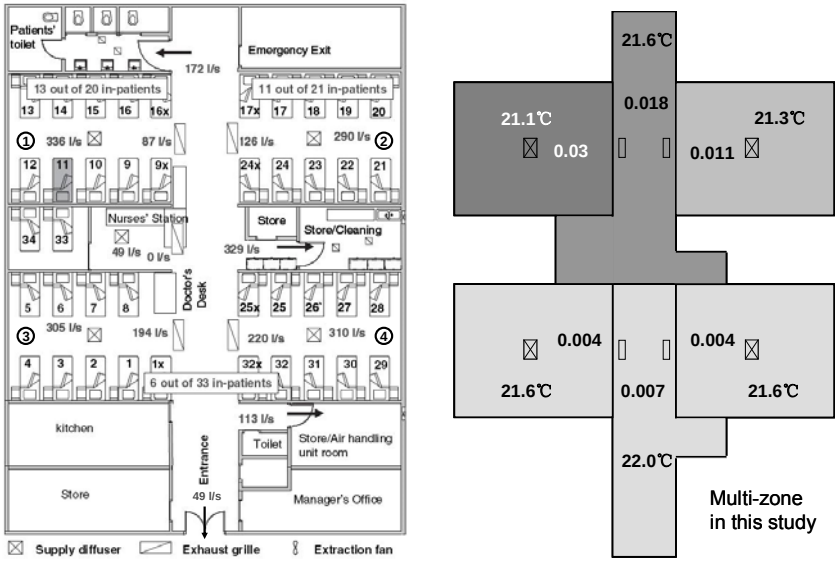

Figure 2-2. (a) Floor plan of Ward 8A during the time of outbreak in March 2003, (b) Results of particle concentration distribution using the multi-zone model (Chen et al., 2011).

To remedy the problem of the well-mixed and multi-zone models, zonal models have been used to predict the distributions of contaminant concentration indoors. Zonal models divide an indoor space into a limited number of cells. The number of cells is typically less than 1000 (Chen, 2009). Normally, zonal models require the information of airflow distribution either from experiment or simulation. Then, the models use mass balance equations to calculate the contaminant concentration in each cell to provide the non-uniform distribution in the room. For example, Song et al. (2008) developed a zonal model by integrating it with source and sink models for contaminants, as shown in Figure 2-3. The review of zonal models by Mergi and Haghighat (2007) indicated that the applications of zonal models were limited because of the availability of airflow patterns.

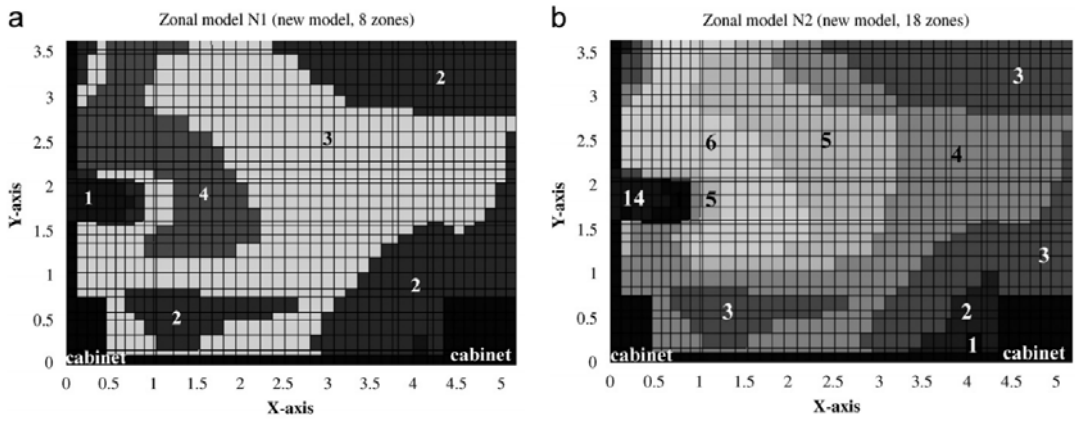

Figure 2-3. Results of particle concentration distributions using a zonal model (a) 8 zones, (b) 18 zones (Song et al., 2008).

2.1.2 Computational Fluid Dynamics Models

The second group of particle models is the Computational Fluid Dynamics (CFD) models. As a powerful airflow and contaminant modeling tool, CFD models have been widely used because they can provide informative and accurate results of transient particle transport in enclosed environments. There are two parts of CFD modeling on person-to-person contaminant transport: airflow modeling and particle modeling.

2.1.2.1 Airflow and Turbulence Models

To obtain the information of airflow distribution, CFD numerically solves a set of partial differential equations for the conservation of mass, momentum (Navier-Stokes equations), energy, and turbulence quantities. The solution includes the distributions of air velocity, pressure, temperature, turbulence parameters, and contaminant concentration. For indoor airflow modeling, there are several turbulence models, which have been systematically reviewed and tested by Zhang et al. (2007), and Wang and Chen (2009). The section summarizes the popular turbulence models for indoor airflow simulations.

The Reynolds-Averaged Navier-Stokes (RANS) models are the most popular CFD models. For an incompressible Newtonian flow, the RANS equation can be written as:

$$\frac{\partial U_i}{\partial t}+\frac{\partial}{\partial x_j}(U_j U_i)=-\frac{1}{\rho}\frac{\partial P}{\partial x_i}+\frac{\partial}{\partial x_j}(\frac{\mu}{\rho}(\frac{\partial U_i}{\partial x_j}+\frac{\partial U_j}{\partial x_i})-\overline{u_i u_j})+S \tag{2.1}$$

where U is the Reynolds average air velocity, t is the time, x represents the coordinate, ρ is the air density, P is the pressure, μ is the air viscosity, u is the fluctuating air velocity, S is the source term, and the bar stands for Reynolds average. For RANS models, they can be generally divided into two categories: eddy-viscosity models and Reynolds-stress models. The eddy-viscosity models use the Boussinesq eddy-viscosity approximation to link the turbulence Reynolds stresses to an eddy-viscosity:

$$-\overline{u_i u_j}=\frac{\mu_t}{\rho}(\frac{\partial U_i}{\partial x_j}+\frac{\partial U_j}{\partial x_i})-\frac{2}{3}\delta_{ij}k \tag{2.2}$$

where $\overline{u_i u_j}$ is the turbulence Reynolds stress, μ_t is the eddy viscosity, and k is the turbulent kinetic energy, which is expressed as:

$$k=\frac{1}{2}\overline{u_i' u_i'} \tag{2.3}$$

Among the eddy-viscosity models, the zero-equation turbulence eddy-viscosity models are the simplest, which have only an algebra equation for turbulent viscosity. For indoor airflow simulations, Chen and Xu (1998) proposed the following function to connect turbulent viscosity to local mean velocity and the distance to the nearest wall:

$$\nu_t = 0.03874UL \tag{2.4}$$

where ν_t is the turbulent viscosity, U is the local mean velocity, and L is the distance to the nearest wall. This model is a very popular zero-equation model for enclosed environments. For instance, the commercial CFD software, Airpak, has included this model as its default.

Although the zero-equation models are very easy to use, they fail to consider the non-local and flow-history effects on turbulent eddy-viscosity. To overcome this problem, one-equation turbulence models were developed, which normally use the turbulent kinetic energy to calculate the eddy viscosity:

$$\nu_t = Ck^{1/2}l \tag{2.5}$$

where C is an empirical coefficient, and l is a turbulence length scale.

Different from using the turbulent kinetic energy to calculate the eddy viscosity, Spallart and Allmaras (1992) developed a model which directly solved a transport equation for the eddy viscosity. This model has been adopted in predicting airflow and turbulence in indoor environments.

In addition to the turbulent kinetic energy equation, two-equation eddy-viscosity models further solve another transport equation. The k-ε model family is the most popular two-equation eddy-viscosity model. Launder and Spalding (1974) developed the standard k-ε model which has been widely used for predicting indoor airflow field. In the k-ε model, the turbulent eddy viscosity is calculated by:

$$\nu_t = C_\mu \frac{k^2}{\varepsilon} \tag{2.6}$$

where C_μ is an empirical constant, k is the turbulence kinetic energy, and ε is the dissipation rate of turbulence energy. In addition to the standard k-ε model, the Re-Normalization Group (RNG) k-ε model (Yakhot and Orszag, 1986; Choudhury, 1993), which accounts for the effects of smaller scales of motion, has also been widely used for indoor environments. Another popular k-ε model is the realizable k-ε model (Shih et al., 1995), which works better for swirling and separation flows. These k-ε models are developed for high Reynolds number flows. To better calculate low Reynolds number flows, Launder and Shamar (1974) further developed a low Reynolds number k-ε model (LRN).

The k-ω model family is another popular two-equation eddy-viscosity model. In the k-ω models, ω is defined as:

$$\omega = \frac{\varepsilon}{k} \tag{2.7}$$

It was found that the performance of k-ω models is better than the k-ε models in predicting equilibrium adverse pressure flows (Wilcox, 1988), but worse in predicting wake region and free shear flows (Menter, 1992). To take advantages of both models, Menter (1994) further developed a shear stress transport (SST) k-ω model, which is essentially a k-ω model in regions near walls and a k-ε model in regions far from walls.

All of the eddy viscosity models introduced above assume isotropic turbulence structures, which may fail for flows with strong anisotropic behaviors. To overcome this problem, some researchers applied the Reynolds stress models (RSM) to calculate airflow field in indoor environments (Murakami et al., 1990; Renz and Terhaag, 1990). Instead of calculating the turbulence eddy viscosity, the RSMs explicitly solve the transport equations of Reynolds stresses. Although the RSMs take the anisotropic turbulence structures into account, it was found that they are only slightly better than the k-ε model but much more time-consuming for indoor airflow simulations (Chen, 1996).

Different from the RANS models which model all of the eddies, the large eddy simulation (LES) directly resolves large eddies and models small eddies. Therefore, the LES requires the separation of small-eddies from large-eddies with a filter (Smagorinsky, 1963). The rationale behind LES is that momentum, mass, energy, and passive contaminants are transported mostly by large eddies, which are more dependent on the geometries and boundary conditions. Thus, these important large eddies should be directly resolved. One the other hand, small eddies are more isotropic and less dependent on the geometries. Thus, modeling small eddies would not introduce significant errors.

Since LES requires superfine grid in the near-wall region and so considerable computing cost, detached eddy simulation (DES) was developed to relax the size of grid in the near-wall region. The only difference between the LES and DES is that DES employs the unsteady RANS models in the near-wall regions. Both the LES and DES include more solid fluid physics than the RANS models do, and contain less than one empirical coefficient. However, even when the flow is steady-state, the transient flow still needs to be solved when one uses LES or DES. Furthermore, the accuracy of LES and DES greatly depends on the grid resolution. Therefore, LES and DES always consume much more computing resource than the RANS models for steady-state airflow simulations. Figure 2-4 summarizes the popular turbulence models that have been applied to predict airflow in enclosed environments.

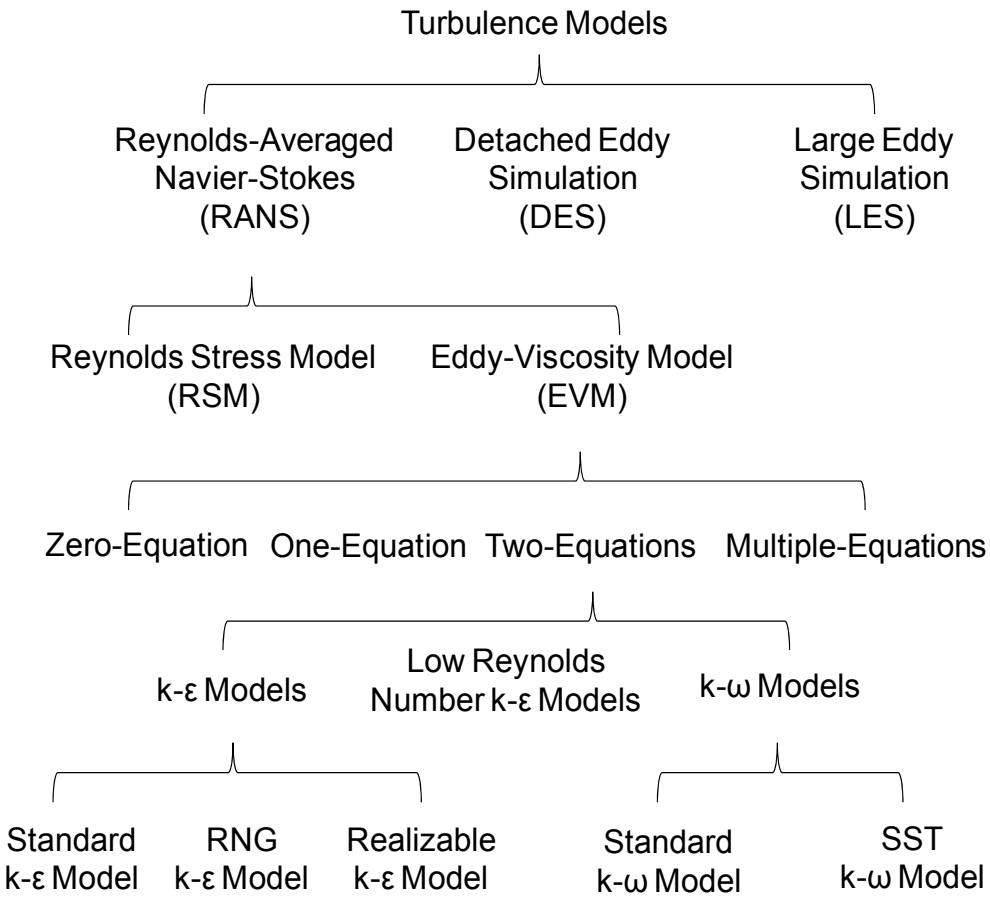

Figure 2-4. Summary of popular turbulence models that have been applied to predict airflow in enclosed environments.

Wang and Chen (2009) systematically compared eight turbulence models for indoor airflow simulations, including an indoor zero equation model (0-eq) (Chen and Xu, 1998), a low Reynolds number k-ε model (LRN) (Launder and Shamar, 1974), an RNG k-ε model (RNG) (Yakhot and Orszag, 1986), an SST k-ω model (SST) (Menter, 1994), a v2f model (v2f) (Davidson et al, 2003), a Reynolds stress model (RSM) (Gibson and Launder, 1978), a detached-eddy-simulation model (DES) (Shur et al, 1999), and a large-eddy-simulation model (LES) (Germano et al, 1996; Lilly, 1992). Figures 2-5 and 2-6 compares the velocity and turbulent kinetic energy profiles, respectively, predicted by the eight turbulence models for one of the cases in Wang and Chen (2009). It was found that

the LES model was the best among the eight models in terms of accuracy. However, the RNG k-ε model had the best overall performance if the accuracy and computing cost are both considered.

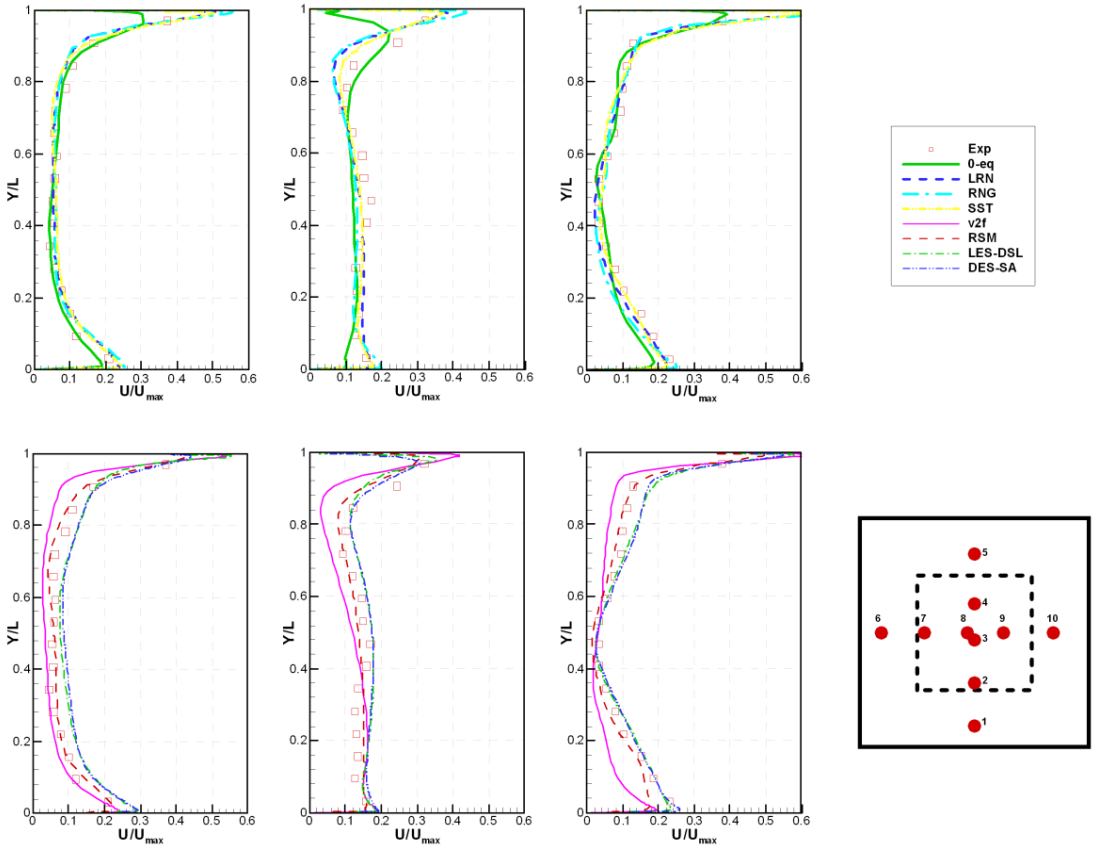

Figure 2-5. Comparison of the velocity profiles predicted by the eight turbulence models for one of the cases in Wang and Chen (2009).

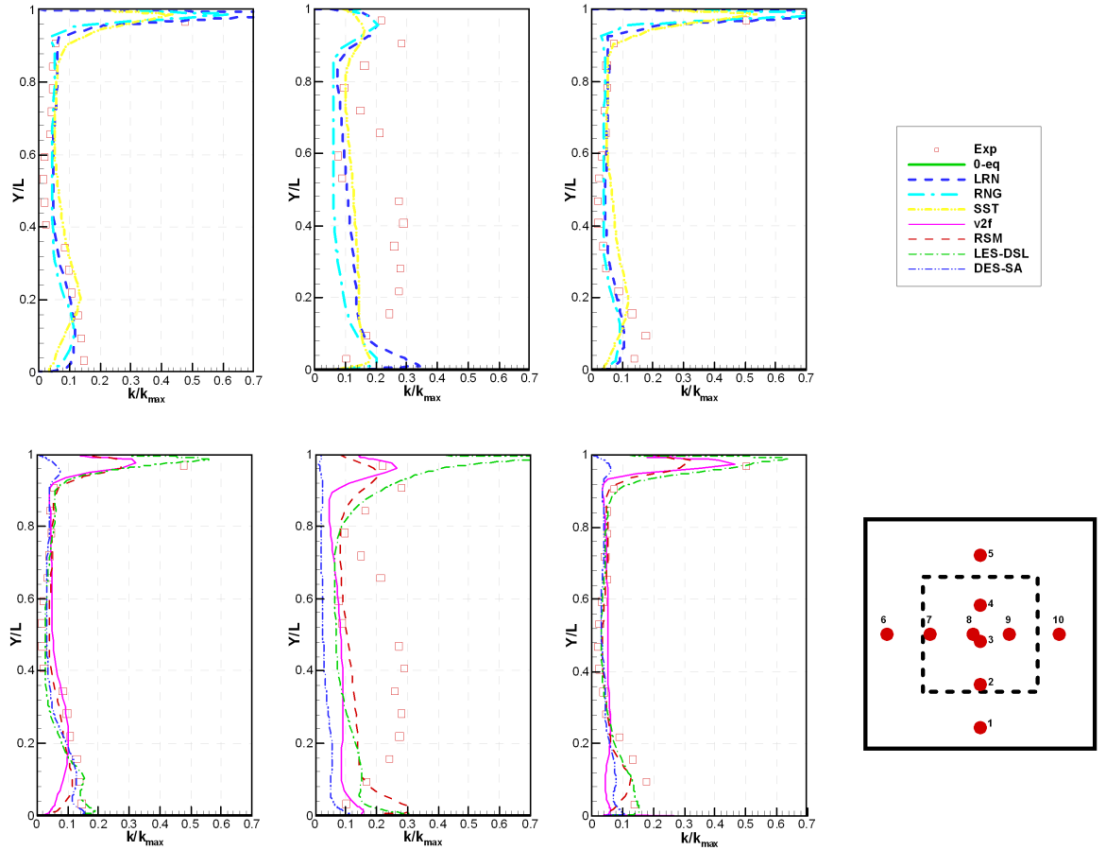

(a) Best (position 10) (b) Worst (position 5) (c) Average (position 6)

Figure 2-6. Comparison of the turbulent kinetic energy profiles predicted by the eight turbulence models for one of the cases in Wang and Chen (2009).

2.1.2.2 Eulerian Model

Based on the airflow predicted by the turbulence models introduced above, one can continue to solve the particle equations to obtain information about person-to-person contaminant transport in enclosed environments. For particle modeling, the Eulerian and Lagrangian are two popular models. The Eulerian model treats the particle phase as a continuum and solves the scalar transport equation:

$$\frac{\partial[(u_j + u_{sj})C]}{\partial x_j} = \frac{\partial}{\partial x_j} \cdot \left(\frac{\upsilon_t}{\sigma_C} \frac{\partial C}{\partial x_j}\right) + S_C \tag{2.8}$$

where u_j is the averaged air velocity; υ_t is the turbulent kinetic viscosity; σ_c is the turbulent Schimit number; and S_c is the particle source term. The particle gravitational settling velocity, u_{sj}, can be calculated by:

$$u_{sj} = \tau_p g_j \tag{2.9}$$

where τ_p is the relaxation time of particle. The τ_p can be calculated by:

$$\tau_p = \frac{C_c \rho_p d_p^{\,2}}{18\mu} \tag{2.10}$$

where C_c is the Cunningham coefficient caused by slippage. The C_c can be calculated by (Hinds, 1999):

$$C_c = 1 + \frac{\lambda}{d_p}(2.514 + 0.8 \times \exp(-0.55\frac{d_p}{\lambda})) \tag{2.11}$$

where λ is the mean air molecules free path. A user-defined function can be implemented in ANSYS Fluent 12.1 to realize the Eulerian model (ANSYS, 2010).

The Eulerian model has been widely used in predicting person-to-person contaminant transport indoors. For instance, Li et al. (2011) used an Eulerian model to study the spatial distribution of exhaled droplet residuals under different ventilation modes. Seepana and Lai (2012) investigated the person-to-person exposure due to sneezing in a full-scale chamber with an Eulerian model. Li et al. (2013) applied an Eulerian model to assess the effectiveness of covering a cough on reducing the exposure to coughed

particles. Hang et al. (2014) studied the effect of human walking on interpersonal exposure to exhaled contaminants in an isolation room using an Eulerian model. The Eulerian model can obtain the distribution of exhaled particle concentrations as an example shown in Figure 2-7.

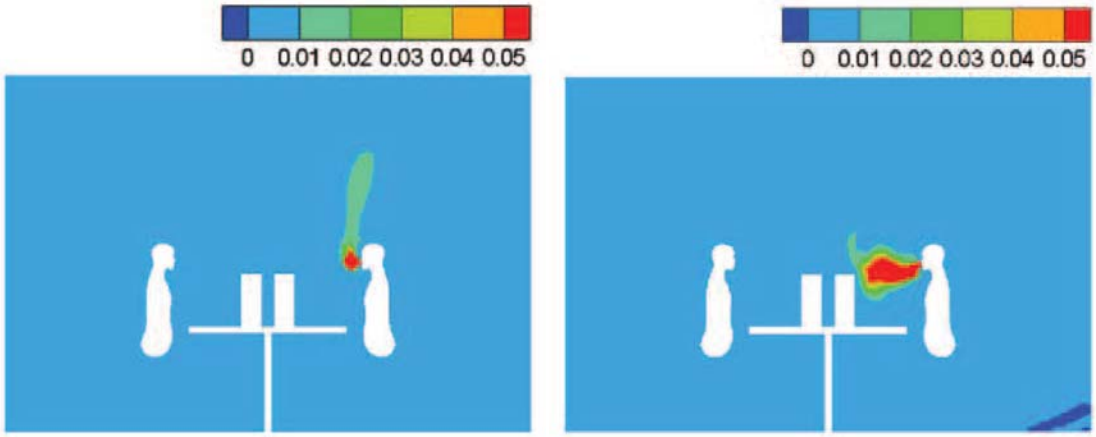

(a) (b)

Figure 2-7. Exhaled particle concentration distributions predicted by an Eulerian model in a room with (a) mixing ventilation and (b) displacement ventilation (Li et al., 2011).

2.1.2.3 Lagrangian Model

Instead of assuming particles to be a continuum as the Eulerian model does, the Lagrangian model calculates the trajectories of numerous individual particles based on Newton's law using the particle momentum equation:

$$\frac{d\vec{u}_p}{dt} = F_D(\vec{u}_a - \vec{u}_p) + \frac{\vec{g}(\rho_p - \rho_a)}{\rho_p} + \vec{F}_a \tag{2.12}$$

where $\vec{u}_p$ is the particle velocity vector; $\vec{u}_a$ is the air velocity vector; $\vec{g}$ is the gravitational acceleration vector; ρ_p and ρ_a is the density of particle and air, respectively; and $\vec{F}_a$ is Brownian motion force. The drag force, $F_D(\vec{u}_a - \vec{u}_p)$, can be calculated by:

$$F_D(\vec{u}_a - \vec{u}_p) = \frac{18\mu_a}{\rho_p d_p^2}\frac{C_D \mathrm{Re}}{24}(\vec{u}_a - \vec{u}_p) \tag{2.13}$$

where μ_α is the air viscosity, d_p is the diameter of particle, R_e is the Reynolds number, and C_D is the drag coefficient (Morsi and Alexander, 1972), which can be calculated by:

$$C_D = a_1 + \frac{a_2}{\mathrm{Re}} + \frac{a_3}{\mathrm{Re}^2} \tag{2.14}$$

where a_1, a_2, and a3 are constants which apply to smooth spherical particles over several ranges of Re given by Morsi and Alexander (1972).

The turbulence dispersion is modeled using the Discrete Random Walk (DRW) model:

$$u'_i = \zeta_i \sqrt{2k_i / 3} \tag{2.15}$$

where ζ_i is a normal random number and k_i is the turbulent kinetic energy in cell i. The particle trajectories can be calculated using ANSYS Fluent 12.1 (ANSYS, 2010).

The Lagrangian model has been also widely used in predicting person-to-person contaminant transport indoors. For example, Chao and Wan (2006) and Gao and Niu (2007) used a Lagrangian model to investigate the dispersion of particles in a room with

different ventilation modes. Chen et al. (2010) use a Lagrangian model to predict the patient to dentist particle transport in a dental clinic. Gupta et al. (2011a) investigated the dispersion of exhaled droplets in a section of an aircraft cabin with the Lagrangian method. Gao et al. (2012) applied a Lagrangian model to study the lock-up phenomenon of exhaled droplets in a room with displacement ventilation. Zhang and Li (2012) studied the transport of exhaled droplets in a fully-occupied high-speed rail cabin using a Lagrangian model. The Lagrangian model can obtain the information about the transport of each individual exhaled particle as an example shown in Figure 2-8.

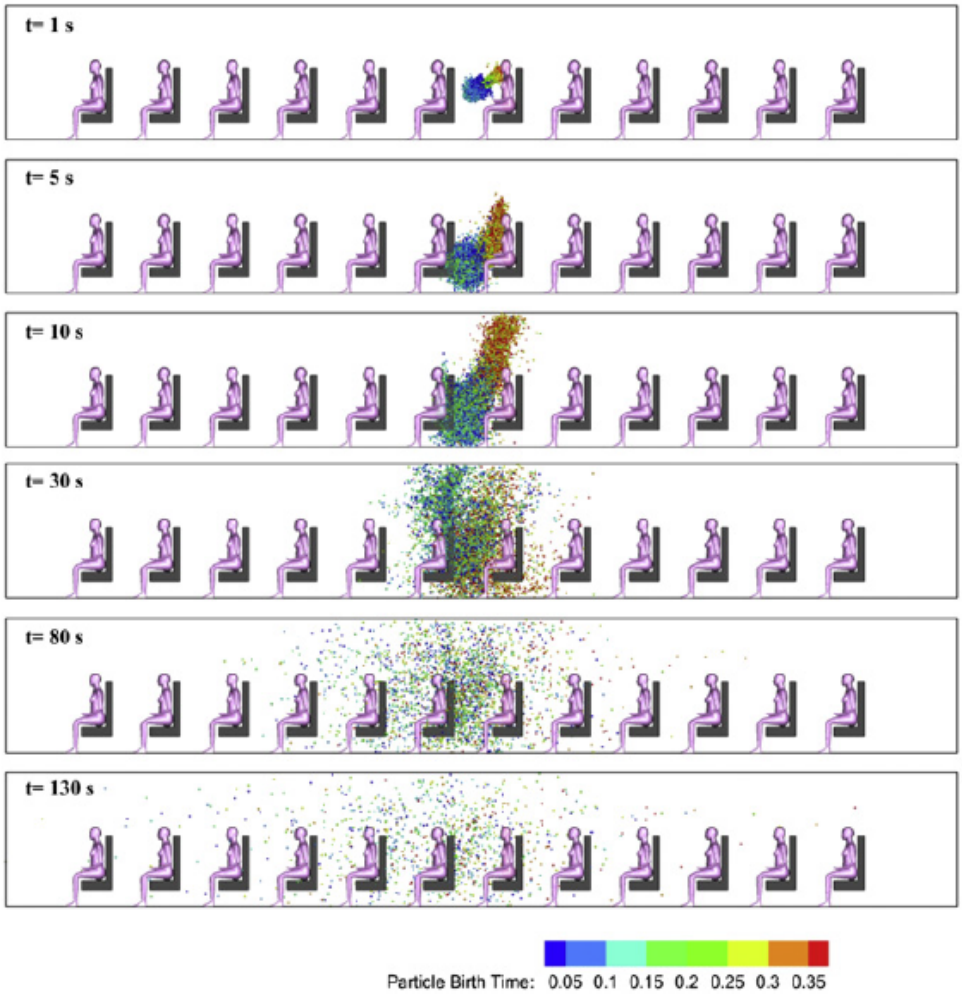

Figure 2-8. The transport of exhaled droplets in a fully-occupied high-speed rail cabin using a Lagrangian model (Zhang and Li, 2012).

One can convert the Lagrangian trajectories to particle number concentrations by implementing a user-defined function in ANSYS Fluent 12.1. The user-defined function counts the particle number in each cell, and then divides it by the volume of the cell, to obtain the particle number concentration.

2.2 Major Problems of Existing CFD Models

Although both the Eulerian and Lagrangian models can provide detailed information about person-to-person particle transport in enclosed environments, there are still some problems of the existing models. This section discusses two major problems of the existing CFD models: unrealistic and time-consuming.

2.2.1 Effect of Covering a Cough/Sneeze

The first major problem is that, when applying the CFD models, most of the existing studies assumed that the index person coughed or sneezed directly without covering the mouth. For example, Seepana and Lai (2012) investigated the person-to-person particle transport due to sneezing in a full-scale chamber with an Eulerian model. The two persons were standing face-to-face with a distance of about 0.3 m. With such a short distance, the index person was still assumed to directly sneeze to the receptor, as shown in Figure 2-9, which is not realistic in a civilized society. In reality, people usually cover their mouths with a hand or a tissue when they cough or sneeze. In health care facilities, patients with respiratory illness are usually asked to wear a mask. Center for Disease Control and Prevention (CDC) has also strongly recommended the public to “cover your cough” (CDC, 2009), since it may reduce the risk of transmission of airborne infectious diseases.

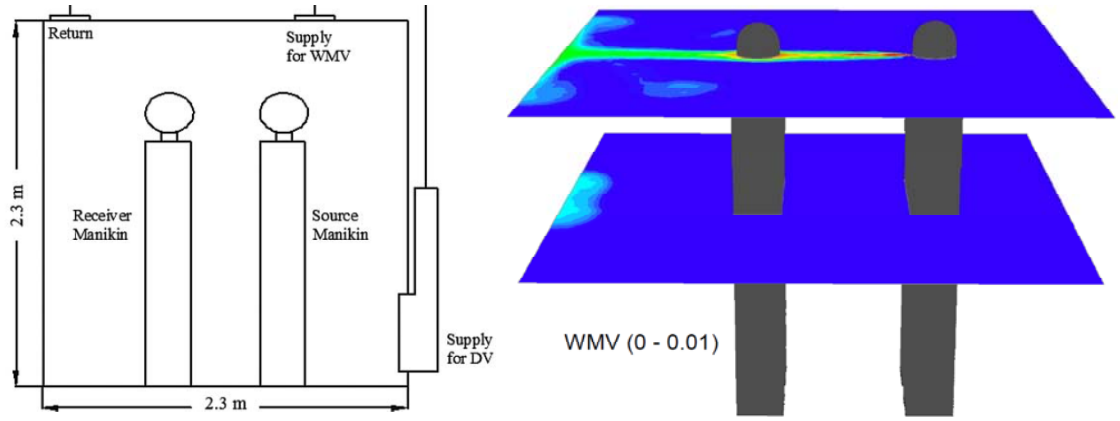

Figure 2-9. Simulation results of person-to-person exhaled particle concentration distribution when sneezing (Seepana and Lai, 2012).

There are a lot of studies experimentally investigated the effect of covering a cough/sneeze on person-to-person contaminant transport. Masks such as surgical and N95 masks have been extensively investigated especially for its effectiveness of removing exhaled particles. For instance, Gupta (2010) conducted a systematic review on the performance of N95 masks and concluded that the penetration through the N95 masks including the face seal leakages to be 10%. However, for surgical masks, Green et al. (2012) found that the removal efficiency of bioaerosols only ranged from 48% to 76%. Milton et al. (2013) showed that the surgical masks can remove 96% of coarse influenza virus aerosols (> 5 μm) but only 55% of fine influenza virus aerosols (≤ 5 μm). Davies et al. (2013) further compared the surgical and homemade mask, and found that the surgical mask was 3 times more effective in blocking transmission than the homemade mask. Furthermore, the fit performance of a mask can significantly affect the effectiveness of removing exhaled particles (Mansour and Smaldone, 2013). In addition to particle removal achieved by masks, other influencing factors about masks were also investigated. Tang and colleagues applied the real-time schlieren and shadowgraph imaging method to visualize the airflow from a cough with and without a mask (Tang et al., 2008; Tang and Settles, 2009; Tang et al., 2009). They found that a N95 mask can block the formation of the cough jet and a surgical mask can redirect the jet in a less harmful direction. Lai et al. (2012) measured the receptor's exposure in an environmental chamber and concluded

that the separation between the source and the receptor was the most influential parameter affecting mask protection. Moreover, it was found that masks on the receptors offered less protection when compared with masks on the sources (Diaz and Smaldone, 2010; Mansour and Smaldone, 2013).

Compared with masks, there are few studies addressing the effectiveness of other mouth coverings, such as a tissue or a hand. Tang and colleagues used the real-time schlieren and shadowgraph imaging method to extensively visualize the airflow from a cough/sneeze with the mouth covered by a tissue, cupped hand, fist, novel 'coughcatcher' device (Tang et al., 2011) and elbow (Tang et al., 2012), as shown in Figure 2-10. The qualitative schlieren and shadowgraph imaging experiments show that covering a cough can significantly reduce the horizontal velocity of the exhaled airflow. However, air jets were still observed from the leakage points between the face and covering. The videos/images produced by Tang and colleagues significantly improve the public understanding on the airflow from a cough/sneeze with the mouth covered. However, the visualization cannot be used for quantitative assessment of the effect of covering a cough.

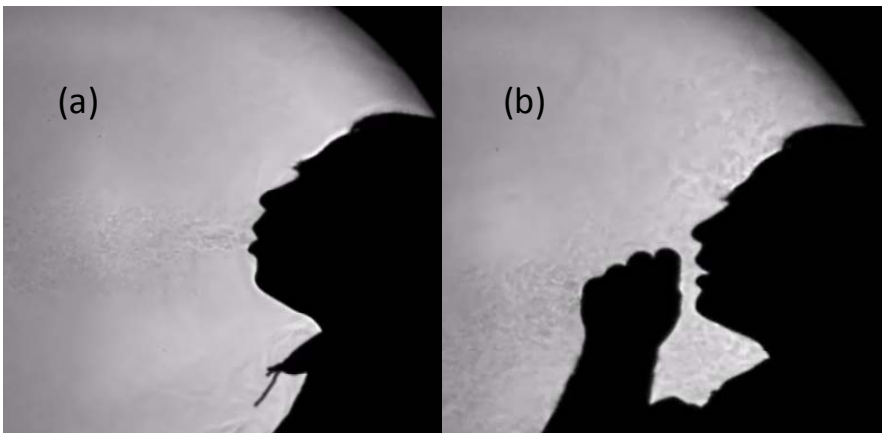

Figure 2-10. Visualization of exhaled airflow by a cough with mouth covering (a) uncovered, (b) fist, (c) cupped hand, (d) tissue, (e) surgical mask, (f) N95 mask (Tang et al., 2011).

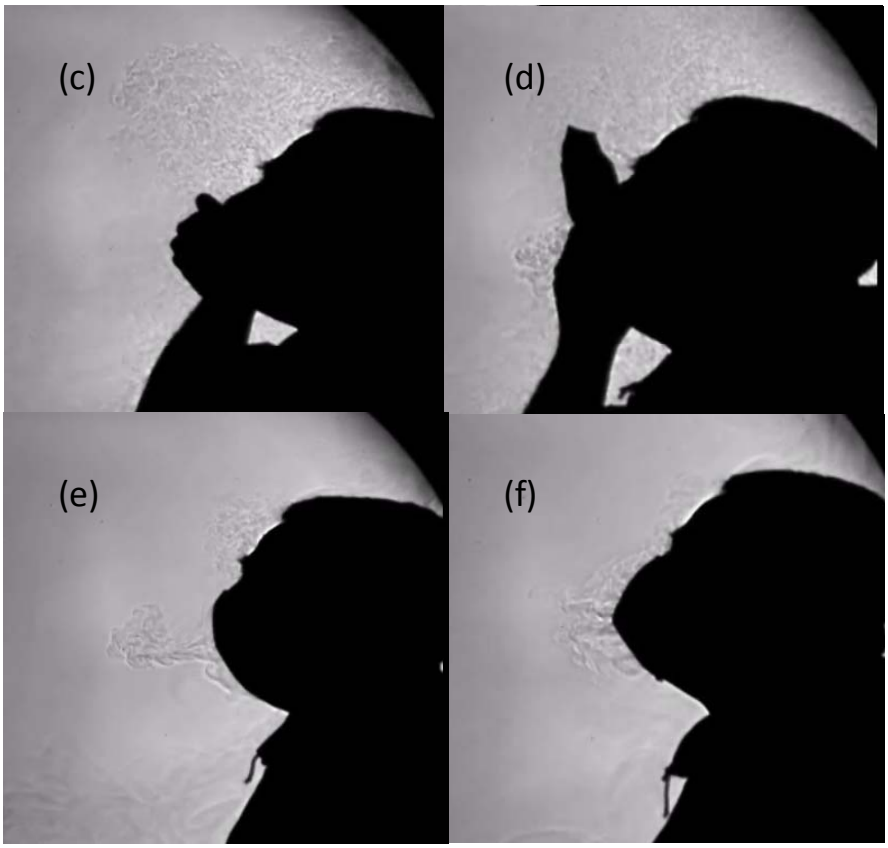

Figure 2-10. continued.

Although great effort has been made on experimental studies about covering a cough, there are surprisingly few numerical studies available in the literature. Li et al. (2013) used CFD simulations to investigate the effects of mouth covering on a co-occupant's exposure under three commonly employed ventilation systems. They concluded that covering the mouth could interrupt the horizontal transport of exhaled air and protect the co-occupant from direct exposure to the coughed particles. Their work has provided a new avenue in studying the effects of a mouth covering on the dispersion of exhaled particles. However, in their simulations, a small plate (0.20 m in length × 0.12 m in height) located 0.03 m in front of the infector's mouth was used to represent the mouth covering, as shown in Figure 2-11. The plate may not be representative of actual mouth coverings used in daily life. Thus, to obtain more realistic information about person-to-

person contaminant transport in indoor environments, it is important to correctly predict the exhaled airflow from a cough with the mouth covered.

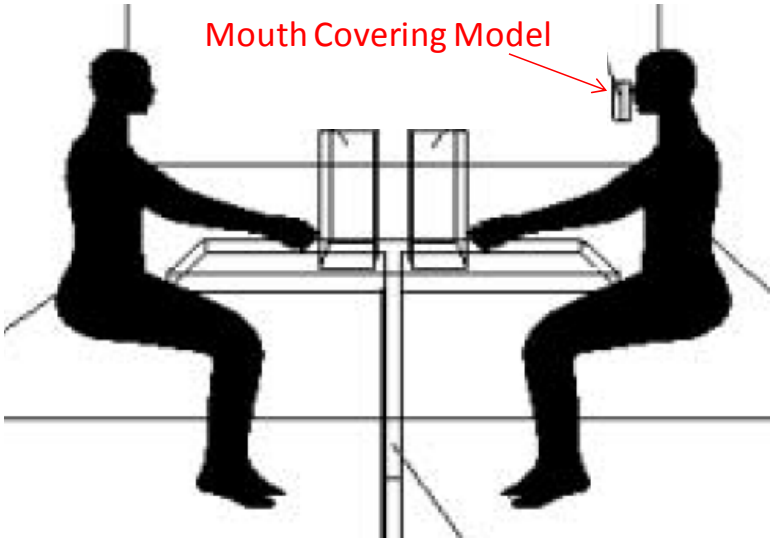

Figure 2-11. A small plate to represent the mouth covering used by Li et al. (2013).

To predict the exhaled airflow from a cough with the mouth covered, one option is to directly build a realistic geometry of the mouth covering, such as a tissue, a cupped hand, a fist, or an elbow. However, it would be very difficult to identify the air leakage points between the face and mouth covering. Furthermore, the complicated geometry of the mouth covering would necessitate a large number of grids in CFD simulations and result in significant computing costs. Therefore it is worthwhile to develop simplified models for predicting the exhaled airflow from a cough with the mouth covered, which can make the simulation of person-to-person particle transport more realistic.

2.2.2 Computing Cost of Existing CFD Models

The studies reviewed above have demonstrated that both the Eulerian and Lagrangian models can provide detailed information about transient particle concentration

distributions. However, both models are considerably time-consuming, especially for transient particle transport calculations (Wang et al., 2012). For instance, four weeks were required to run a four-minute real-time simulation of particle transport in a seven-row aircraft cabin using the Lagrangian model on an eight-parallel-processor computer cluster (Gupta et al., 2011a). Wang et al. (2012) tested the computing times of the Eulerian and Lagrangian models with different turbulence models for calculating transient particle transport in a typical room on an eight-core cluster with two 2.5 GHz AMD quad-core processors, as shown in Table 2-1. It can be seen that, such a calculation requires at least 62.2 and 84.9 hours for the Eulerian and Lagrangian models, respectively.

Table 2-1. Computing costs of different particle simulation models (Wang et al., 2012).

Method		Computing time (hour)*
Eulerian	RANS	62.2
	LES	323.3
	DES1	367.0
	DES2	396.6
Lagrangian	RANS	84.9
	LES	360.5
	DES1	389.2
	DES2	434.3

* The computing time was estimated on an eight-core cluster.

For the Lagrangian model, it calculates the trajectories of individual particles on the basis of Newton's law. The discrete random walk (DRW) model is typically used to calculate the turbulence dispersion. Statistically speaking, a large number of particles are needed in the calculations in order to ensure accuracy. Traditionally, modelers have conducted an independence test in order to find a reasonable value for this particle number. For instance, as shown in Figure 2-12, Zhang and Chen (2006) conducted a particle number independence test by comparing the particle concentration solutions from different tracked particle numbers. It was found that 10,000 particles are needed to obtain statistically meaningful results in their case. However, this unguided process of an

independence test can be highly time-consuming when no simple method is available for estimating the necessary particle number. Furthermore, the computing cost of the Lagrangian model is positively associated with the particle number in the calculation. If this number is very large, the computing cost may not be affordable. Therefore, it is worthwhile to develop a method for estimating and reducing the necessary particle number, in order to accelerate the Lagrangian method for modeling transient particle transport in indoor environments.

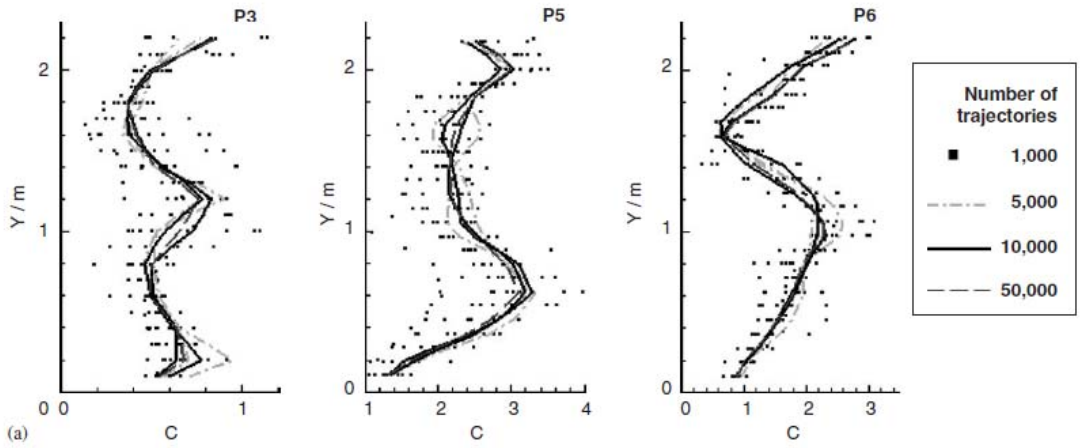

Figure 2-12. A particle number independence test at three poles in one of the cases in Zhang and Chen (2006).

Wang et al. (2012) systematically compared the Eulerian and Lagrangian models with various turbulence models and found that the Eulerian model was faster than the Lagrangian model. However, even with the Eulerian model, the unsteady-state calculation with iterations in each time step is considerably time-consuming for engineering applications, as shown in Table 2-1.

Several studies have demonstrated the ability of the Markov chain technique to quickly predict spatial and temporal particle concentrations. For instance, Nicas (2000) and Jones and Nicas (2014a,b) applied the Markov chain technique in a multi-zone model, as shown in Figure 2-13. However, these models can only work for an extremely coarse grid.

Therefore, a new model that not only works on a fine grid, as do the Eulerian and Lagrangian methods, but also runs faster than these two methods, is desirable. Note that, when solving the particle equations, the Markov chain technique does not require any iteration in a time step. Compared with the Eulerian model which requires iterations in each time step, the Markov chain technique has the potential to reduce the computing cost. Therefore, it is worthwhile to develop a new CFD model on the basis of a Markov chain frame, which can be much faster than the traditional models, for predicting detailed transient particle concentration distributions in enclosed environments.

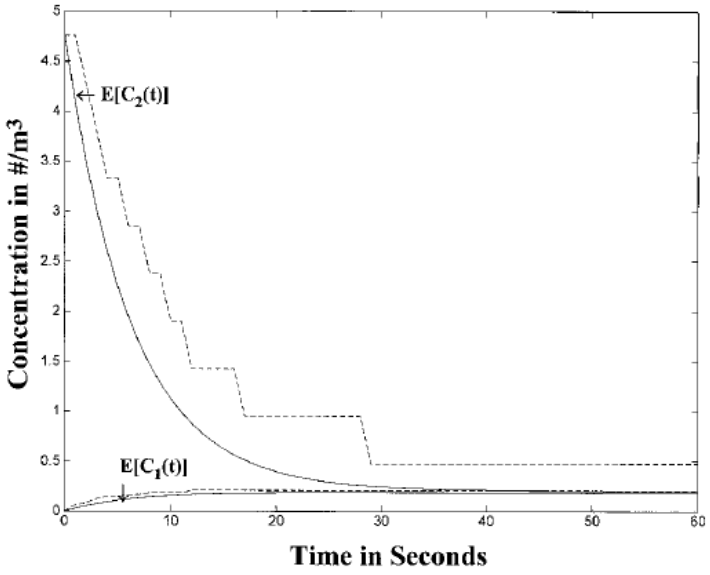

Figure 2-13. The Mycobacterium tuberculosis particle concentrations in the near-field and far-field zones in the first 60 seconds following a pulse release of 10 particles into the near field at time zero using a two-zone model based on a Markov chain frame. (Nicas, 2000).

According to the review conducted in this chapter, the following tasks are proposed in this study to improve and accelerate the computer models for predicting person-to-person contaminant transport in enclosed environments:

(1) Developing simplified models for predicting the exhaled airflow from a cough with the mouth covered;

(2) Develop a method for estimating and reducing the necessary particle number in order to accelerate the Lagrangian model;

(3) Develop a new CFD model on the basis of a Markov chain frame, which can be much faster than the traditional models.

CHAPTER 3. EXPERIMENTAL STUDY

The major objective of this study is to improve and accelerate the computer models for predicting person-to-person contaminant transport in enclosed environments. To assess the performance of the computer models, experimental data of airflow, temperature, and contaminant concentration distributions are required. Therefore, this chapter aims to conduct experimental measurements for person-to-person transient particle transport in an office mockup with an under-floor air-distribution (UFAD) system and the first-class cabin of an MD-82 airplane.

3.1 Steady-State Experiment in an Office Mockup

This study first conducted experimental measurements of steady-state distributions of airflow, temperature, and passive contaminant concentration in an office mockup with a UFAD system. Although the person-to-person contaminant transport is transient in nature, the steady-state experimental measurements are still useful for validating the basic features of CFD simulations.

3.1.1 Experimental Setup

This investigation built a full-scale office using an environmental chamber with dimensions of 4.8 m in length, 4.3 m in width, and 2.4 m in height, as shown in Figure 3-1(a). A UFAD system was installed in the chamber. There were two inlets installed at floor level, and the exhaust was located at ceiling level. Figure 3-2 shows the linear type of diffusers used in the experiment. The environmental chamber could provide a

controlled air supply at various airflow rates. The enclosures were well insulated so that the chamber could maintain a stable thermal condition.

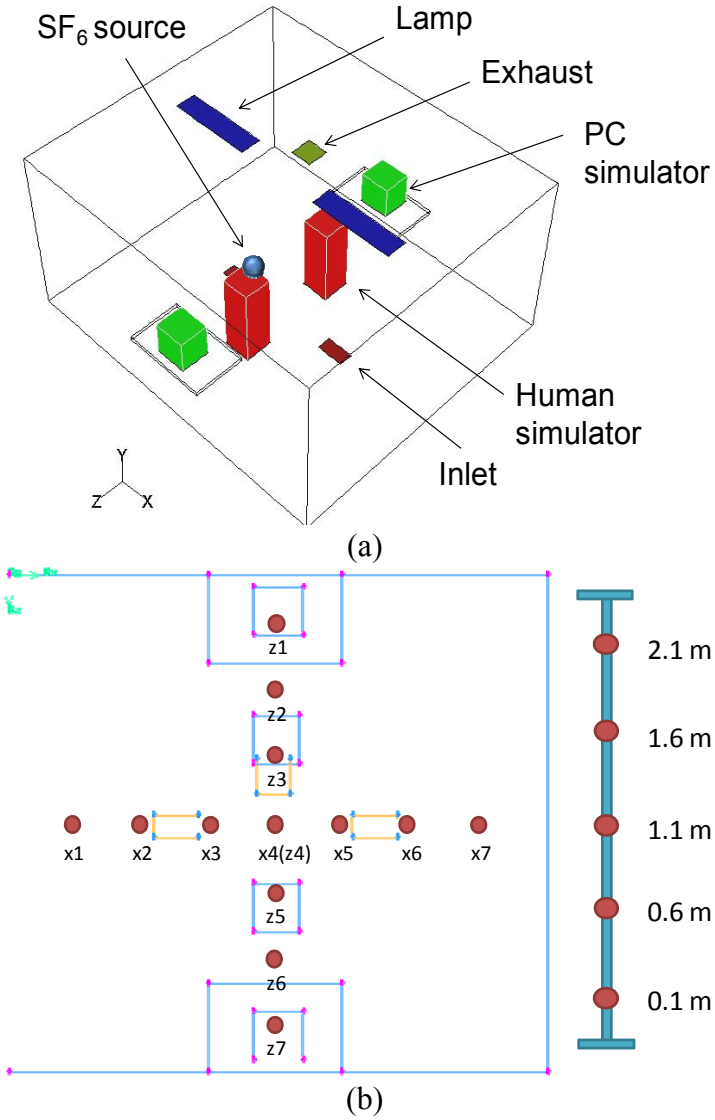

Figure 3-1. (a) Schematic of the office and (b) measuring locations and heights for air velocity, temperature and SF_6 concentration.

Figure 3-2. Linear diffuser used in the UFAD system.

The ventilation rate was set at 3, 6, and 9 ACH, and the person-to-person distance was set at 0.5, 1.1, and 1.8 m. This study used sulfur hexafluoride, SF_6, as a tracer gas to simulate the exhaled contaminants. The SF_6 source was located in the breathing zone of one of the human simulators, as shown in Figure 3-1. Before each measurement, this investigation operated the heating, ventilation, and air-conditioning (HVAC) system for 6 to 8 hours to reach a thermally steady-state condition. The measurement started after a steady-state concentration distribution of SF_6 was reached.

The air velocity, temperature, and SF_6 concentration distributions were measured in the experiment. As depicted in Figure 3-1(b), the air velocity, temperature, and SF_6 concentration were measured in two sections at 13 locations in the plane. At each location the measurements were conducted at five different heights along a pole. The experiment used 30 hot-sphere anemometers to measure the air velocity and air temperature. The hot-sphere anemometers had an accuracy of 0.02 m/s for velocity and 0.2 K for air temperature. A photo-acoustic multi-gas analyzer (INNOVA model 1312) with a multipoint sampler (INNOVA model 1309) was employed to measure the SF6 concentration with an accuracy of 0.001 ppm. The measurement duration of air velocity, air temperature, and SF_6 at each point was five minutes. Moreover, the air velocity magnitude and direction at the inlets were measured using ultrasonic anemometers. All the surface temperatures were measured using thermocouples as shown in Table 3-1.

Table 3-1. Measured boundary conditions.

Boundary	Temp. (°C)	Boundary	Temp. (°C)	Heat Power (W)
North wall (-X)	24.7	Lamps (north)	-	87
South wall (+X)	23.6	Lamps (south)	-	70
East wall (-Z)	24.8	Human simulator (east)	27.7	84
West wall (+Z)	24.3	Human simulator (west)	28	93.3
Ceiling (+Y)	24.8	PC simulator (east)	31.4	105
Floor (-Y)	24.3	PC simulator (west)	30.8	90
Supply air (north)	21.1	Supply air (south)	20.2	

3.1.2 Validation of Steady-State CFD Model

This study used the experimental data to first validate the steady-state CFD model in terms of airflow, temperature, and passive contaminant concentration fields. A RANS model with the Eulerian method for steady-state was used in this study because of the reasonable accuracy and low computing cost associated with the model (Wang et al., 2012). The renormalization group (RNG) k-ε model (Choudhury, 1993) was applied to calculate the airflow and turbulence because it has the best overall performance among all RANS models for enclosed environments (Wang and Chen, 2009). For contaminant modeling, because the mean diameter of the droplets exhaled through breathing was 0.4 μm (Gupta et al., 2010), the effect of gravitational settling on droplet dispersion was negligible (Zhao et al., 2009). Furthermore, Chen and Zhao (2010) have indicated that the transient process from a droplet to a droplet nucleus due to evaporation is also negligible for particles with a diameter of 0.4 μm. Furthermore, this case is to simulate a continuous breathing scenario, thus, modeling the breathed droplets as gaseous contaminants is reasonable.

Numerical simulations were conducted using the CFD program, ANSYS Fluent 12.1 (ANSYS 2010). A user-defined function (UDF) was implemented to realize the Eulerian model. Three grid resolutions (101,709, 729,304, and 1,476,360) were tested for CFD

grid independence. The 729,304 grid resolution was sufficiently fine to capture such a turbulent flow in the office mockup.

Figure 3-3 compares the measured and calculated air velocity profiles for the six validation cases. The lower and upper bounds of the error bars represent the 10th and 90th percentiles of the measurement data, respectively. There was a large quantity of data; therefore, in order to keep the paper concise, this study shows only representative results at poles x1 and x3. It can be seen in Figure 3-3 that both the measured and calculated air velocities were higher at the lower region of pole x3, which was near an inlet. At that location, the model predicted higher air velocities when the ventilation rate increased, which agrees well with the measurements. At the locations that were far away from the inlets, such as pole x1, both the measurements and the modeling results show relatively low air velocities. For all the cases, the average relative error of air velocity was 45%.

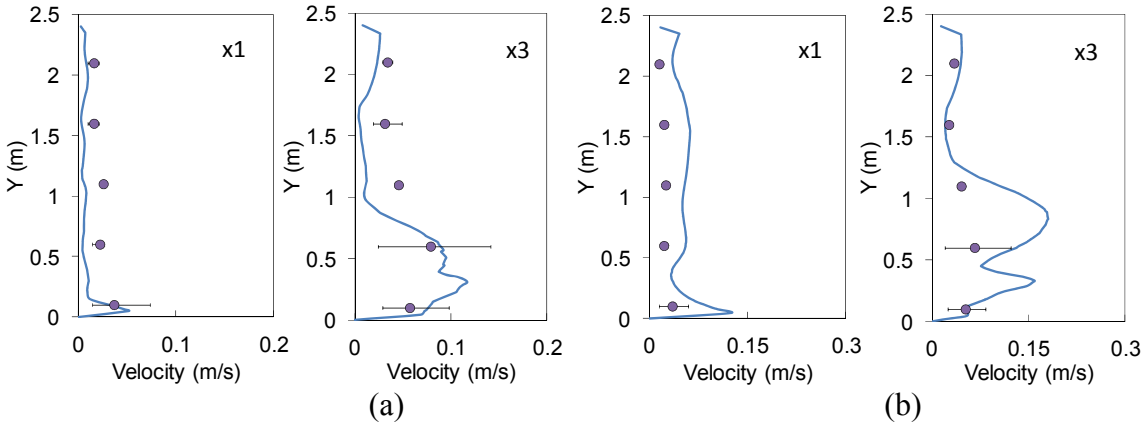

Figure 3-3. Comparison of the measured and calculated air velocity profiles for (a) Case 1: 3 ACH and 0.5 m distance; (b) Case 3: 3 ACH and 1.1 m distance; (c) Case 9: 6 ACH and 0.5 m distance; (d) Case 11: 6 ACH and 1.1m distance; (e) Case 21: 9 ACH and 0.5 m distance; and (f) Case 23: 9 ACH and 1.1 m distance.

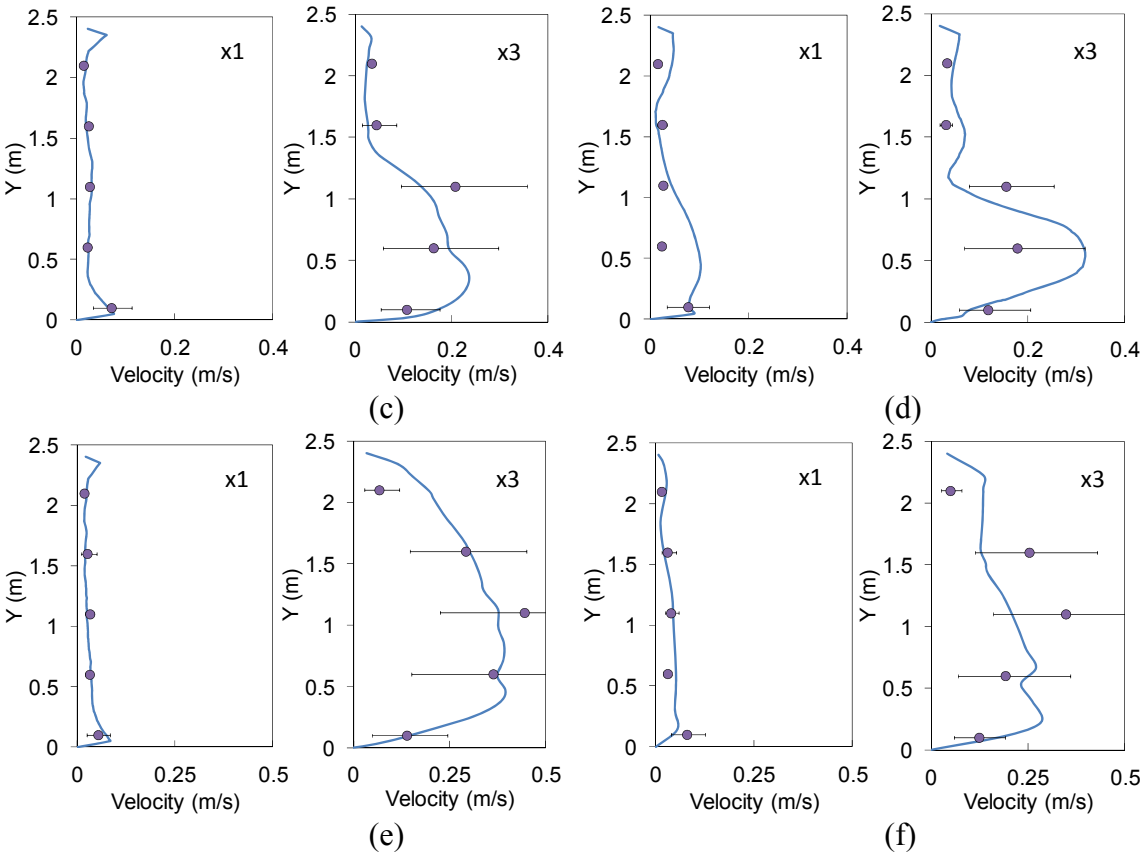

Figure 3-3. Continued.

Figure 3-4 shows a comparison of the measured and calculated air temperature profiles at poles x3 and z2. The air temperature was normalized by

$$\theta = \frac{T - T_{in}}{T_{out} - T_{in}} \tag{3.1}$$

where T is the local temperature, and T_{in} and T_{out} are the temperatures at the inlets and exhaust, respectively.

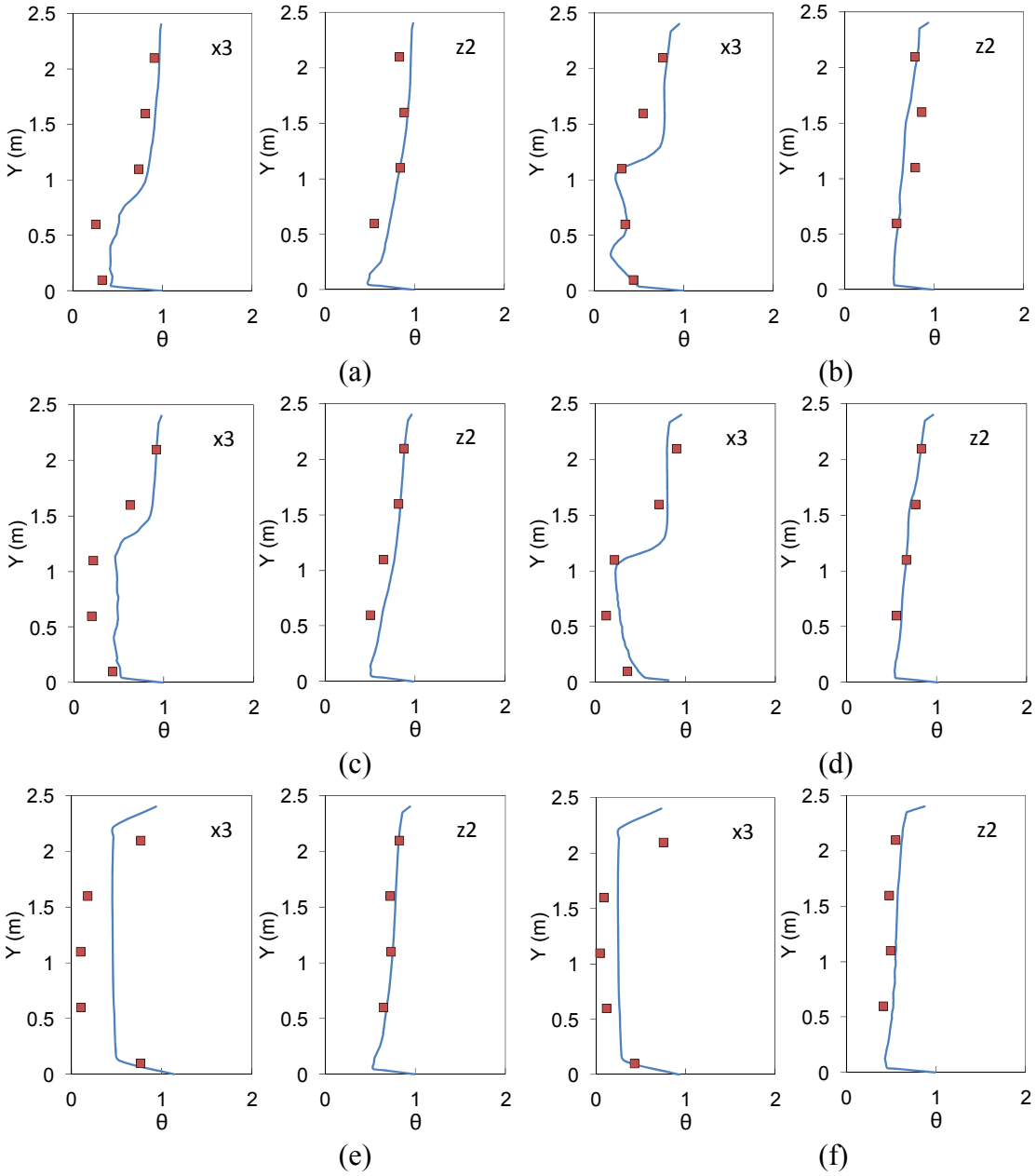

Figure 3-4. Comparison of the measured and calculated air temperature profiles for (a) Case 1: 3 ACH and 0.5 m distance; (b) Case 3: 3 ACH and 1.1 m distance; (c) Case 9: 6 ACH and 0.5 m distance; (d) Case 11: 6 ACH and 1.1m distance; (e) Case 21: 9 ACH and 0.5 m distance; and (f) Case 23: 9 ACH and 1.1 m distance.

Both the measured and calculated results show positive vertical temperature gradients for all the cases. At pole x3, which was close to an inlet, the temperature gradients tended to

be small when the ventilation rate was increased to 9 ACH. The reason was that such high air velocities near the inlet caused mixing and destroyed the stratification. The model can predict such a phenomenon in good agreement with the measurements. For all the cases, the average relative error of air temperature was 31%.

Figure 3-5 compares the measured and calculated SF_6 concentration profiles for the six cases. Again, the SF_6 concentration was normalized by

$$C^* = \frac{C - C_{in}}{C_{out} - C_{in}} \tag{3.2}$$

where C is the local concentration, and C_{in} and C_{out} are the concentrations at the inlets and exhaust, respectively. When the ventilation rate was 3 and 6 ACH, both the measured and calculated results show that the SF_6 concentration had a positive vertical gradient. This confirmed that the UFAD system could create a stratified air distribution. With a high ventilation rate of 9 ACH, the SF_6 concentration was uniform. The high air velocities near the inlets caused the mixing type of air distribution at pole x3. In Figure 3-5(a), remarkable differences existed between measurement and simulation. For pole x5, the simulation shows that there was a sudden change of concentrations at the height between 1.6 to 1.7 m. A single measurement point here was difficult to capture such a sudden change of concentrations. This might be the major reason for the remarkable difference between measurement and simulation. However, it can be seen that the measured data at 1.6 m matches well with the calculated data at 1.7 m. The measured data did fell in the range of calculated results at the height between 1.6 to 1.7 m. The similar explanation may apply to the remarkable difference at pole z2. For all the cases, the average relative error of SF_6 concentration was 44%.

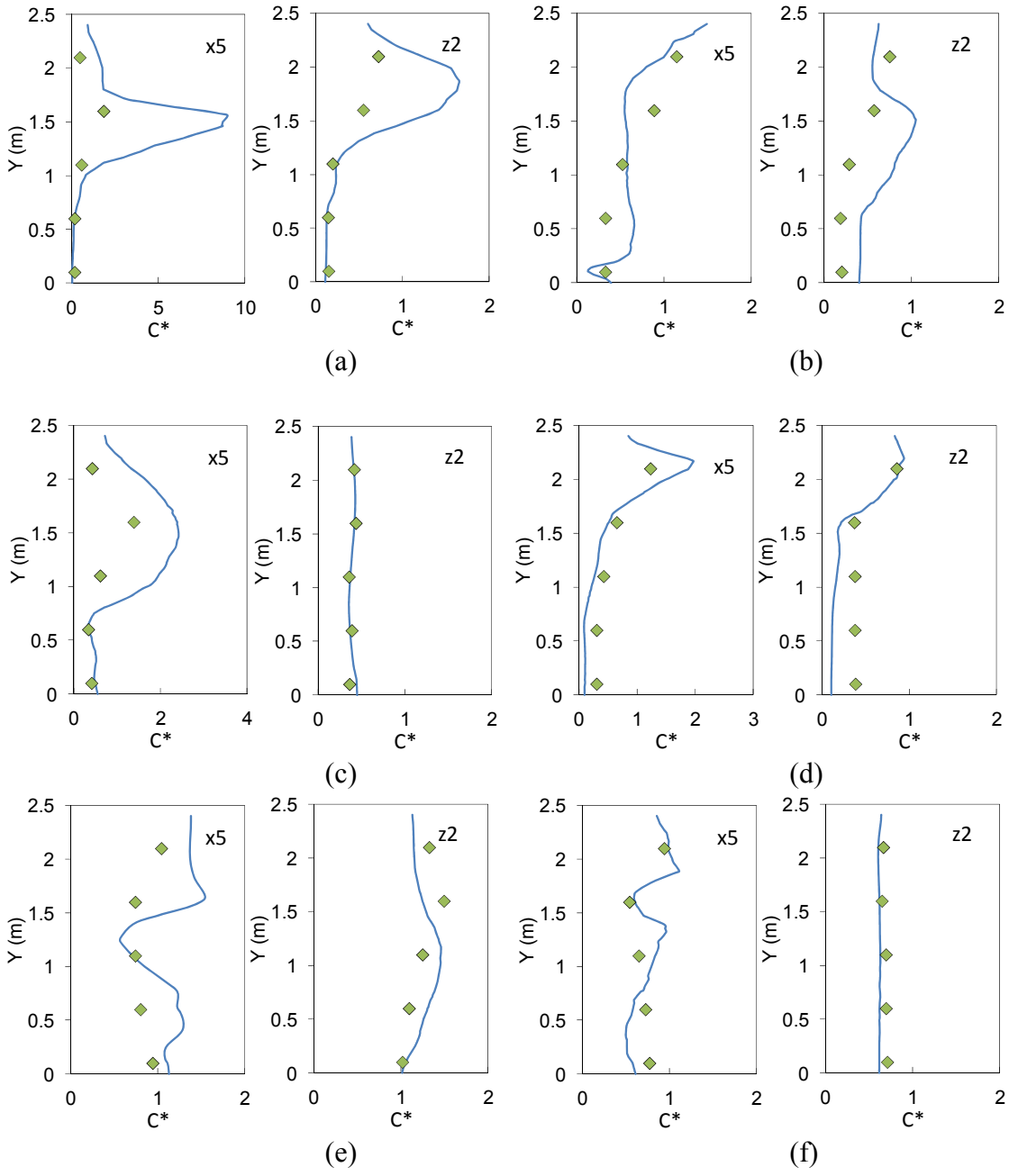

Figure 3-5. Comparison of the measured and calculated air temperature profiles for (a) Case 1: 3 ACH and 0.5 m distance; (b) Case 3: 3 ACH and 1.1 m distance; (c) Case 9: 6 ACH and 0.5 m distance; (d) Case 11: 6 ACH and 1.1m distance; (e) Case 21: 9 ACH and 0.5 m distance; and (f) Case 23: 9 ACH and 1.1 m distance.

Generally speaking, the calculated results agree reasonably well with the experimental data in terms of air velocity, temperature, and contaminant concentration distributions. Therefore, the RNG k-ε model can be used for predicting steady-state airflow and temperature distribution in enclosed environment. Furthermore, the steady-state Eulerian model is very fast and can be used for predicting steady-state contaminant concentration distribution indoors. The validated steady-state model has been applied to investigate the influence of ventilation mode, ventilation rate, and person-to-person distance on steady-state person-to-person contaminant transport indoors. This work is shown in Appendix A instead of the main body because the major focus of this thesis is for transient particle transport.

3.2 Experiment of Transient Particle Transport in an Aircraft

The section above has validated the steady-state CFD model for airflow and temperature prediction in enclosed environments. For person-to-person particle transport, it is transient in nature. Therefore, experimental data of transient particle transport is needed to validate the transient particle models. This section reports our effort in measuring person-to-person transient particle transport in the first-class cabin of an MD-82 aircraft.

3.2.1 Experimental Setup

Figure 3-6(a) shows the schematic model of the fully-occupied first-class cabin of the MD-82 aircraft. The dimension of the cabin was 3.28 m (L) × 2.91 m (W) × 2.04 m (H). The cabin contained three rows of seats, and each row had four seats as numbered in Figure 3-6(b). There were three and a half pieces of diffusers installed on each side in the cabin. Each diffuser of the supply inlet contained 280 linear slots which were arranged in two rows. The size of each slot was 124 mm (L) × 3 mm (W). Seven exhausts were located on each side of the cabin near the floor. The heated manikins were built by wrapping solid manikins with nickel-chromium wires. The sensible heat production of

the manikin was 75 W (Liu et al., 2013). A detailed description of the cabin can be found in Liu et al. (2012). The airflow and thermal boundary conditions of the first-class cabin were measured previously by Liu et al. (2012, 2013). This case was an ideal and realistic one for studying person-to-person transient particle transport in a mechanical ventilated space.

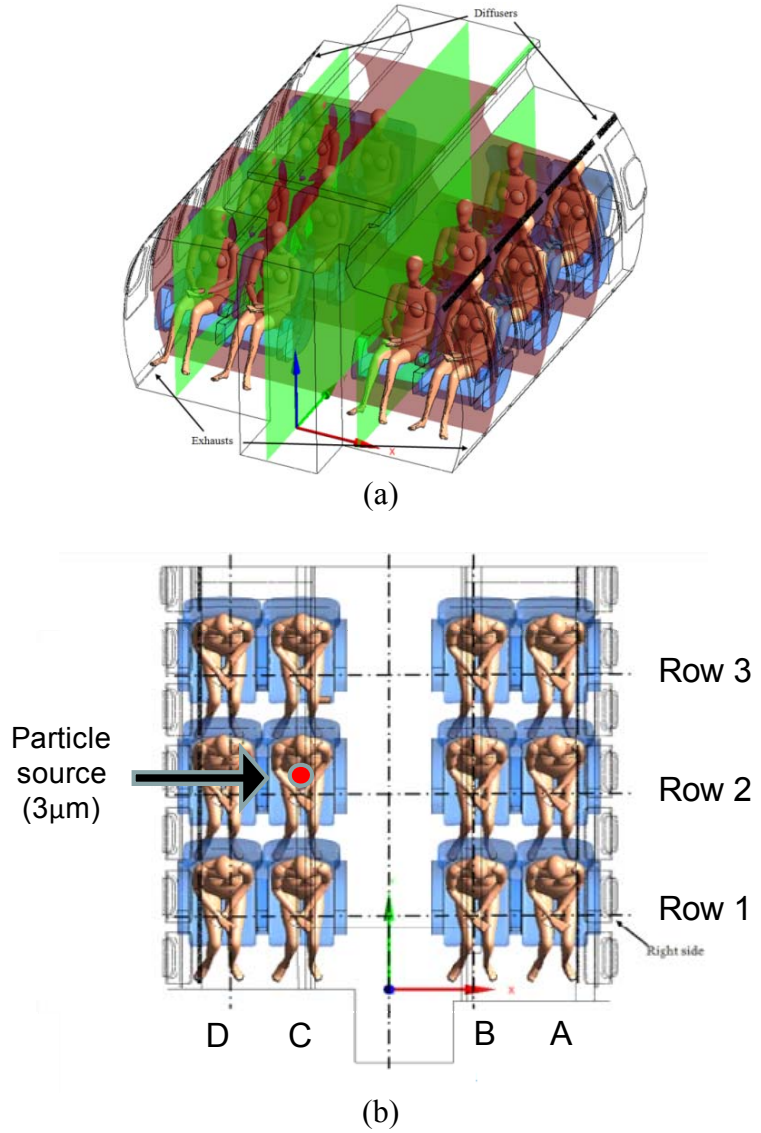

Figure 3-6. Schematic of the fully-occupied first-class cabin: (a) perspective view and (b) plane view (Liu et al., 2013).

The manikin 2C was set as the index passenger with a particle source. At the mouth, particles were released to the cabin air through a tube of 0.01 m in diameter at a speed of 1.03±0.02 m/s. To simulate a cough, an electromagnetic valve was installed in the tube, as shown in Figure 3-7. Then the particle release time could be controlled accurately. It was tested that the release time can be controlled within an error of 0.1 s. A MAG 3000 PALAS particle generator was used to generate Di-Ethyl-Hexyl-Sebacate (DEHS) mono-size particles with a diameter of 3 μm. DEHS is a non-soluble liquid with a low evaporation rate and a density of 912 kg/m^3. The DEHS particles have been widely used in experiments for indoor particle transport. For instance, Zhang et al. (2009) used DEHS particles to represent the exhaled particles in an airliner cabin mockup and measured their distributions under a half-occupied scenario.

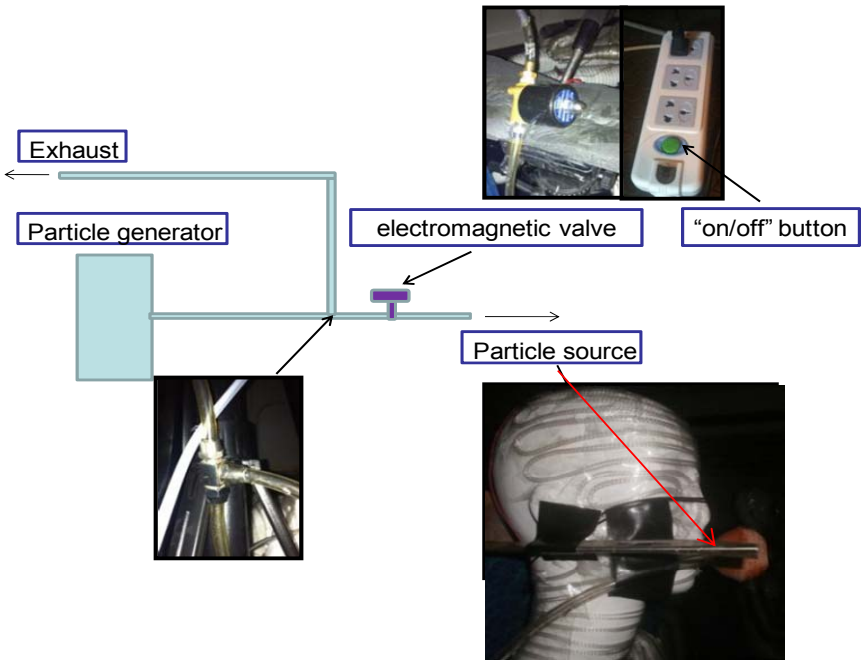

Figure 3-7. Particle source with an electromagnetic valve.

The particle concentrations versus time at the breathing zones were measured in front of each passenger's mouth. An aerodynamic particle sizer (APS 3321, TSI Inc., St. Paul,

MN) spectrometer was used to measure the particle concentration. To measure the transient particle concentration in a location, the sampling time should be larger than the response time of the aerodynamic particle sizer but should also be as short as possible. The response time of the instrument was 1 s so it was used in the experiment. To verify this sampling time, we measured the particle concentrations versus time were measured 5 mm in front of the source with different sample time intervals, 1, 2, 3 s. The source release time was set at 20 s (determination of the source release time is discussed in the next sub-section). In addition, the average particle concentration of the constant source (continuously releasing source) was also measured to be a reference. Figure 3-8 shows the comparison of particle concentrations in front of the source when the sample time interval was set at 1, 2, 3 s, respectively, and the average particle concentration of the constant source. Each profile was the average one of three-time measurements. The difference of the peak particle concentration when sample time interval was 1 s and the average concentration of the constant source was only 3.1%. Therefore, the sample time interval can be set at 1 s in the experiments to obtain detailed information with acceptable measurement accuracy.

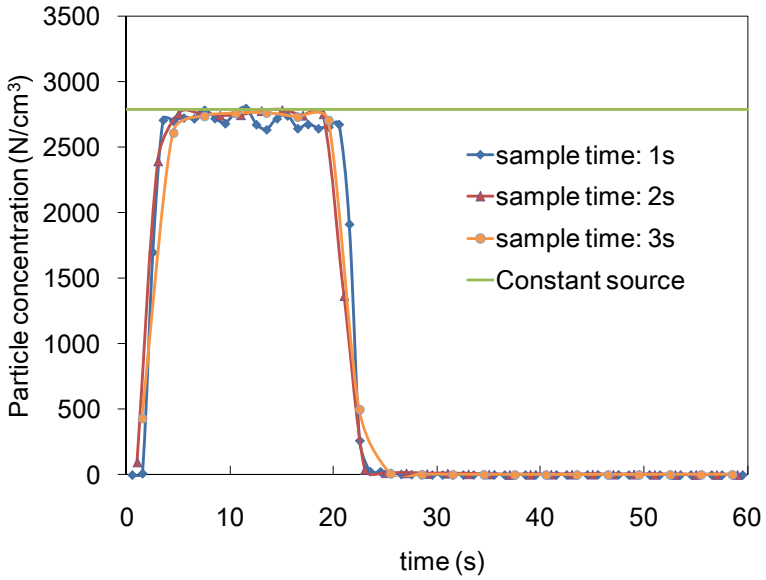

Figure 3-8. Comparison of particle concentrations in front of the source for different sample time intervals.

The source release time is also an important factor of experimental data quality. A single cough lasts for less than 1 s (Gupta et al., 2009). With such a short source release time in the experiment, the particle concentrations in the cabin may be too low to be detected by the aerodynamic particle sizer, so the data quality would be poor. Therefore, the source release time should be increased to some extent. Although the increased source release time was different from the real coughing case, the experiment was still meaningful since the aim of this study was to provide reliable experimental data to validate the CFD models. If the source release time had been too long, the experiment might have become a steady-state case. Hence, the source release time still needs to be as short as possible to meet the purpose of this study, while the particle concentrations at the breathing zone of other manikins should be detectable with the aerodynamic particle sizer.

This investigation compared the particle concentration versus time at 1A and 2A under three different source release times: 5, 20, and 60 s, as shown in Figure 3-9. It can be seen that a 5 s source release time cannot result in obvious particle concentration peaks. Therefore, a 5 s source release time was too short so that the particle concentrations in the cabin were too low to be detected by the aerodynamic particle sizer. A 20 s source release time can generate a peak concentration that is more than 5 times the background concentration. Obviously, a 20 s source release time can result in sufficient particle numbers at the breathing zone of the manikins so that the peak concentrations can be easily detected and observed. It can be seen that a 60 s source release time can result in even higher and more obvious peaks. However, the goal was to make the source release time be as short as possible to meet the purpose of this study. Therefore, a 60 s source release time may be too long for a transient particle transport case. Hence, a 20 s source release time was applied in the experiment.

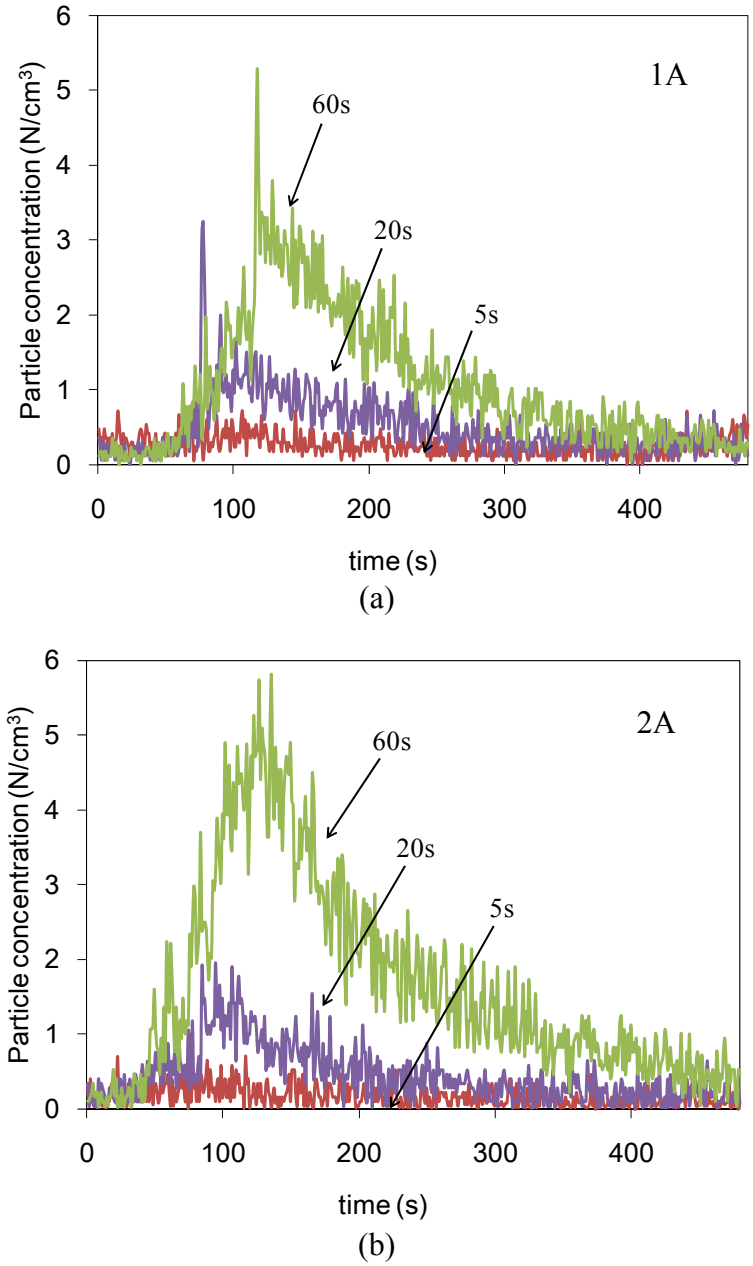

Figure 3-9. Comparison of the particle concentration levels when the source release time was 5, 20, and 60 s for (a) 1A and (b) 2A.

Since only one particle sizer spectrometer was available, the particle concentrations versus time were measured for one passenger at a time. The measurement time for each passenger was set as 500 s, so the entire experiment for measuring 11 passengers took about 2 hours. The complete experiment was repeated 3 times on different days. Since the

experimental data quality is related to the repeatability of the experiment, Figure 3-10 compares the three independent measurements of particle concentration versus time, taking 1B and 2A as examples. It can be seen that the three independent measurements matched very well with each other. Hence, the repeatability of the experiment is acceptable.

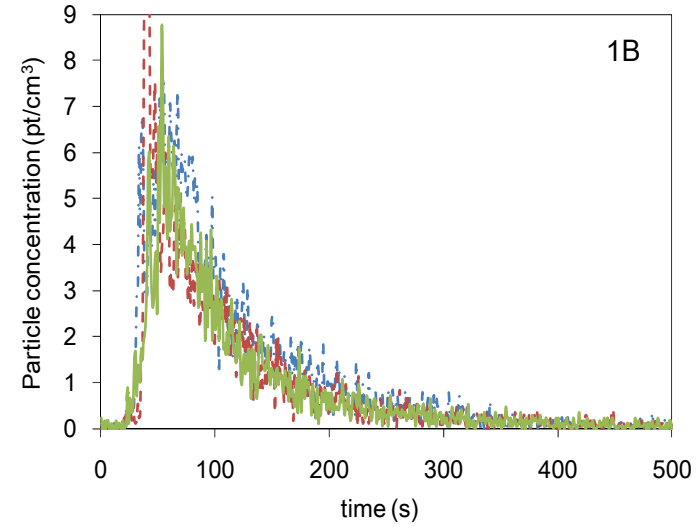

(a)

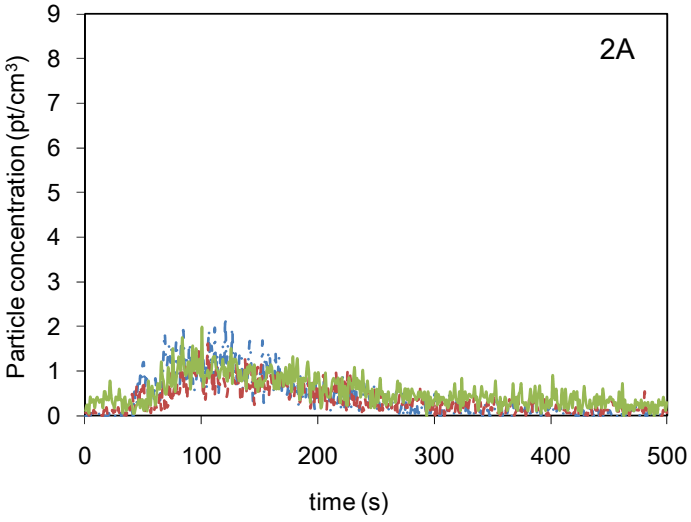

(b)

Figure 3-10. Comparison of three independent measurements of particle concentration versus time for (a) 1B and (b) 2A.

3.2.2 Experimental Data

Figure 3-10 showed that the transient particle concentrations were fluctuating to some extent. For easy observation and comparison with modeling results, the experimental data should be rearranged. Figure 3-11 compares different average metrics of the experimental data, i.e. averaged every 1, 5, 10, and 15 seconds. It can be seen that the 15 second averaged particle concentration versus time is smooth enough and easy to observe. Thus, the experimental data were averaged every 15 s.

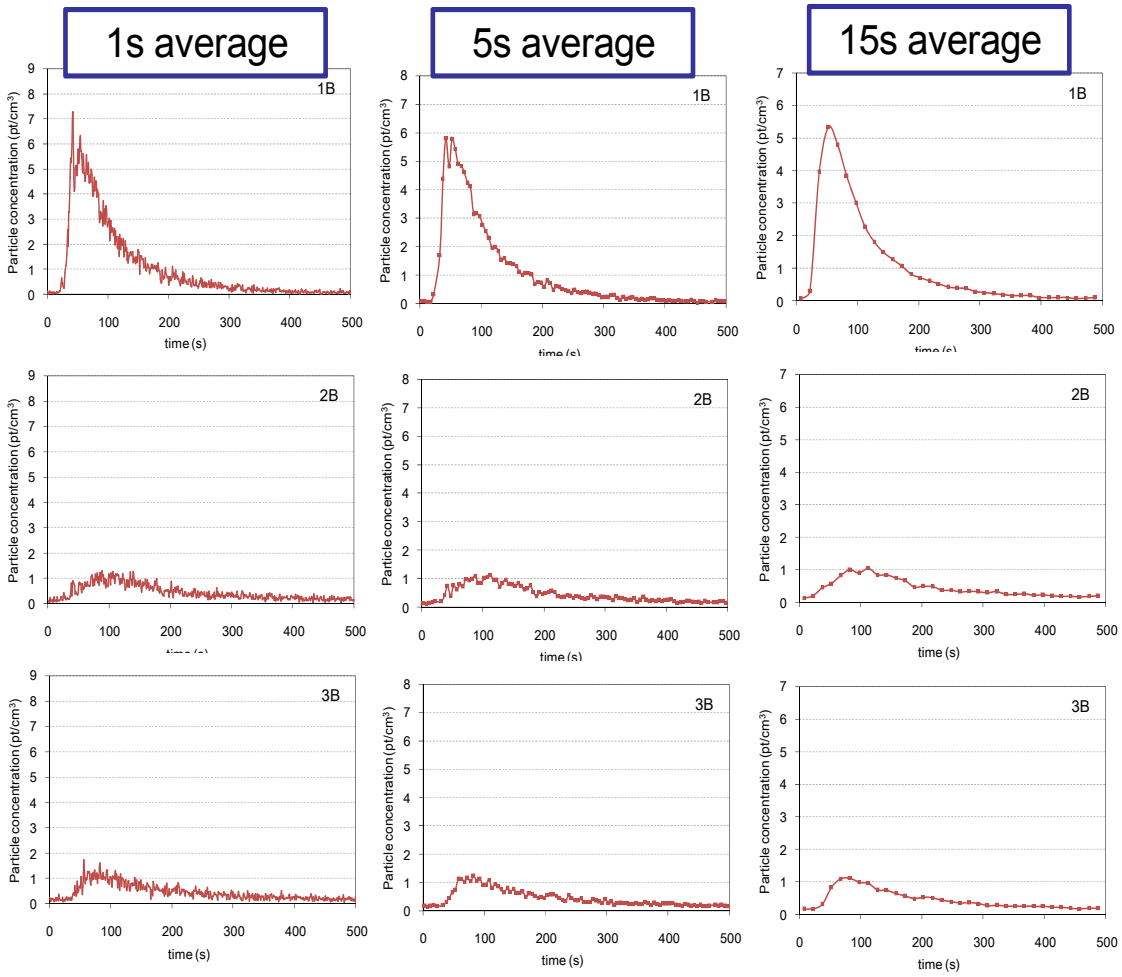

Figure 3-11. Comparison of different average metrics of the experimental data.

Figure 3-12 shows the transient particle concentrations at the breathing zone of each passenger. Since the experiment was repeated 3 times, each solid point in the figure represents the average value of the 45 data points (15×3=45). The lower and upper bound of the error bars represents the 10^{th} and 90^{th} percentile of the 45 data points, respectively. The experimental data were normalized by the maximum concentration among the monitoring points for the entire experiment. The particle concentration at the breathing zone of each passenger reached to a very low level after 500 s. The particle concentrations at Seat 1B, 1C were relatively high, while that at the other seats were relatively low. A large portion of the released particles moved forward from 2C to 1B, and 1C and resulted in relatively high peak concentrations. The rest of the particles dispersed to other locations and also led to peaks but with lower concentrations. The experimental data measured in the first-class cabin of the MD-82 aircraft can be used in evaluating the performance of the models studied and developed in this study.

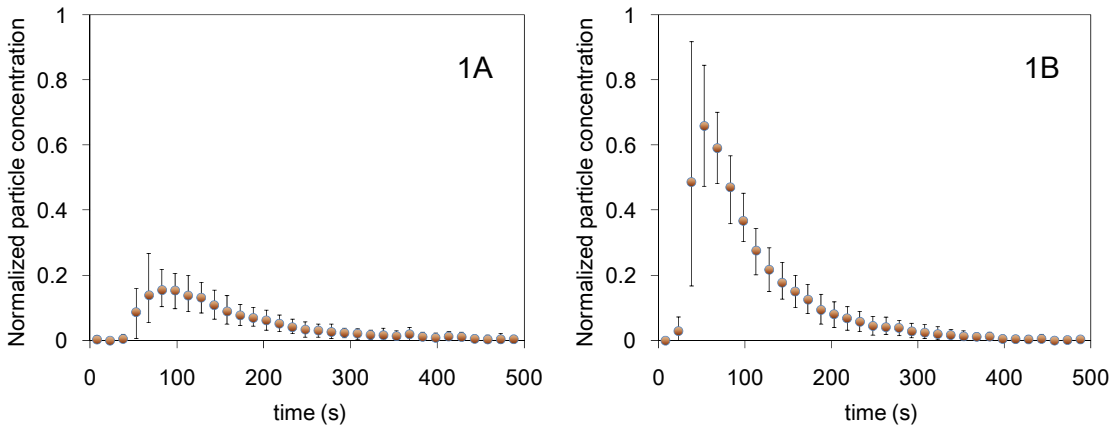

Figure 3-12. Experimental data of transient particle concentrations at the breathing zone of each passenger.

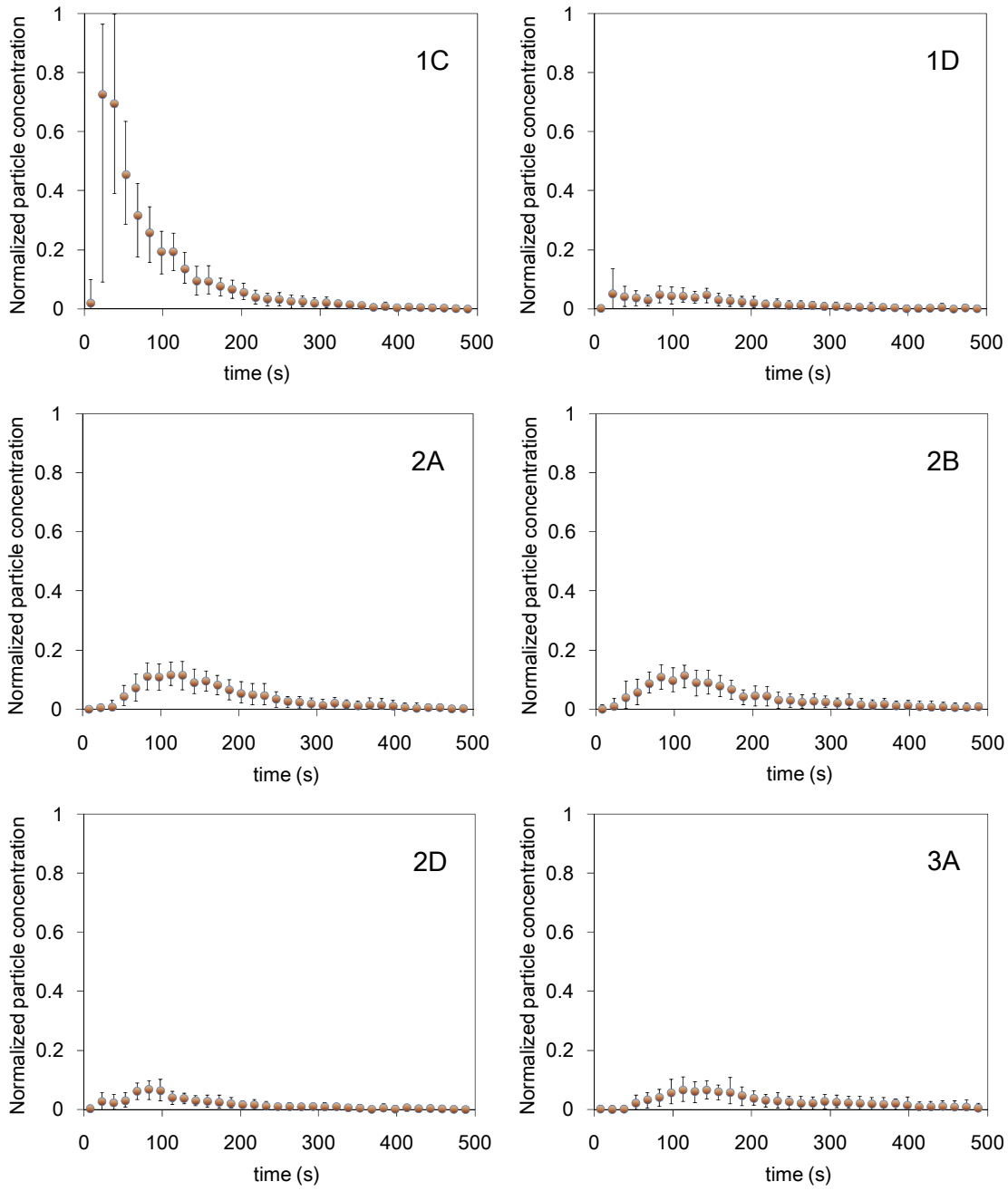

Figure 3-12. continued.

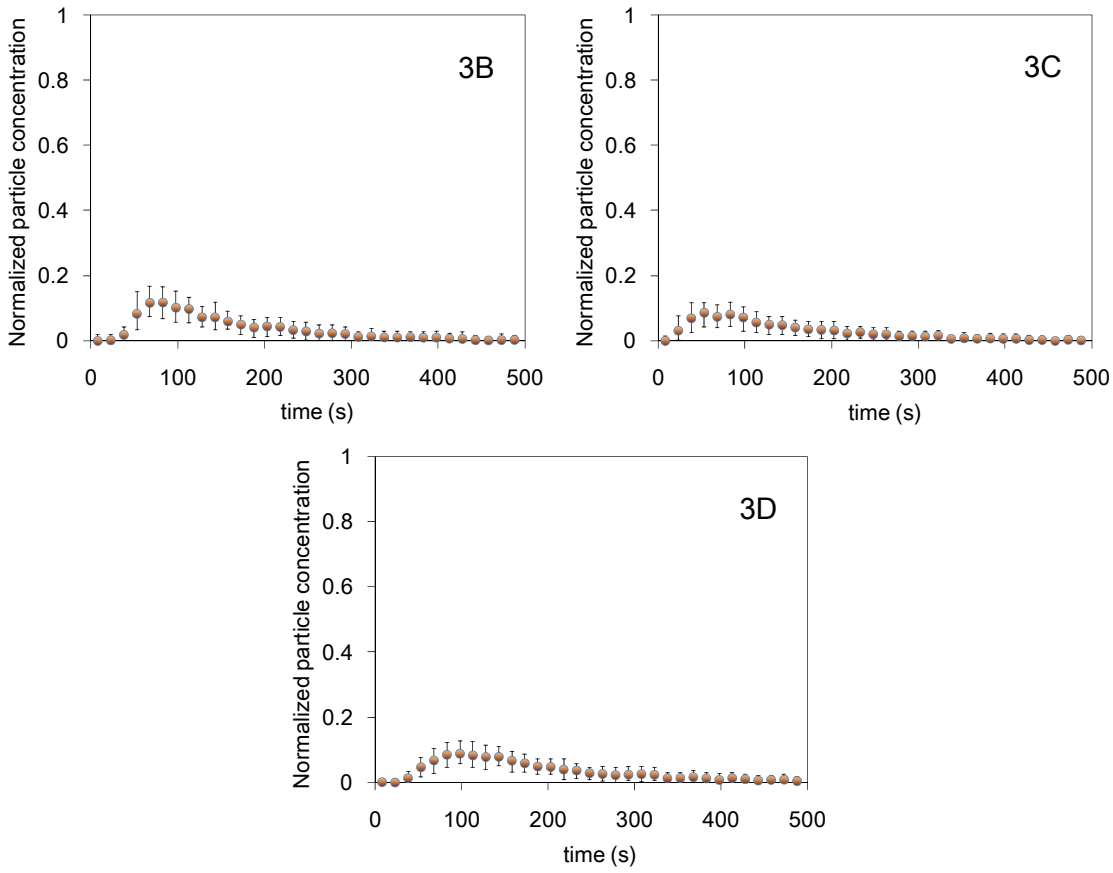

Figure 3-12. continued.

3.3 Conclusions

This chapter conducted experimental measurements for person-to-person particle transport in an office mockup with a UFAD system and the first-class cabin of an MD-82 airplane. The investigation has led to the following conclusions:

(1) The experimental data measured in the office mockup can be used in evaluating the performance of steady-state airflow and contaminant distribution models.

(2) The RNG k-ε model can be used for accurately predicting steady-state airflow and temperature distribution in enclosed environments.

(3) The steady-state Eulerian model is very fast and can be used for predicting steady-state contaminant concentration distribution in enclosed environments.

(4) The experimental data measured in the first-class cabin of the MD-82 aircraft can be used in evaluating the performance of the transient particle models in the next chapters.

CHAPTER 4. SIMPLIFIED MODELS FOR COVERING A COUGH

People usually cover their mouths with a hand or a tissue when they cough or sneeze. To predict the exhaled airflow from a cough with the mouth covered, one option is to directly build a realistic geometry of the mouth covering, such as a tissue, a cupped hand, a fist, or an elbow. However, it would be very difficult to identify the air leakage points between the face and mouth covering. Furthermore, the complicated geometry of the mouth covering would necessitate a large number of grids in CFD simulations and result in significant computing costs. Therefore this chapter aims to develop simplified models for predicting the exhaled airflow from a cough with the mouth covered, to make the simulation of person-to-person particle transport more realistic.

4.1 Visualization of Exhaled Airflow

4.1.1 Experimental Methods

In order to understand the characteristics of exhaled airflow from a cough with the mouth covered, this study used tobacco smoke to visualize the airflow from 16 human subjects (15 males and 1 female). The median diameter of tobacco smoke particles is about 0.2 μm (Klepeis and Nazaroff, 2002) and the temperature of exhaled tobacco smoke is close to that of pure exhaled air (Gupta et al., 2009). Thus, the exhaled smoke flow should closely follow the cough airflow.

The subjects were healthy smokers, and the experimental procedures were approved by an institutional review board for human subject experimentation. The subjects were

informed of the objectives of this research and the associated risks. Each subject signed a consent form before participating in the experiment. The pictures of the exhaled flows were obtained by moderate-speed photography at a frequency of 80 Hz. Five types of mouth covering methods were tested: a tissue, a cupped hand, a fist, and an elbow with a sleeve and without a sleeve, as well as an uncovered cough. Each test was repeated at least twice for each subject. The subjects were asked to exhale smoke through a single cough. To ensure high-quality flow visualization, a light source and a dark background were used. The pictures were taken from both the front and side view. However, the results showed that the exhaled airflow visualized from the front view was much more limited than that from the side view. Therefore, this study only discusses the characteristics of coughed airflow from the side view.

4.1.2 Characterizing Exhaled Airflow from a Cough with the Mouth Covered

In representative photographs of a cough covered by a tissue (Figure 4-1), the transient exhaled airflow profiles can be seen in detail. A forward jet penetrated the tissue, and an upward jet escaped from the upper leakage point between the face and tissue. Further visualization results are provided in Figure 4-2. Some subjects exhaled both forward and upward jets, as shown in Figure 4-2(a), while others exhaled only a forward jet or only an upward jet, as shown Figures 4-2(b) and 4-2(c), respectively. The visible horizontal transport distance of the smoke was quantitatively estimated using the digital color Y'UV model. Averagely, the visible smoke flow from a cough covered by a tissue can travel by 0.10 m in the horizontal direction. Note that the estimated visible horizontal transport distance does not necessarily represent the actual stopping distance of the cough air, since the smoke may be too weak to be detected outside the "edge" of the visible smoke. This parameter is provided for comparison between different covering methods.

Figure 4-1. Representative photographs of a cough covered by a tissue.

(a) (b) (c)

Figure 4-2. Visualization of a cough covered by a tissue (a) with both forward and upward jets, (b) with only a forward jet, and (c) with only an upward jet.

When a cough was covered by a cupped hand, upward and downward jets escaped the upper and lower leakage points, respectively, between the face and hand. Moreover, the upward jet tended to move forward to some extent. The visualization results (Figure 4-3) indicate that the cough could lead to both upward and downward jets, only an upward jet, or only a downward jet. The average horizontal transport distance for a cough covered by a cupped hand was 0.13 m.

(a) (b) (c)

Figure 4-3. Visualization of a cough covered by a cupped hand (a) with both upward and downward jets, (b) with only an upward jet, and (c) with only a downward jet.

When a cough was covered by a fist, jets moved through the hole in the subject's fist (Figure 4-4(a)), through the side leakage points between the fist and face (Figure 4-4(b)), or through both locations (Figure 4-4(c)). The average horizontal transport distance for a cough covered by a fist was 0.30 m, which was remarkably larger than a cough covered by a tissue or cupped hand.

(a) (b) (c)

Figure 4-4. Visualization of a cough covered with a fist (a) with a jet through the hole in the fist, (b) with jets through the leakage points between the face and fist, and (c) with both types of jets.

When a cough was covered by an elbow with a sleeve, there was a relatively strong upward jet and a relatively weak downward jet through the leakage points between the

face and elbow (Figure 4-5). An elbow with a sleeve can significantly redirect the exhaled airflow.

Figure 4-5. Visualization of a cough covered by an elbow with a sleeve.

Without a sleeve, the jet can move further than with a sleeve, as illustrated in Figure 4-6. Therefore, the effectiveness of covering a cough by an elbow without a sleeve is worse than that with a sleeve. The average horizontal transport distance for a cough covered by an elbow without a sleeve (0.25 m) was relatively larger than that with a sleeve (0.18 m). As a reference, this study also visualized the airflow from an uncovered cough. The average horizontal transport distance for an uncovered cough was 0.38 m.

Figure 4-6. Visualization of a cough covered by an elbow without a sleeve.

4.2 Developing the Simplified Models

From the images captured in the experiments, the jet velocity and direction from the coughs can be determined, and these parameters can be used as boundary conditions for modeling person-to-person contaminant transport in ventilated spaces. This section details the determination of jet velocity and direction.

4.2.1 Methods for Determining Jet Velocity, Direction, and Flow Ratio

Figure 4-7 shows an example of the first image captured after the start of exhalation. Because the image capture frequency was 80 Hz, the image was captured at t = 0.0125 s. The distance traveled by the jet was Δs, which was quantitatively determined using the digital color Y'UV model. It was found that the peak velocity occurred at the very beginning of exhalation, and thus the peak velocity of the jet can be calculated by

$$V = \frac{\Delta s}{\Delta t} \tag{4.1}$$

where Δt is equal to 0.0125 s.

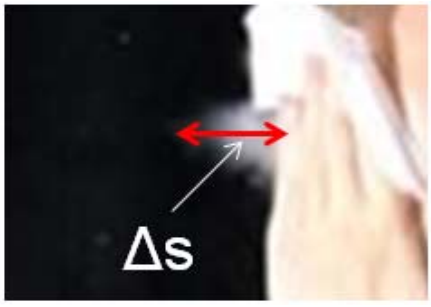

Figure 4-7. An example of the first image captured after the start of exhalation.

To verify the method, this investigation also visualized the airflow from an uncovered cough and compared it with detailed measurement data from Gupta et al. (2009). The average calculated peak velocity (11.8 m/s for 15 males and 1 female) agrees reasonably well with the measurement data (12.6 m/s for 25 males). Thus, this method can be used to determine the jet velocity from a cough with the mouth covered.

The direction of the jet's central line was visually approximated as a line that equally divided the smoke in the two-dimensional plane as shown in Figure 4-8. Two angles, θ_1 and θ_2, were used to describe the direction of the jets. For cases in which two jets were observed, the ratio of the airflow rates can be estimated by the volumes of the two smoke jets.

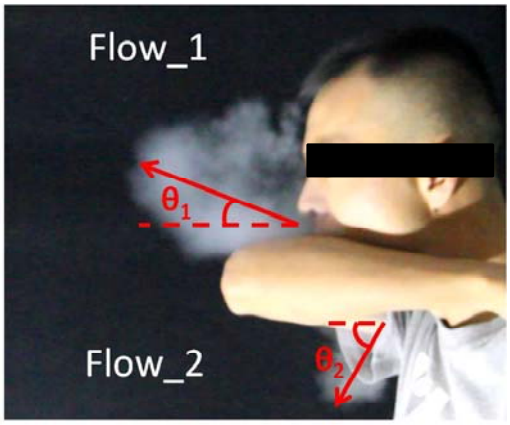

Figure 4-8. Directions of jets' central lines.

4.2.2 Simplified Models

The average, 10th percentile, and 90th percentile of initial jet velocity, direction, and flow ratio were determined for coughs with the mouth covered, as shown in Figure 4-9. The average velocities of the forward and upward jets from a cough covered by a tissue were 2.6 and 3.8 m/s, respectively, which were lower than in the other cases. Since the use of tissues can also prevent the transmission of infectious diseases by eliminating direct

contact with hands, covering a cough with a tissue should be the best approach. Covering a cough with a cupped hand is the second best approach, with an average upward jet velocity of 6.3 m/s and an average angle of 59.2°. When coughs were covered by an elbow with and without a sleeve, the average initial jet velocity was similar between them, but the average angle with a sleeve was relatively large. Thus, the sleeve is beneficial for redirecting the airflow and reducing the risk of horizontal transport of exhaled particles. Covering a cough with a fist is probably the worst approach, with a relatively high velocity of 8.5 m/s and a small angle of 25.8°.

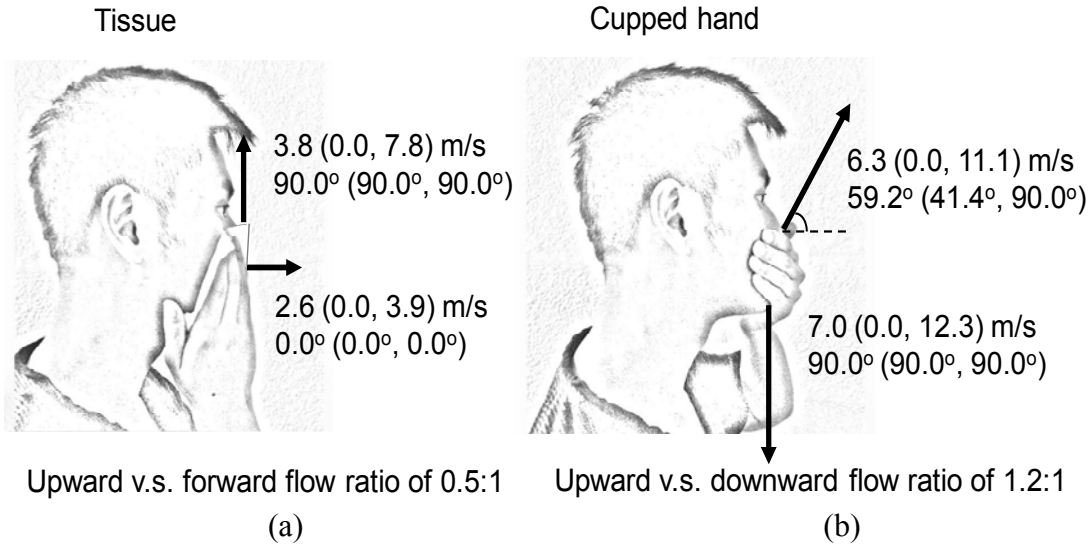

Figure 4-9. Average jet velocity, direction, and flow ratio for coughs covered by (a) a tissue, (b) a cupped hand, (c) an elbow with a sleeve, (d) an elbow without a sleeve, and (e) a fist; and (f) an uncovered cough. The numbers in parentheses are the 10th and 90th percentiles, respectively.

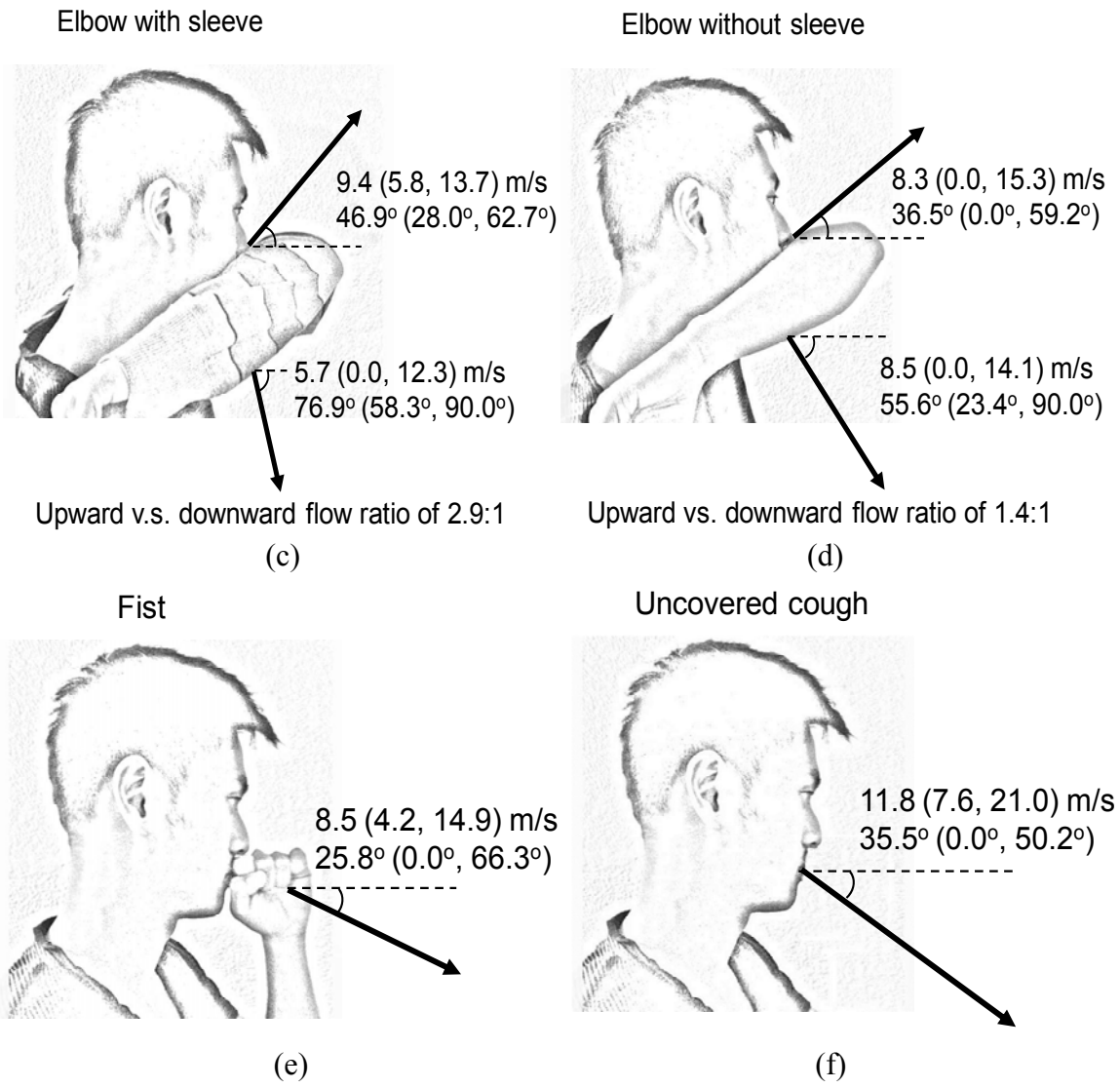

Figure 4-9. continued.

A covered mouth can be represented by a simplified method that separates the opening into four equal sections with a total area of 8 cm^2, as shown in Figure 4-10. The jet velocity and direction are defined at two of these sections, and the other two sections are defined as solid walls. Thus, the remaining area of the opening is 4 cm^2, which is the actual area of a mouth opening (Gupta et al., 2009). The various mouth coverings (Figure 4-10) are defined according to the following rule. If the angle shown in Figure 4-9 is larger than 45°, the jet is defined at the upper or lower section of the opening, whereas, if

the angle is smaller than 45^{o}, the jet is defined at the upper-front or lower-front section of the opening. Under this simplification, the complicated geometries of mouth coverings are avoided, and the models can be used more easily for engineering applications.

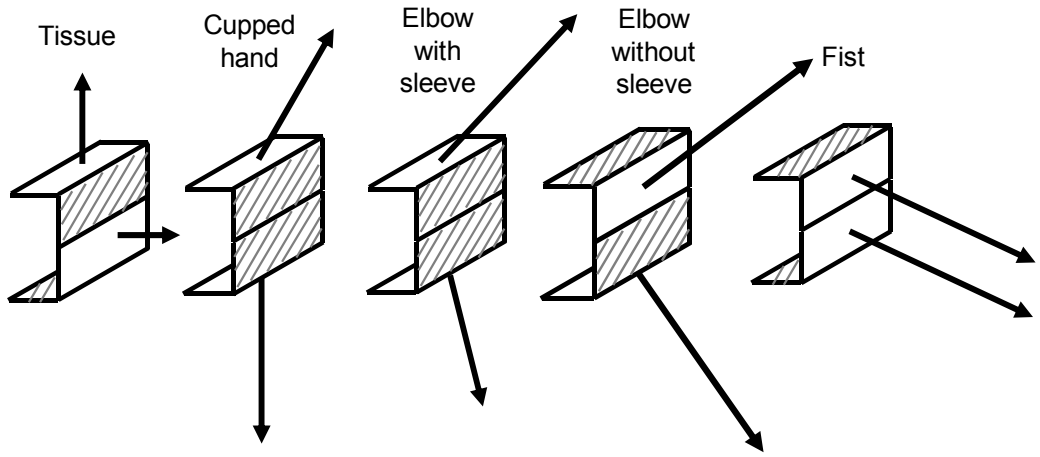

Figure 4-10. Definition methods for different mouth coverings in CFD simulations.

4.3 Model Verification and Case Study

This investigation designed multiple cases and applied the proposed simplified models to calculate the particle concentration distribution as a function of time. The CFD results were then qualitatively compared with the images of smoke flow in order to verify the models to some extent. Finally, this study explored the influence of mouth coverings on the receptor's exposure.

4.3.1 Case Setup and Simulation Models

Figure 4-11 illustrates the configuration of the room used in this study. The room was 3.0 m in length, 3.0 m in width, and 2.3 m in height. There were two persons sitting face to face, with a distance of about 1.0 m between their noses. The person on the left was assumed to be the index person, while the one on the right was the receptor. The index

person was assumed to have a single cough at time zero. The room was ventilated by a mixing ventilation system with an air change rate of 3 ACH. The temperature of the supplied air was 21 ^{o}C, and the surface temperature of the persons was 32 ^{o}C. All the walls were adiabatic.

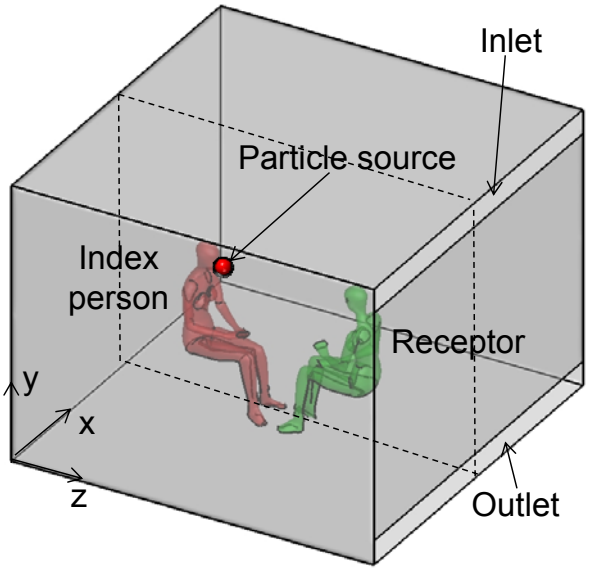

Figure 4-11. Configuration of the room studied in this study.

Eight cases were investigated, including a cough covered by a tissue, a cupped hand, a fist, an elbow with a sleeve, and an elbow without a sleeve, an uncovered cough with average and maximum velocity and a hypothetical release of particles with zero velocity. The total particle emission rates were exactly the same for all cases. This study assumed a constant exhaled velocity for a cough. The constant velocity was assumed to be the peak velocity. The cough duration was set at 0.15 s so that the cough expired volume matches with the measurement data by Gupta et al. (2009). A particle size of 1.0 μm was assumed in order to represent fine particles. The densities of particles were assumed to be uniform. Obviously, this case is more complicated than the previously discussed validation cases because of the complicated manikin geometry with unstructured tetrahedral grids. This

study used the case to further assess the performance of the Markov chain model in a realistic scenario.

4.3.2 Verification of the Simplified Models

Figure 4-12 provides a qualitative comparison of the CFD simulation results (at 0.05 s) with images of the smoke flows. The experimental images of (a) to (f) depict the coughs with an initial jet velocity and direction that is close to the average values shown in Figure 4-9. The experimental image of (g) depicts an uncovered cough with an initial jet velocity that is the maximum of the initial jet velocities of all uncovered coughs. The proposed simplified models can predict the general trend of exhaled airflow reasonably well. For instance, the models predicted the relatively weak jet generated by a cough covered by a tissue. For a cough covered by a cupped hand and an elbow, the model correctly predicted an upward and a downward jet. Furthermore, the model reflects the fact that covering a cough with an elbow with a sleeve can redirect the airflow more significantly than an elbow without a sleeve. In addition, the predicted horizontal jet from a cough covered by a fist was the strongest jet from coughs with the various mouth covering methods.

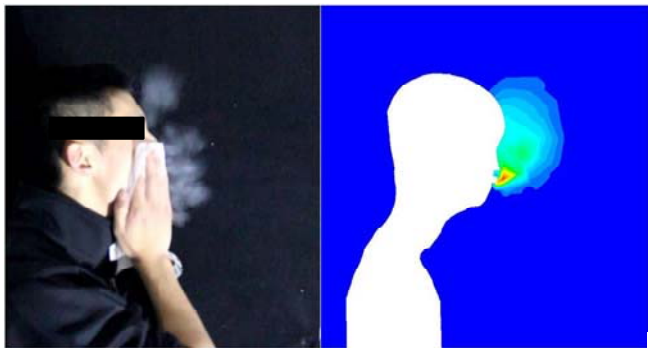

(a)

Figure 4-12. Qualitative comparison of airflow in experimental images and as depicted by simplified models, from coughs covered by (a) a tissue, (b) a cupped hand, (c) an elbow with a sleeve, (d) an elbow without a sleeve, and (e) a fist; and uncovered coughs with (f) average velocity and (g) maximum velocity.

(b)

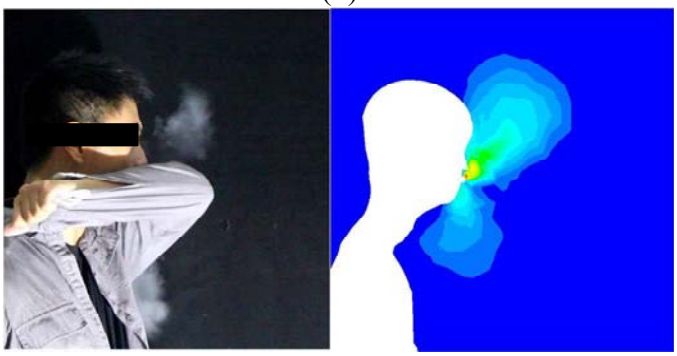

(c)

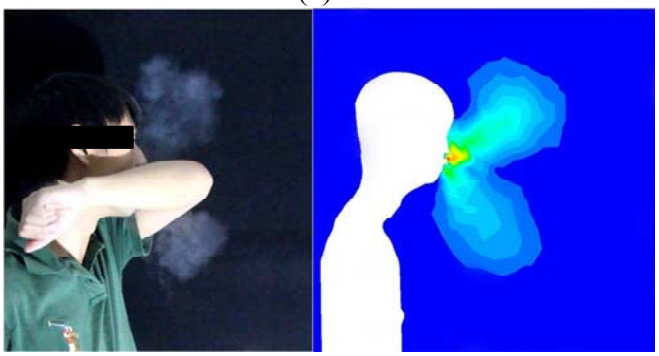

(d)

(e)

Figure 4-12. continued.

(f)

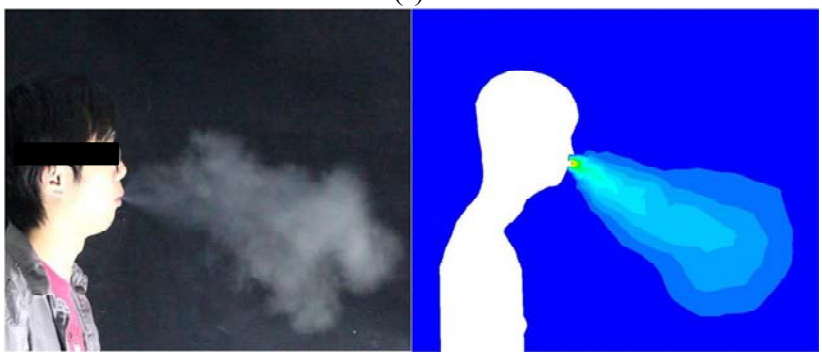

(g)

Figure 4-12. continued.

The comparison showed that the CFD simulation results agreed well with the experimental observations. Thus, these simplified models can be used to predict the airflow from a cough with the mouth covered.

4.3.3 Influence of Mouth Coverings on Receptor's Exposure

The background airflow distribution predicted by CFD simulation shows that there was no strong advective airflow moving from the index person to the receptor. This feature allows us to examine the influence of a cough and mouth coverings on receptor's exposure with minimized impact of background advective airflow. The particle concentration distribution at t = 5.0 s is shown in Figure 4-13 for each of the eight cases. For a hypothetical release of particles with zero velocity and for coughs covered by a tissue, a cupped hand, and an elbow, the exhaled particles moved upward with the thermal plumes generated by human bodies. For these cases, the horizontal transport

distances of the particles at this moment were less than 0.5 m. For a cough covered by a fist and an uncovered cough with an average velocity, the particles penetrated the thermal plumes and moved forward to some extent. The horizontal transport distance of the particles for covering by a fist was about 0.7 m. For an uncovered cough with a maximum velocity, the particles directly entered the breathing zone of the receptor, i.e. the horizontal transport distance of the particles was at least 1.0 m. The results indicate that the mouth coverings, with the exception of the fist, can significantly reduce the horizontal air velocity and cause the particles to move upward with the thermal plumes. Furthermore, when the horizontal air velocity is sufficiently high, or the person-to-person distance sufficiently small, the particles can directly enter the breathing zone of the receptor and result in serious exposure.

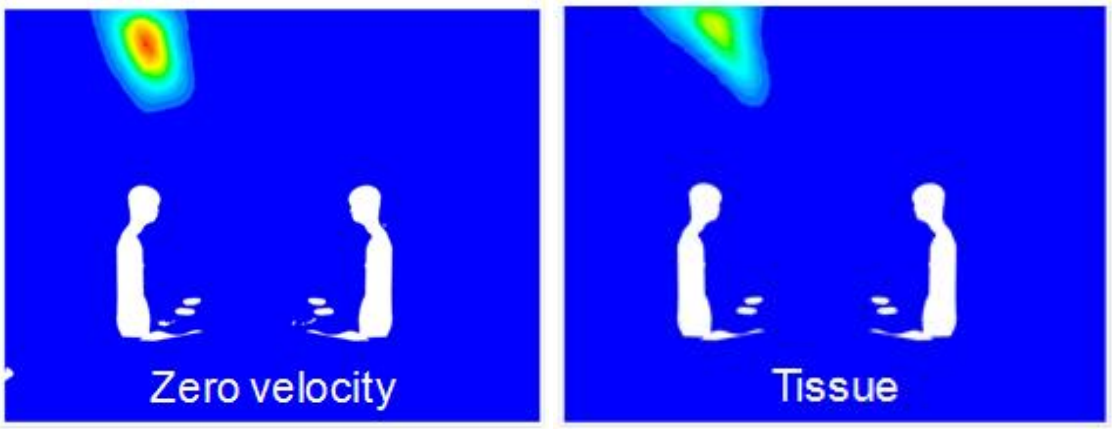

(a) (b)

Figure 4-13. Comparison of particle concentration distributions at 5.0 s for (a) a hypothetical release of particles with zero velocity; coughs covered by (b) a tissue, (c) a cupped hand, (d) an elbow with a sleeve, (e) an elbow without a sleeve, and (f) a fist; and uncovered coughs with (g) average velocity and (h) maximum velocity.

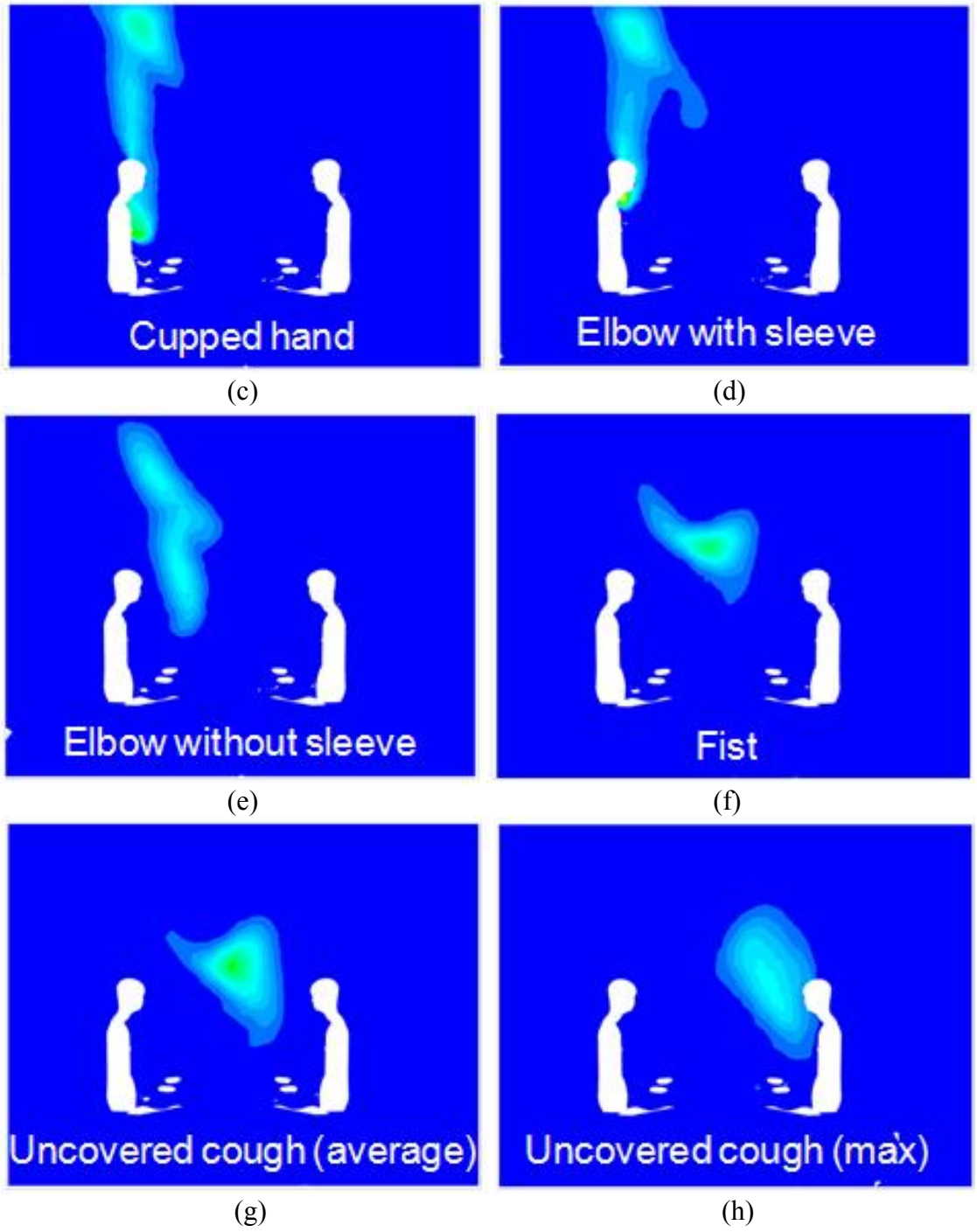

Figure 4-13. continued.

Figure 4-14 compares the normalized particle concentration as a function of time in the breathing zone of the receptor for the eight cases. The particle concentrations were

normalized by the maximum concentration observed in the breathing zone of the receptor among all the cases. For uncovered coughs, the exhaled particles directly entered the breathing zone of the receptor. The receptor also experienced indirect exposure because the particles dispersed throughout the room and again reached the receptor. However, if the mouth was covered, the receptor experienced only indirect exposure.

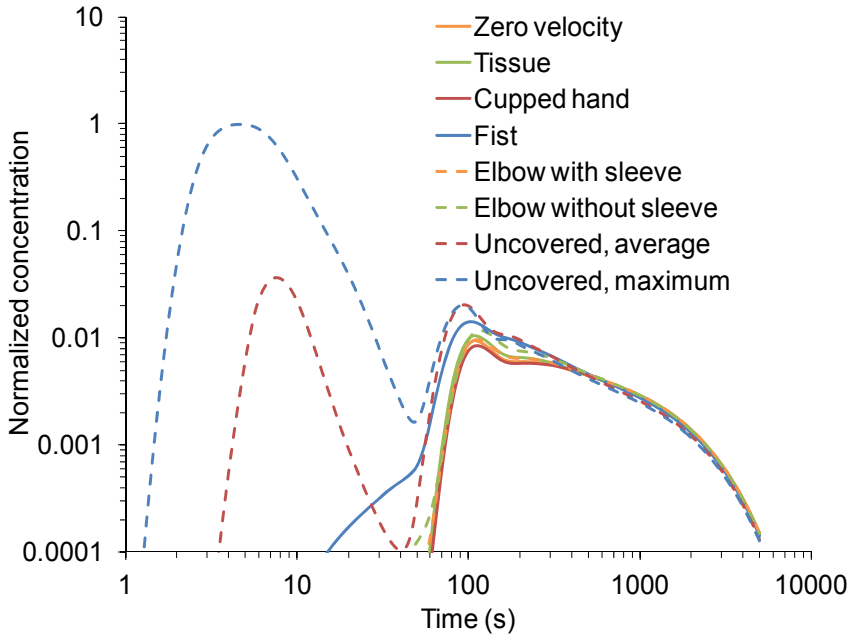

Figure 4-14. Comparison of particle concentration as a function of time in the breathing zone of the receptor for the eight cases.

As compared with the particle concentration as a function of time, the total exposure of the receptor may be more important for estimating the risk of infection. This study calculated the inhaled dose, ID, by

$$ID = \int_{t=0}^{t'} C(t)dt \cdot q \tag{4.2}$$

where C(t) is the particle concentration in the breathing zone of the receptor, t is the time, q is the breathing flow rate which was set at 0.00053 m^3/s, which corresponds to the ISO standard for an adult 1.88 m tall with a mass of 85 kg engaged in moderate work (ISO, 2007). The inhaled dose was further separated into direct exposure from 0 to 50 s and indirect exposure from 50 to 5000 s, as shown in Figure 4-15. All the inhaled doses were normalized by the total inhaled dose for an uncovered cough with maximum velocity. The results show that, for an uncovered cough with maximum velocity, direct exposure was 44.7% of the total exposure. However, if the mouth was covered, no direct exposure was observed. Thus, covering a cough can eliminate approximately 45% of the total exposure as compared with an uncovered cough with maximum velocity. Note that this percentage did not include the particles that were removed from the mouth covering. The removal of particles by the mouth covering will be discussed in section 4.4. Interestingly, the indirect exposure for all the cases was similar to that of a hypothetical release of particles with zero velocity, which indicates that indirect exposure was determined primarily by the ventilation rather than the cough itself.

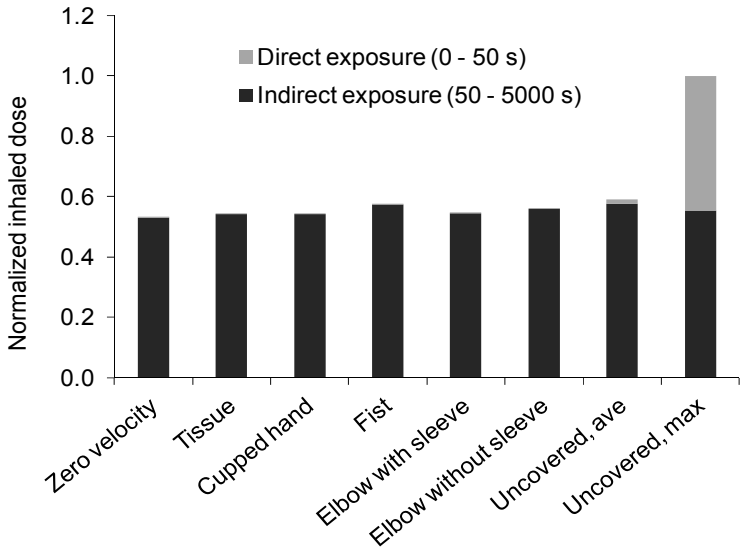

Figure 4-15. Comparison of inhaled dose for the eight cases.

4.3.4 Influence of Turning the Head Away on Receptor's Exposure

The results above demonstrate the benefits of covering a cough. Covering can prevent direct exposure, which suggests that turning the head away may also reduce direct exposure. The person on the left was assumed to have turned her head by 90^{o} when she coughed. Three cases were calculated in which the head was turned away, including an uncovered cough with an average velocity and maximum velocity, and a cough covered by an elbow with a sleeve. Figure 4-16 compares the total exposure when the head was turned away with the total exposure when there were face-to-face uncovered coughs. If the index person turned her head away, the receptor experienced only indirect exposure. Moreover, the total exposure when the head was turned away was similar to that of a hypothetical release of particles with zero velocity. It should be noted that although turning the head away can prevent direct exposure, it cannot remove the coughed particles in the same way that covering a cough can do. Therefore, covering a cough is still a better choice. It is likely that turning the head away while simultaneously covering the mouth is the best way to reduce the risk of infection.

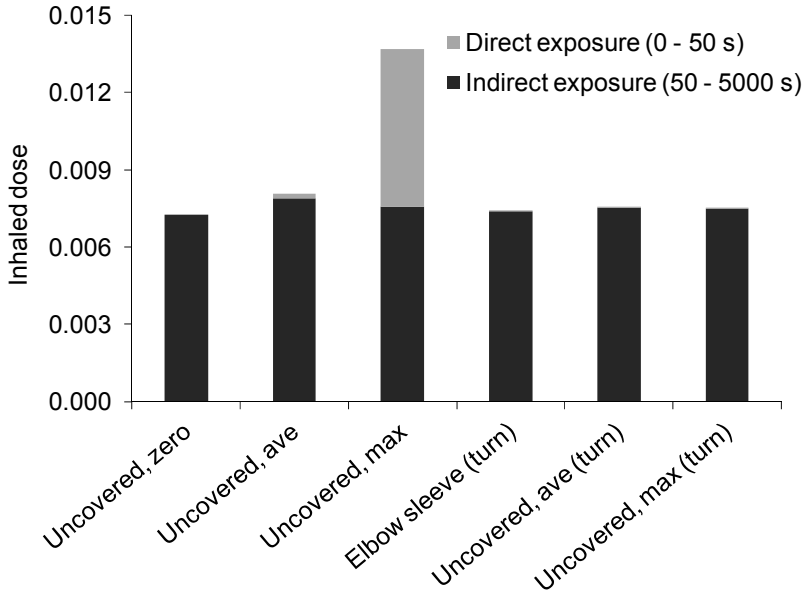

Figure 4-16. Comparison of the inhaled dose when the head was turned away with the inhaled dose when there were face-to-face uncovered coughs.

4.3.5 Possibility in Further Simplifying the Model

The above results show that the total exposures of the mouth covering cases were close to that of the zero momentum case. Thus, it is possible to use the zero momentum assumption for these cases to calculate reasonable results of the total exposure of receptor. Table 4-1 shows the relative errors of using the zero momentum assumption for the mouth covering cases. The relative error was defined by

$$\varepsilon = \frac{\left| ID_{\text{zero}} - ID_{\text{covering}} \right|}{ID_{\text{covering}}} \times 100\% \tag{6.3}$$

where ID_{zero} is the inhaled dose of the zero momentum case and $ID_{covering}$ is the inhaled dose of the mouth covering cases. It was found that the relative errors of using the zero momentum assumption were all below 3% for covering a cough with a tissue, a cupped hand and an elbow with a sleeve. Using the zero momentum assumption for covering a cough with a fist resulted in the largest relative error of 7.9%. It was because the exhaled droplets by a cough with covering a fist penetrated the human thermal plume while the droplets moved upward with the human thermal plume if assuming emission with zero momentum. It should be noticed that the relative errors shown in the table were obtained based on this particular case. Other settings may result in either higher or lower relative errors. In principle, as long as the mouth coverings can make the exhaled droplets move with the human thermal plume, the relative error of using the zero momentum assumption can be minimized.

Table 4-1. Relative errors of using the zero momentum assumption for the mouth covering cases.

Mouth covering approach	Relative error
Tissue	2.4%
Cupped hand	2.1%
Fist	7.9%
Elbow with a sleeve	2.8%
Elbow without a sleeve	5.3%

4.4 Estimating Droplet Removal Achieved by Mouth Covering

Mouth covering not only can re-direct the exhaled airflow but also can remove a portion of the coughed droplets. This section uses theoretical analysis to estimate removal of droplets achieved by a mouth covering.

4.4.1 Original Size Distribution of Coughed Droplets

To estimate the removal efficiency of the total number of droplets or mass droplet concentration by a mouth covering, information about the original size distribution of coughed droplets is required. There have been a number of studies and excellent reviews (Nicas et al., 2005; Morawska, 2006) on the size distribution of coughed droplets. Early studies suggested that the majority of droplets generated through coughs are in the super-micrometer size (Duguid, 1945; Loudon and Roberts, 1967). Chao et al. (2009) also reported that the coughed droplets in close proximity to the mouths are in the super-micrometer size. Yang et al. (2007) reported that droplet size spans from 0.6 to 16 μm, with the average at 8.35 μm during coughing. However, some other studies indicated that the majority of coughed droplets are within the sub-micrometer size range (Papineni and Rosenthal, 1997; Morawska et al., 2009). The discrepancy of these studies on the size distribution of droplets is more because of the instrument and measurement methodology (Chen and Zhao, 2010). Table 4-2 summarizes the representative diameter, concentration, measurement technique and limitations of the previous studies. It can be found that the

studies before 2009 had certain limitations including not considering the effect of evaporation, nucleation and water partitioning onto sample media. Furthermore, when using microscopic technique after collection of droplets on a media, the sub-micrometer droplets cannot be captured. On the other hand, when using modern aerodynamic particle sizers, the accuracy of super-micrometer droplets is a major issue. Considering the measurement accuracy, the size distribution and concentration of sub-micrometer droplets measured by Morawska et al. (2009) tends to be the most reliable. The representative diameter is less than 0.8 μm and the average total number concentration for sub-micrometer droplets is 0.64 cm^{-3}. For super-micrometer droplets, the size distribution measured by Chao et al. (2009) tends to be the most reliable. The results show that the geometric mean diameter of super-micrometer droplets by coughs is 13.5 μm. Although their technique cannot measure the actual concentrations, they roughly estimated the droplet concentration using four different methods based on some unverified assumptions. The first method was to convert the size-dependent droplet numbers measured by Duguid (1946) to the total volume of droplets. Then the total volume of droplets and the size distribution were used to estimate the concentrations. The second method was analogous to the first one but using the data by Loudon and Roberts (1967). The third method was to directly use the total volume of droplets reported by Zhu et al. (2006). The fourth method was to divide the total number of droplets captured by the total laser measurement volume. However, they acknowledged that significant uncertainties existed for all the methods. Figure 4-17 shows the combination of the size distribution obtained by Morawska et al. (2009) and Chao et al. (2009) (the first method in their study) for the entire size range. There are two peaks in the size distribution for the entire size range. The total concentration including sub-micrometer and super-micrometer droplets is 2.91 cm^{-3}. It should be noticed that the considerable uncertainty in the concentration of super-micrometer droplets may lead to significant error of the size distribution for the entire size range.

Table 4-2. Summary of the previous studies on coughed droplets.

Reference	Representative diameter (μm)	Concen. (cm^{-3})	Technique	Limitations
Duguid (1946)	14	5[a]	Count of large droplets using microscopy after collection on a slide	Sampling losses for submicron droplets, evaporation, nucleation, water partitioning NOT considered
Loudon & Roberts (1967)	12	0.47[a]	Count of large droplets using microscopy after collection on a filter	Sampling losses for submicron droplets, evaporation, nucleation, water partitioning NOT considered
Fairchild & Stamper (1987)		0.6	Sample aerosol from a respirator mask using a laser aerosol spectrometer	Sampling losses for submicron droplets, evaporation, nucleation, water partitioning NOT considered
Papineni & Rosenthal (1997)	<0.6	0.024–0.22	A subject coughed into a funnel connected to an OPC[b]	Sampling losses for supermicron droplets, evaporation, nucleation NOT considered
Yang et al. (2007)	8.35	881–2355	Measure size distribution and concentration using APS[c] after collection in an air bag	Sampling losses for supermicron droplets, evaporation, nucleation, water partitioning NOT considered
Chao et al. (2009)	13.5	2.368–5.212[d]	Measure size distribution immediately at mouth opening using IMI[e]	Sampling losses for submicron droplets NOT considered
Morawska et al. (2009)	<0.8	0.64	Measure size distribution and concentration using APS immediately at the mouth opening	Sampling losses for supermicron droplets NOT considered

[a] Assuming the Cough Expired Volume (CEV) to 1.0 L (Gupta et al., 2009)
[b] OPC: Optical Particle Counter
[c] APS: Aerodynamic Particle Sizer
[d] Concentration estimated based on four different methods
[e] IMI: Interferometric Mie Imaging

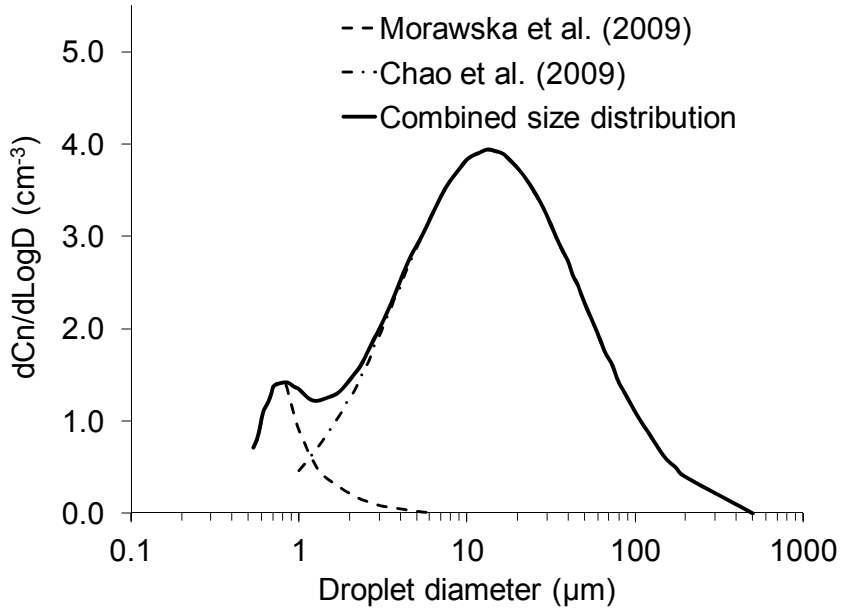

Figure 4-17. Size distribution and concentration of coughed droplets as combined from the data of Morawska et al. (2009) and Chao et al. (2009) (the first data set in their study).

4.4.2 Droplet Removal by Mouth Covering

Droplets can deposit onto the mouth-covering surface by several mechanisms, such as Brownian and turbulent diffusion, gravitational settling, inertial impaction, etc. Lai (2002) reviewed and collected the particle deposition velocities associated with Brownian and turbulent diffusion, gravitational settling, and other mechanisms such as thermopheresis, as measured in indoor environments. The deposition velocity, V_d, has a magnitude in the range of 10^{-6} to 10^{-3} m/s (Lai, 2002). The deposition area, i.e., the surface area of the mouth covering, Ad, has a magnitude of 10^{-2} m^2. Thus, the droplet deposition "flow rate", V_dA_d, has a magnitude in the range of 10^{-8} to 10^{-5} m^3/s. However, the cough airflow rate has a magnitude of 10^{-3} m^3/s (Gupta et al., 2009), which is much larger than the deposition "flow rate." Thus, the droplet deposition due to diffusion and gravitational settling onto the surface of the mouth covering is negligible, and this finding agrees with that of Li et al. (2012).

To determine the droplet deposition due to inertial impaction, this study referred to the impactor theory (Hinds, 1999). Particle removal efficiency is a function of the square root of the Stokes number, as shown in Figure 4-18 (Marple and Liu, 1974).

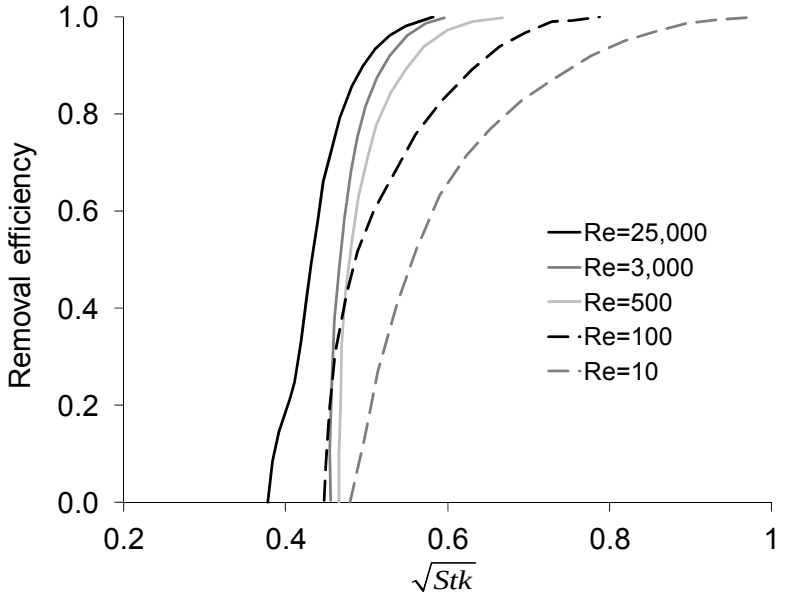

Figure 4-18. Relationship between particle removal efficiency and square root of Stokes number (Marple and Liu, 1974).

The Stokes number is expressed as (Hinds, 1999)

$$Stk = \frac{\rho_p d_p^{\,2} U C_c}{9 \mu h} \tag{6.4}$$

where ρ_p is the particle density, d_p is the particle diameter, U is the air velocity of the cough, μ is the dynamic viscosity of air, h is the height of the mouth opening, and C_c is the Cunningham coefficient caused by slippage. Furthermore, the relationship between particle removal efficiency and the square root of the Stokes number depends on the

Reynolds number. Because the average air velocity of a cough is 11.8 m/s and the height of the mouth opening is about 0.02 m (Gupta et al. 2009), the Reynolds number is equal to 15,051. Thus, the curve for a Reynolds number of 25,000 in Figure 4-18 should be used.

This study also calculated the effect of droplet evaporation. As summarized by Nicas et al. (2005), respiratory droplets are composed of an aqueous solution containing inorganic and organic ions, glycoprotein, and protein, and the equilibrium diameter of a completely evaporated particle (d_{ep}) is related to the initial diameter (d_0) by

$$d_{ep} = 0.44 d_0 \tag{6.5}$$

Figure 4-19 shows the size distribution of coughed droplets at the origin, after they have been removed by the mouth covering, and after evaporation. Droplets with a diameter larger than 10 μm are removed by the mouth covering. However, fine droplets can move with the airflow through the leakage points between the face and mouth covering. After the removal of larger droplets by the mouth covering, the representative diameter drops from 13.5 to 5.4 μm. When the remaining droplets have been completely evaporated, the representative diameter is further reduced to 2.4 μm. It is expected that at this size, droplet nuclei can follow the airflow very closely (Yin et al., 2011). In regard to particle removal efficiency, the mouth covering can remove 64.8% of the total number of coughed droplets. If the droplets are all assumed to be spherical and of the same density, then it can be said that 99.99% of the total mass of coughed droplets is removed by the mouth covering. This is because large droplets tend to contain most of the mass. For the various data sets provided in Chao et al. (2009), the removal efficiency of the total number of coughed droplets varies from 58.6% to 64.8%.

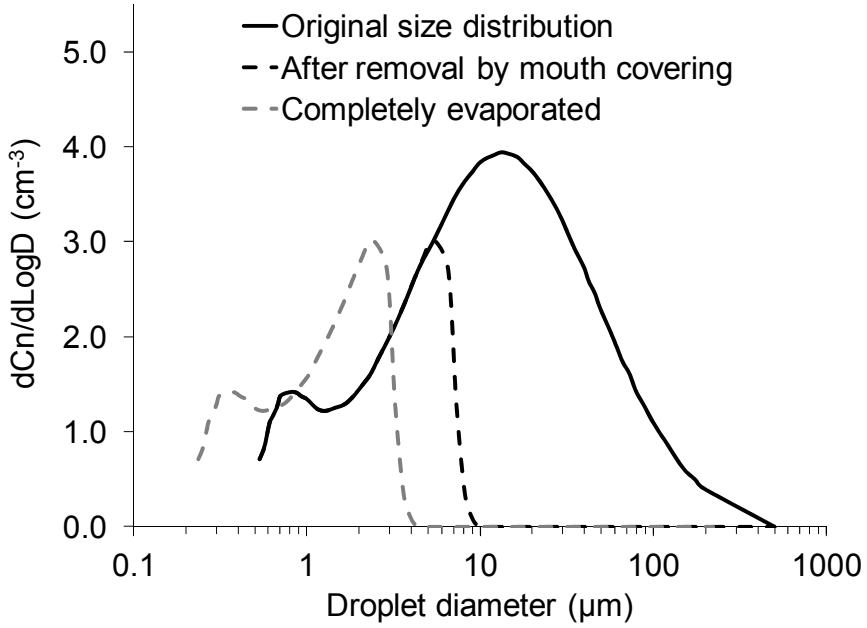

Figure 4-19. Size distributions of coughed droplets at the original site, after removal of large droplets by a mouth covering, and after evaporation.

4.5 Discussion

There are a number of limitations to the present study, beginning with the use of smokers as human subjects. Smokers may suffer from chronic obstructive pulmonary disease (COPD) so that their respiratory patterns may be different from non-smokers (Decramer et al., 2012). Typically, a smoker may generate a larger volume of cough air than a non-smoker (Tang et al., 2012). Therefore, this study recruited "healthy" smokers who reported no COPD in their consent forms to minimize this influence, although the experimental results may still be somewhat biased. Another limitation was that only 1 female subject was recruited in this study due to the difficulty of finding female smokers. Thus, the proposed models should work better for males than females. To avoid the influence of smokers as human subjects, Tang and colleagues proposed to use the real-time schlieren and shadowgraph imaging method to visualize the exhaled airflow (Tang and Settles, 2009; Tang et al., 2008; 2009; 2011; 2012). This method does not require the introduction of visualization media such as tobacco smoke. Furthermore, as shown in

Tang et al. (2008, 2009), this method can obtain instantaneous velocity vectors of a cough. Thus, it is hoped that this investigation will encourage the researchers who have access to the schlieren and shadowgraph imaging systems to develop similar models as presented in this study based on the advanced experimental technique.

This study developed the simplified models based on the average values of initial jet velocity and direction. As shown in Figure 9, the initial jet velocity and direction can vary significantly among subjects. Thus, the proposed simplified models predict the general patterns of airflow from a cough with the mouth covered, other than the pattern for a particular person. Furthermore, this study limited the models to two dimensions since the exhaled airflow visualized from the front view was much more limited than from the side view. This assumption may result in a certain error since there might be some small airflow in the third direction. Moreover, this study did not consider the effect of the speed with which the user can put their hands/tissues into effective position to cover the cough. It was reported that this factor could significantly affect the effectiveness of covering a cough (Tang et al., 2011). In addition, the movement of the head when coughing may also affect the airflow movement (Tang et al., 2011), which was not included in the present analysis. Furthermore, mouth covering not only can re-direct the exhaled airflow but also can remove a portion of the coughed droplets, which deserves further study.

When estimating the removal of droplets by the mouth covering, this study assumed that some of the droplets were first removed, and then the size of the rest of the droplets decreased because of evaporation. However, these two processes may occur simultaneously. That is to say, it is possible that a droplet is evaporating when it is removed by the mouth covering, or even a droplet is completed evaporated before it is removed. Therefore, to better estimate the removal and size distribution change of the droplets, the time scale of the droplet removal by the mouth covering and the droplet evaporation should be further considered.

4.6 Conclusions

This chapter used smoke to visualize the airflow exhaled by a cough from 16 human subjects with covered mouths. On the basis of the smoke data, simplified models were developed for predicting airflow. Finally, the effects of a mouth covering on the receptor's exposure were discussed. Within the scope of this research, the following conclusions can be drawn:

(1) The proposed simplified models can be used to predict the airflow from a cough when the mouth is covered, which make the simulation of person-to-person particle transport more realistic.

(2) Covering a cough with a tissue, a cupped hand, or an elbow can significantly reduce the horizontal velocity and cause the exhaled particles to move upward with the thermal plumes generated by human bodies.

(3) Covering a cough or turning the head away can prevent the receptor's direct exposure.

CHAPTER 5. ACCELERATING THE LAGRANGIAN MODEL

The Lagrangian model calculates the trajectories of individual particles on the basis of Newton's law. The discrete random walk (DRW) model is typically used to calculate the turbulence dispersion. Statistically speaking, a large number of particles are needed in the calculations in order to ensure accuracy. Traditionally, modelers have conducted an independence test in order to find a reasonable value for this particle number. However, the unguided process of an independence test can be highly time-consuming when no simple method is available for estimating the necessary particle number. Furthermore, the computing cost of the Lagrangian method is positively associated with the particle number in the calculation. If this number is very large, the computing cost may not be affordable. Therefore, this chapter aims to develop a method for estimating and reducing the necessary particle number, in order to accelerate the Lagrangian method for modeling transient particle transport in indoor environments.

5.1 Methods for Accelerating the Lagrangian Model

5.1.1 Estimating the Necessary Particle Number

When performing Lagrangian particle tracking, the number of particles injected from the source is one of the inputs. This section proposes a method for estimating the necessary particle number in the Lagrangian method that can provide statistically meaningful results.

For the purpose of estimating the necessary particle number, this study assumed a well-mixed condition in the indoor environments that were studied. The particle mass balance equation is:

$$\frac{dC(t)}{dt} = -\frac{Q}{V_{\text{room}}}C(t) + \frac{Q}{V_{\text{room}}}C_{\text{in}}(t) + \frac{S(t)}{V_{\text{room}}} \tag{5.1}$$

where C(t) and $C_{in}(t)$ are the particle number concentration in the room and at the inlet, respectively, t is the time, Q is the airflow rate from the inlet, S(t) is the particle emission rate from an indoor source, and V_{room} is the volume of the room. With a certain boundary condition, Eq. (5.1) can be easily solved either analytically or numerically.

To demonstrate the method, this study used an example in which particles are emitted from the inlet over duration of t_s. The boundary condition can be expressed as:

$$C_{\text{in}}(t) = \begin{cases} \dfrac{N}{Q \cdot t_s} & 0 \le t \le t_s \\ 0 & t > t_s \end{cases} \quad \text{and} \quad S(t) = 0 \tag{5.2}$$

where N is the total number of particles emitted from the inlet. The goal of this section is to estimate the lower bound of this N, i.e., the necessary particle number, N_{nec}. Solving Eq. (5.1) with this boundary condition, the particle number concentration as a function of time is:

$$C(t) = \begin{cases} \dfrac{N}{Q \cdot t_s}\left(1 - \exp\left(-\dfrac{Q}{V_{\text{room}}}t\right)\right) & 0 \le t \le t_s \\ C(t_s)\exp\left(-\dfrac{Q}{V_{\text{room}}}(t - t_s)\right) & t > t_s \end{cases} \tag{5.3}$$

The peak particle concentration over time, $C(t)_{max}$, is:

$$C(t)_{\max} = \frac{N}{Q \cdot t_s}(1 - \exp(-\frac{Q}{V_{\text{room}}} t_s)) \tag{5.4}$$

To obtain statistically meaningful results for particle concentrations in a target zone, the particle number in this zone for Lagrangian tracking should be sufficiently large. Considering a target zone with a volume of V_{target}, the particle number in this target zone is:

$$N_{\text{target}}(t) = C(t) \cdot V_{\text{target}} \tag{5.5}$$

The peak particle number over time in this zone, $N_{target}(t)_{max}$, is:

$$N_{\text{target}}(t)_{\max} = C(t)_{\max} \cdot V_{\text{target}} \tag{5.6}$$

Assuming that the necessary particle number in the target zone is N_{target}^{*}, then,

$$N_{\text{target}}(t) \geq N_{\text{target}}^{*} \tag{5.7}$$

so that the particle number in this zone at every time point is statistically sufficient. According to the law of large numbers, the greater the number of particle samples used, the closer the estimate will be to the true value (Durrett, 2010). Therefore, theoretically, there is no cut-off value for N_{target}^{*}. However, in real-life applications, a sample size of 30

is normally large enough for a statistical analysis (Student, 1908). This is because the t-distribution becomes a close fit for the normal distribution when the number of samples reaches 30 (Student, 1908). Thus, N_{target}^{*} can be set at 30.

However, for a transient particle transport case, theoretically, Eq. (5.7) may not hold at every time point. For instance, $N_{target}(t)$ would approach zero as the time approaches infinity, causing Eq. (5.7) to become problematic. Therefore, to make the method workable for engineering applications, Eq. (5.7) is replaced by:

$$\alpha \cdot N_{\text{target}}(t)_{\max} \geq N_{\text{target}}^{*} \tag{5.8}$$

where α is a coefficient ranging from 0% to 100%. According to Eq. (5.8), if this α is equal to 1%, the results will be statistically meaningful even when the particle concentration has decreased to 1% of the peak value ($N_{target}(t)_{max}$). Therefore, the value of α depends on the tolerance of error.

When Eqs. (5.4), (5.6), and (5.8) are solved together, the following equation is obtained:

$$N \geq \frac{\frac{t_s}{\tau} V_{\text{room}}}{\alpha(1-\exp(-\frac{t_s}{\tau}))V_{\text{target}}} N_{\text{target}}^{*} \tag{5.9}$$

where τ is the time constant of the room:

$$\tau = \frac{V_{\text{room}}}{Q} \tag{5.10}$$

Therefore, the necessary number of particles injected from the source for Lagrangian tracking, i.e., the lower bound of N, is:

$$N_{nec} = \frac{\frac{t_s}{\tau} V_{\text{room}}}{\alpha(1-\exp(-\frac{t_s}{\tau}))V_{\text{target}}} N_{\text{target}}^{*} \tag{5.11}$$

Note that Eq. (5.11) was derived under the assumption of a well-mixed condition. If the room is ventilated with a displacement ventilation system, there will be a negative particle concentration gradient along the vertical axis. In that case, the proposed method may underestimate the necessary particle number when the target zone is located in the lower part of the room. Even if the room is ventilated with a mixing ventilation system, the particle concentration distribution may not be uniform. In that case, the proposed method may underestimate the necessary particle number when the particle concentration in the target zone is lower than the average level. Therefore, it is important to note that the proposed method can only estimate a reasonable magnitude of the necessary particle number instead of determining a precise value.

5.1.2 Reducing the Necessary Particle Number

5.1.2.1 Superimposition Method

The superimposition method has been successfully used to convert the transient particle concentration distributions from a single pulsed source to one from multiple pulsed sources (Gupta et al., 2011b). Eq. (5.11) shows that the necessary particle number can be reduced as the duration of particle emission is shortened. It implies that the superimposition method has the potential to reduce the necessary particle number. Instead of injecting particles in each time step, the superimposition method injects particles only

in one time step. Then, the transient particle transport from this single pulsed source is calculated with Lagrangian particle tracking. Finally, by superimposing the calculated particle concentrations with a time shift, the total particle concentration can be calculated by:

$$C(t) = \sum_{for\ all\ i} C_{\text{single}}(t - t_i) \tag{5.12}$$

where $C_{single}(t\text{-}t_i)$ is the particle concentration at time $t\text{-}t_i$ as a result of emission from the single pulsed source that started at time t_i. With the superimposition method, only the calculation of particle transport from a single pulsed source is needed for Lagrangian particle tracking. Therefore, the necessary particle number is:

$$N_{nec,\text{sup}} = \frac{\frac{\Delta t}{\tau} V_{\text{room}}}{\alpha(1 - \exp(-\frac{\Delta t}{\tau}))V_{\text{target}}} N_{\text{target}}^{*} \tag{5.13}$$

where Δt is the time step size. Normally, the time step size is much smaller than time constant of the room, τ. Therefore, one can take the Taylor expansion for the exponent in Eq. (5.13) and keep only the first term, and Eq. (5.13) becomes:

$$N_{nec,\text{sup}} = \frac{V_{\text{room}}}{\alpha \cdot V_{\text{target}}} N_{\text{target}}^{*} \tag{5.14}$$

Compared with the pure Lagrangian method, the combined Lagrangian and superimposition method can reduce the necessary particle number by a factor of:

$$\frac{N_{\text{nec}}}{N_{\text{nec,sup}}} = \frac{\frac{t_s}{\tau}}{1-\exp(-\frac{t_s}{\tau})} \tag{5.15}$$

5.1.2.2 Time-Averaging Method

This method performs time-averaging of the particle concentrations within certain time steps. If the number of particles tracked in a time step is N', then the total number of particles tracked in n time steps is N'×n. Therefore, theoretically, if time-averaging is performed over every n time steps, the necessary particle number can be reduced by n times.

However, if the particle number in the calculation is too small, it is possible that no particles will be tracked in the target zone. Therefore, at least one particle should be tracked in this zone; i.e., the N_{target}^{*} in Eq. (5.11) should be at least 1. When $N_{target}^{*} = 1$, Eq. (5.11) becomes:

$$N_{\text{nec,sup+time-ave}} = \frac{V_{\text{room}}}{\alpha \cdot V_{\text{target}}} \tag{5.16}$$

Compared with the pure Lagrangian method, the combined Lagrangian and time-averaging method can reduce the necessary particle number by a factor of:

$$\frac{N_{\text{nec}}}{N_{\text{nec,time-ave}}} = N_{\text{target}}^{*} \tag{5.17}$$

when time-averaging is performed taken over every N_{target}^{*} time steps.

5.1.2.3 Combined Superimposition and Time-Averaging Method

To further reduce the particle number in the Lagrangian tracking calculation, one can use both the superimposition and time-averaging methods. When using only the superimposition method, the necessary particle number can be calculated by Eq. (5.14). If the time-averaging method is then used for every N_{target}^{*} time steps, the particle number can be further reduced by a factor of N_{target}^{*}. Therefore, the necessary particle number when both methods are used can be calculated by:

$$N_{\text{nec,sup+time-ave}} = \frac{V_{\text{room}}}{\alpha \cdot V_{\text{target}}} \tag{5.18}$$

Therefore, compared with the pure Lagrangian method, the combined Lagrangian, superimposition, and time-averaging method can reduce the necessary particle number by a factor of:

$$\frac{N_{\text{nec}}}{N_{\text{nec,sup+time-ave}}} = \frac{\frac{t_s}{\tau}}{1-\exp(-\frac{t_s}{\tau})} N_{\text{target}}^{*} \tag{5.19}$$

5.2 Verification and Validation of the Proposed Methods

5.2.1 Case Description

This investigation used the case of transient particle transport in an isothermal ventilated chamber (Zhang et al., 2009) to verify the proposed methods. Figure 5-1 shows the

configuration of the chamber with spatial dimensions of 4 m in length, 2.1 m in width, and 2.4 m in height. The size of both the supply inlet and exhaust was 0.3 m × 0.3 m. The supply inlet was located 0.3 m from the ceiling, while the exhaust was located 0.3 m from the floor. The averaged supply-air velocity magnitude and turbulence intensity were 0.84 m/s and 20%, respectively. The incident angle of the supply air was 10° downward. Particles with a size of 1 μm were injected through the inlet into the chamber. Transient particle concentrations were measured at two locations on a vertical line in the z-directional center-cutting plane and 1 m away from the inlet. The measurement locations, Point 1 and Point 2, were 1.8 and 0.9 m from the floor, respectively. In the experiment, two optical particle counters were used to measure the transient particle concentrations at the inlet and one of the measurement locations (Point 1 and Point 2) simultaneously. Therefore, the experiment was conducted twice in order to obtain the results at the two locations. The two profiles exhibit similar trends, but there are some differences. In general, at the inlet, there was an initial peak in particle concentration, and then the concentration decreased significantly to a stable level.

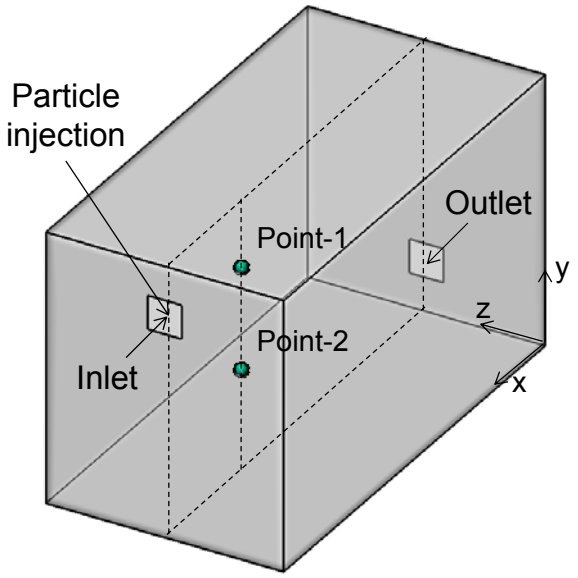

Figure 5-1. Configuration of the chamber studied by Zhang et al. (2009).

Numerical simulations were performed using ANSYS Fluent 12.1 (ANSYS, 2010). Three grid resolutions (4,934, 18,009, and 134,090) were tested for CFD grid independence. The resolution of 18,009 was sufficiently fine to capture the turbulent flow in the chamber. The time step was set at 0.05 s. An independence test regarding the time step size was conducted to ensure that 0.05 s was small enough to obtain accurate results. Particle deposition, resuspension, and droplet evaporation are negligible at a particle size of 1 μm (Zhao et al., 2009, Zhu et al., 2012, Chen and Zhao, 2010).

5.2.2 Verification of the Method for Estimating the Necessary Particle Number

This study designed three cases to verify the method for estimating the necessary particle number in the Lagrangian method (Eq. (5.11)), as listed in Table 5-1. The target zone in Cases 1 and 3 was the breathing zone, while that in Case 2 was the whole room. The center of the breathing zone was Point 2. The volume of the breathing zone was set at 0.027 m^3 (OSHA, 2014). The duration of the particle source in Cases 1 and 2 was one time step (Δt), i.e., a pulsed source, while the duration in Case 3 was equal to the time constant of the room (τ). The airflow rate (Q) was 0.074 m^3/s, the volume of the room (Vroom) was 20.2 m^3, the necessary particle number in the target zone (N_{target}^*) was set at 30 (Student, 1908), and the coefficient (α), which depends on the tolerance of error, was set at 1%. A sensitivity analysis of the coefficient (α) is discussed in Section 5.3.1. The values of these parameters were the same for all the cases discussed in this paper.

Table 5-1. Cases designed to verify the method of estimating the necessary particle number.

Case No.	Target zone	Volume of target zone (m^3)	Characteristics of source duration	Duration of particle source(s)	Calculated necessary particle number (millions)
1	breathing zone	0.027	Δt	0.05	2.24
2	whole room	20.2	Δt	0.05	0.003
3	breathing zone	0.027	τ	273	3.55

This study conducted particle number independence tests for the designed cases to determine whether or not the calculated particle numbers were sufficient for obtaining statistically meaningful results. The necessary particle numbers calculated by Eq. (5.11) were 2.24, 0.003, and 3.55 million, respectively, for Cases 1, 2, and 3. This study used the Lagrangian method with the calculated particle number to predict the particle concentration as a function of time in the target zone. To conduct the particle number independence tests, this study repeated the simulations with a particle number that was increased by a factor of 10. Figure 5-2 compares the normalized particle concentrations predicted from the calculated particle number with those predicted from particle number that is 10 times larger. All the particle concentrations were normalized by the total particle number injected in the room. For all three cases, the Lagrangian method with the calculated particle number provided similar results to those with a 10-times-larger particle number. Therefore, the proposed method can provide a necessary particle number with a reasonable magnitude. This method avoids the unguided process of the particle number independence test and thus significantly accelerates the entire calculation process.

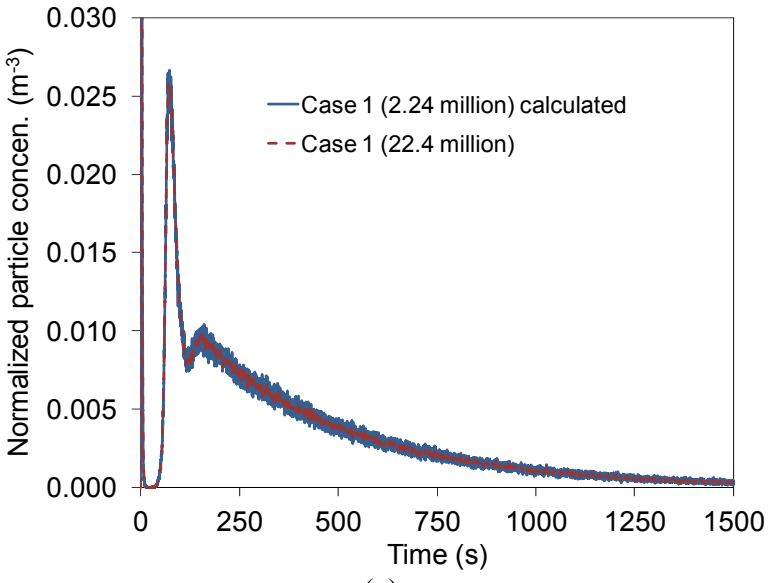

(a)

Figure 5-2. Particle number independence tests for (a) Case 1, (b) Case 2, and (c) Case 3.

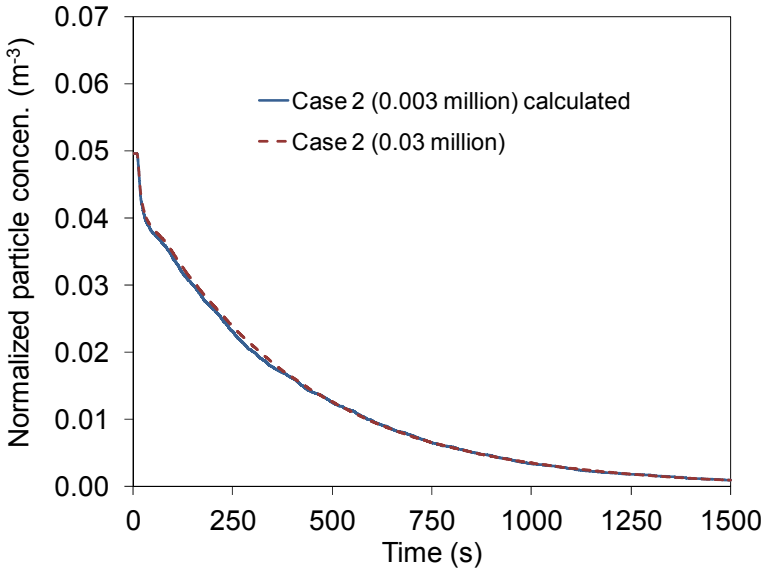

(b)

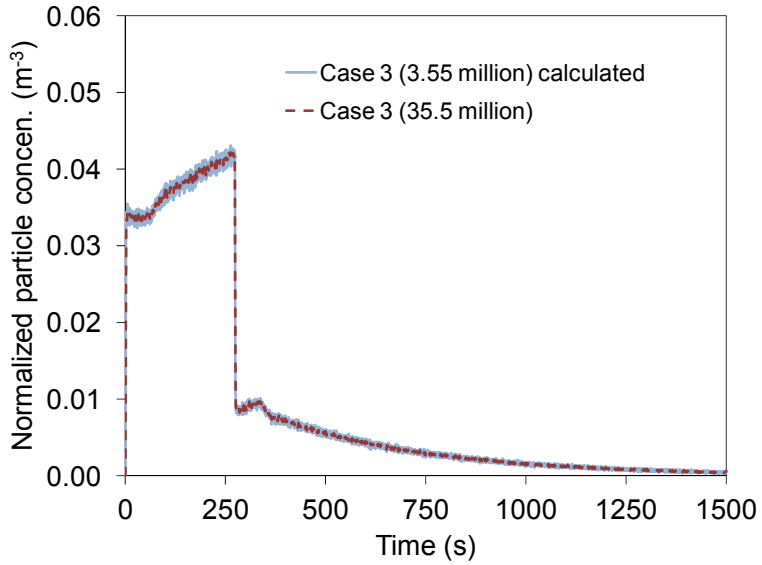

(c)

Figure 5-2. continued.

5.2.3 Verification of the Method for Reducing the Necessary Particle Number

5.2.3.1 Superimposition Method

This study compared the normalized particle concentrations predicted by the combined Lagrangian and superimposition method and the pure Lagrangian method for Case 3. The

necessary particle number for the pure Lagrangian method calculated by Eq. (5.11) was 3.55 million, while that for the combined method calculated by Eq. (5.14) was 2.24 million. As shown in Figure 5-3, the particle concentrations predicted by the combined Lagrangian and superimposition method agreed well with that predicted by the pure Lagrangian method. However, the necessary particle number in the combined method (2.24 million) was reduced by 1.6 times in comparison with that in the pure Lagrangian method (3.55 million).

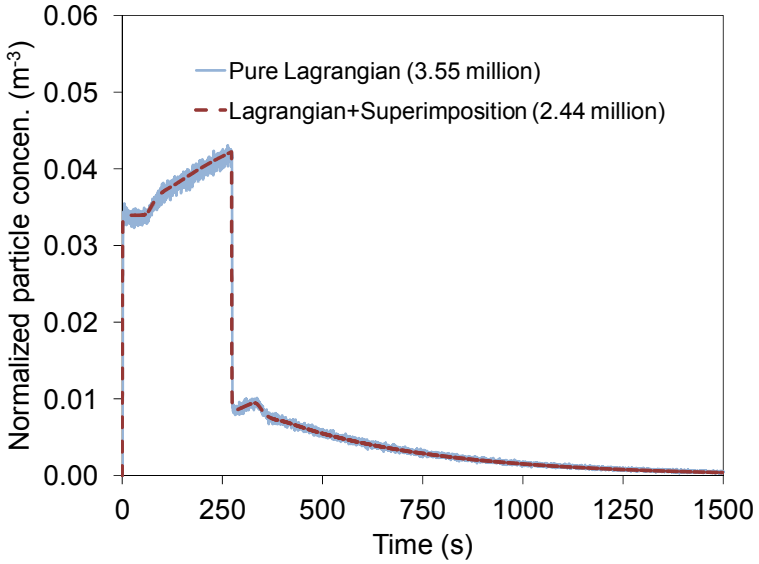

Figure 5-3. Comparison of normalized particle concentrations predicted by the combined Lagrangian and superimposition method and the pure Lagrangian method.

Eq. (5.15) indicates that the reduction in particle number when using the superimposition method depends on the duration of the particle source. Figure 5-4 shows the factor of reduction in particle number when using the superimposition method as a function of source duration (Eq. (5.15)). The factor of reduction in particle number is positively associated with the particle source duration. For example, if the duration was 0.1τ, the necessary particle number could be reduced only slightly when using the superimposition method. However, if the duration was increased to 5τ, the necessary particle number

could be reduced by five times when using the superimposition method. Therefore, the superimposition method can reduce the necessary particle number in the Lagrangian method when the particle source duration is relatively long.

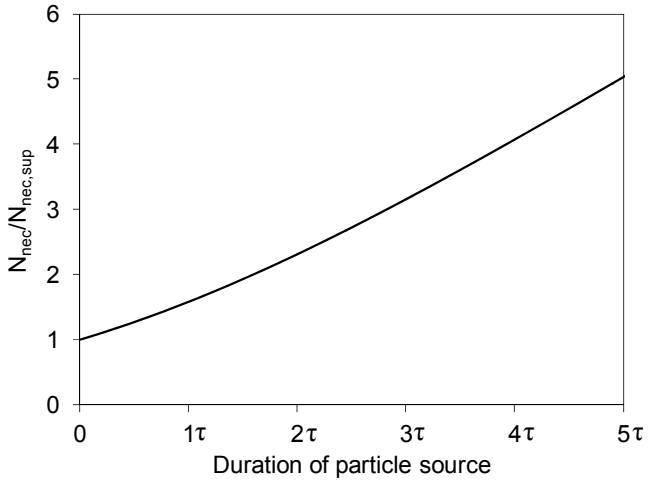

Figure 5-4. Factor of reduction in particle number as a function of particle source duration when the superimposition method is used.

5.2.3.2 Time-Averaging Method

This study compared the normalized particle concentrations predicted by the combined Lagrangian and time-averaging method and the pure Lagrangian method for Cases 1 and 3. The necessary particle numbers in the pure Lagrangian method calculated by Eq. (5.11) were 2.24 million for Case 1 and 3.55 million for Case 3. In comparison, the necessary particle numbers in the combined method calculated by Eq. (5.16) for Cases 1 and 3 were 0.074 and 0.12 million, respectively. As discussed in Section 5.1.2.2, time-averaging can be performed over every $N_{target}^{*} = 30$ time steps.

As shown in Figure 5-5, the particle concentrations predicted by the two methods agreed well with each other for both cases. Furthermore, the necessary particle number in the combined method was reduced by 30 times as compared with that in the pure Lagrangian

method. Thus, the hypothesis that the time-averaging method can reduce the necessary particle number has been verified. It should be noted that the number of time steps to be averaged depends on the level of detail required in the results. For instance, if the calculated particle concentration as a function of time with a time step size of 0.05 s is to be compared with experimental data with a measurement time interval of 0.5 s, time-averaging over more than 10 time steps is not suitable. Furthermore, the particle concentrations may vary significantly in certain time steps. To ensure that the peak particle concentrations are captured, the time-averaging method should not be used in such time steps.

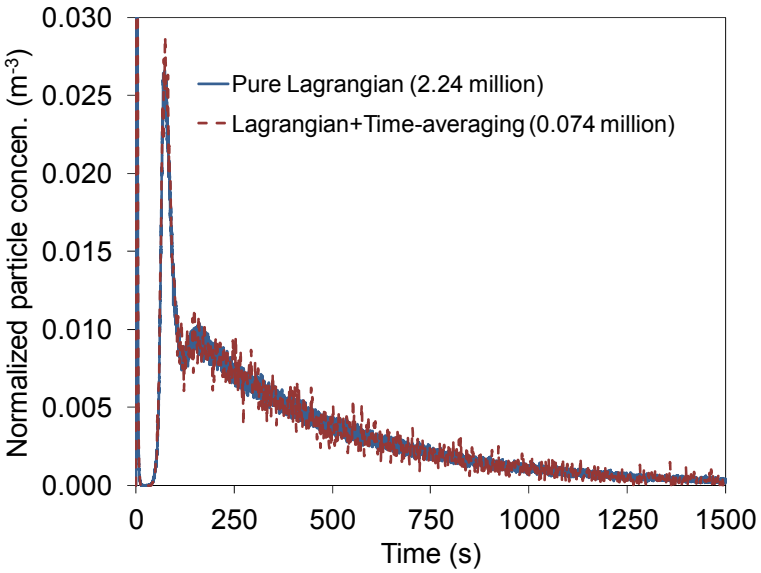

(a)

Figure 5-5. Comparison of normalized particle concentrations predicted by the combined Lagrangian and time-averaging method and the pure Lagrangian method for (a) Case 1 and (b) Case 3.

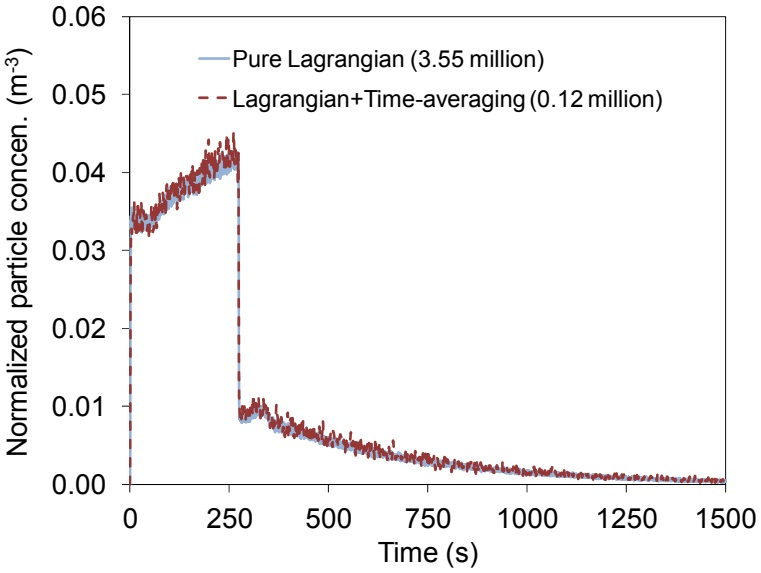

(b)

Figure 5-5. continued.

5.2.3.3 Combined Superimposition and Time-Averaging Method

This study further compared the normalized particle concentrations predicted by the combined Lagrangian, superimposition, and time-averaging method and the pure Lagrangian method for Case 3. The calculated necessary particle number for the pure Lagrangian method was 3.55 million according to Eq. (5.11), while that for the combined method was 0.074 million according to Eq. (5.18). As shown in Figure 5-6, the particle concentration profiles predicted by the two methods matched well with each other. Furthermore, the necessary particle number in the combined method was reduced by 48 times as compared with that in the pure Lagrangian method. Therefore, this comparison verifies that the combined method can further reduce the necessary particle number in the Lagrangian method.

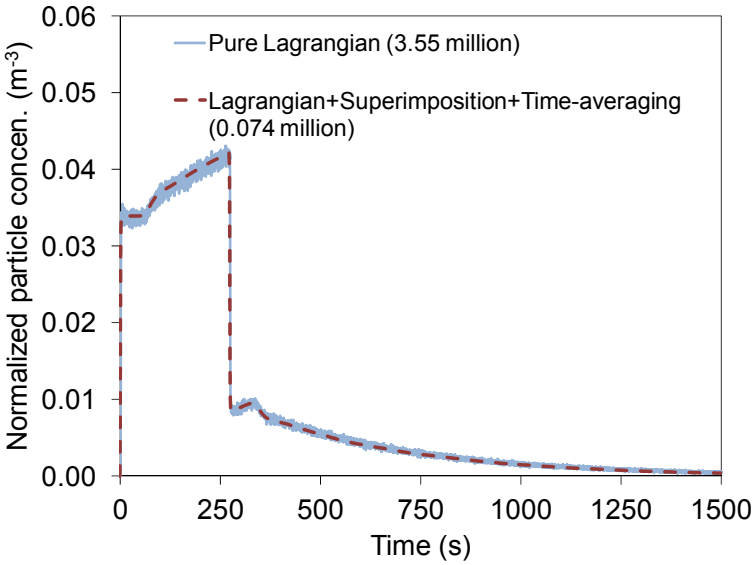

Figure 5-6. Comparison of normalized particle concentrations predicted by the combined Lagrangian, superimposition, and time-averaging method and the pure Lagrangian method.

As indicated in Eq. (5.19), the reduction in particle number when using the combined method increases as the particle source duration becomes longer. For instance, if the duration of the particle source was 0.1τ, the necessary particle number in the combined method would be reduced by 30 times as compared with that in the pure Lagrangian method. If the duration was increased to 5τ, the combined Lagrangian, superimposition, and time-averaging method would reduce the necessary particle number by 150 times compared with that in the pure Lagrangian method.

5.2.3.4 Comparison of Computing Cost

Table 5-2 compares the computing time of the pure Lagrangian method and the combined methods. The computing time was estimated on a single core computer with two 3.2 GHz Intel(R) Xeon(R) processors and 12 GB of memory. For Case 1, the combined Lagrangian and time-averaging method can reduce the computing time by 30 times when compared with the pure Lagrangian method. For Case 3, the combined Lagrangian,

superimposition, and time-averaging method can reduce the computing time by 40 times when compared with the pure Lagrangian method. Therefore, the proposed method can significantly save the computing resources.

Table 5-2. Comparison of computing cost.

Case No.	Pure Lagrangian	Lagrangian + Superimposition	Lagrangian + Time-averaging	Lagrangian + Superimposition + Time-averaging
	Computing time (hour) *			
1	48.9	N/A	1.6	N/A
3	64.8	48.9	2.2	1.6

* The computing time was estimated on a single core computer, with two 3.2 GHz Intel(R) Xeon(R) processors and 12 GB of memory.

5.2.4 Validation with Experimental Data

5.2.4.1 Particle Transport in an Isothermal Ventilated Chamber

This study first used the experimental data obtained by Zhang et al. (2009) to validate the proposed methods for predicting transient particle transport in indoor environments. This case was the same as the previous cases in all aspects except the boundary condition at the inlet. In the experiment, two optical particle counters were used to measure the transient particle concentrations at the inlet and one of the measurement locations (Point 1 and Point 2) simultaneously. Therefore, the experiment was conducted twice in order to obtain the results at the two locations. The inlet particle concentration profiles at Points 1 and 2 are shown in Figure 5-7(a) and 5-7(b), respectively. The two profiles exhibit similar trends, but there are some differences. In general, at the inlet, there was an initial peak in particle concentration, and then the concentration decreased significantly to a stable level.

With the grid resolution (18,009) used in this study, the volume of the CFD cell at Points 1 and 2 was 0.0012 m^3. The calculated necessary particle number in the combined Lagrangian, superimposition, and time-averaging method was 1.72 million on the basis of the proposed method. The time step size in the simulation was 0.05 s. Figure 5-7 compares the numerical results for transient particle concentration with the experimental data. Note that two sets of simulations were performed on the basis of the corresponding inlet particle concentration profiles.

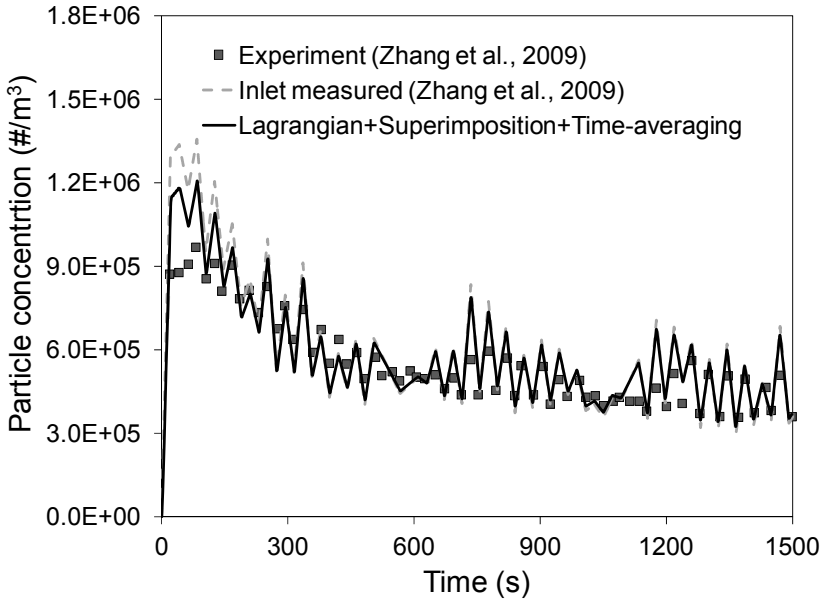

(a)

Figure 5-7. Comparison of the numerical results for transient particle concentration with the corresponding experimental data: (a) Point 1 and (b) Point 2.

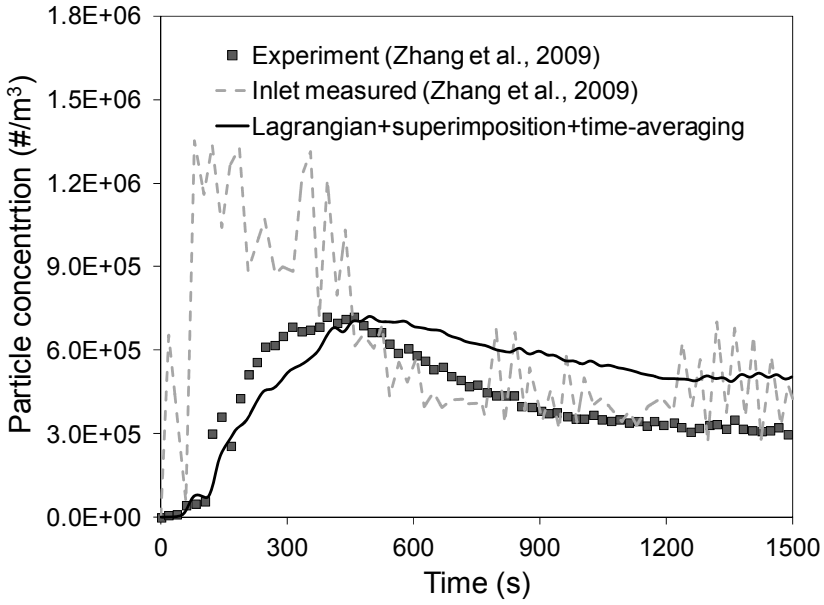

(b)

Figure 5-7. continued.

In Figure 5-7(a), the simulation and the experiment at Point 1 both show particle concentration profiles that are similar to that at the inlet. This similarity occurred because Point 1 was close to the inlet. The fluctuations in particle concentration at this location were caused primarily by the fluctuations measured at the inlet. In Figure 5-7(b), both the simulation and the experiment at Point 2 exhibit peak particle concentrations that are lower than that at the inlet. Moreover, the peak at Point 2 is delayed in time compared with that at the inlet. This delay indicates a weaker response to the source because of a greater distance between the source and Point 2. In comparison with the experimental data, the proposed method overestimated the particle concentrations after about 500 s. Zhang et al. (2009) compared the results predicted by an Eulerian method with experimental data. They also found that the Eulerian method overestimated the particle concentrations after about 500 s. The differences between the simulation and the experiment may be attributed to the discrepancies between the predicted airflow field and the actual one (Zhang et al., 2009). In general, the trends in transient particle concentration predicted by the combined Lagrangian, superimposition, and time-averaging method agreed reasonably well with the experimental data. Therefore, the

proposed method can be used for predicting transient particle transport in indoor environments with reasonable accuracy.

5.2.4.2 Particle Transport in an Aircraft Cabin

This study then used the experimental data of transient particle transport in the first-class cabin of the MD-82 aircraft to further validate the proposed combined Lagrangian, superimposition, and time-averaging method. According to the proposed method, the necessary particle number injected from the source was 1.76 million. Figure 5-8 compares the transient particle distributions predicted by the combined method with the corresponding experimental data.

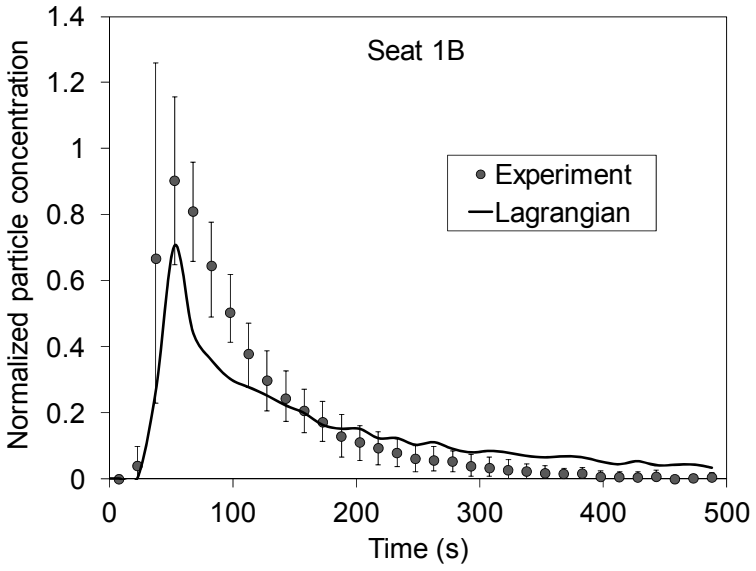

(a)

Figure 5-8. Comparison of the numerical results of transient particle concentrations predicted by combined Lagrangian, superimposition, and time-averaging method with the corresponding experimental data at seats: (a) 1B, (b) 1C, (c) 2B, and (d) 3B..

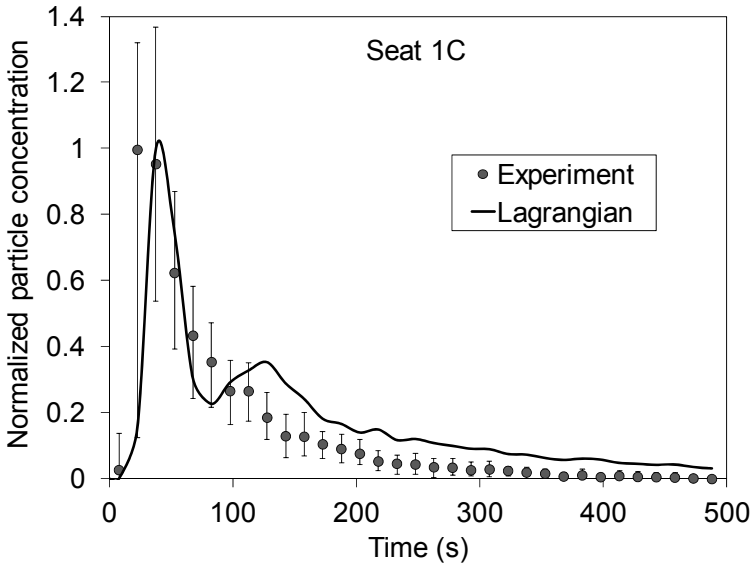

(b)

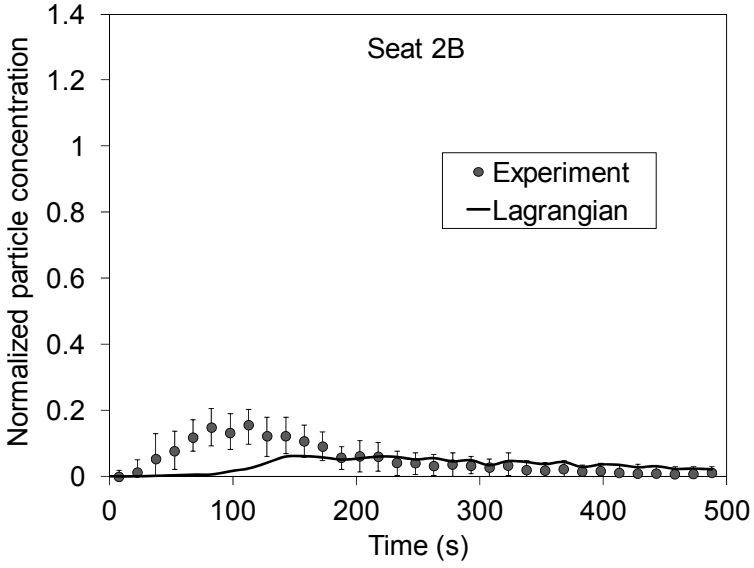

(c)

Figure 5-8. continued.

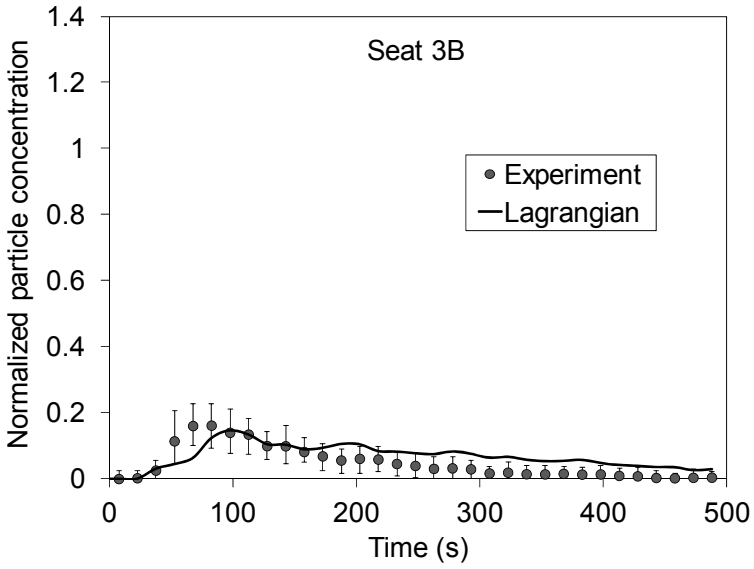

(d)

Figure 5-8. continued.

As shown in Chapter 3, the particle concentrations at Seat 1B, 1C were relatively high, while that at the other seats were relatively low. Figures 5-8(a) and 5-8(b) shows that the combined method accurately predicted relatively high peak concentrations at Seats 1B and 1C when compared with the experimental data. For the other seats where the concentrations were relatively low, only the comparison results at Seats 2B and 3B are shown here in Figures 5-8(c) and 5-8(d) to keep the main body of thesis concise. Seat 3B was a representative location where the agreement between simulation and experiment was very good, while Seat 2B was a representative location where the agreement was worse. Generally speaking, the proposed method can predict the general trends of person-to-person particle transport in the aircraft cabin with reasonable accuracy. The validation cases have demonstrated that the proposed method can estimate the necessary particle number and thus reduce the effort that is normally required for evaluating different numbers of particles in order to achieve statistically meaningful results.

5.3 Discussion

5.3.1 Influence of the Coefficient α

The coefficient α in Eq. (5.11) can influence the calculated necessary particle number in the Lagrangian tracking calculations. If this α is equal to 1%, the results will be statistically meaningful even when the particle concentration has decreased to 1% of the peak value. Therefore, the value of α depends on the tolerance of error. This study conducted a sensitivity analysis of α for Case 1. Figure 5-9 compares the normalized particle concentrations predicted by the Lagrangian method with particle numbers that were estimated using α values of 1%, 10%, and 100%. The corresponding calculated necessary particle numbers were 2.24, 0.224, and 0.0224 million, respectively. It can be seen that a smaller α provides better results, with fewer fluctuations and uncertainties. Theoretically, there is no cut-off value for α. For engineering applications, as shown in the figure, an α value of around 1% should minimize fluctuations and uncertainties in the results.

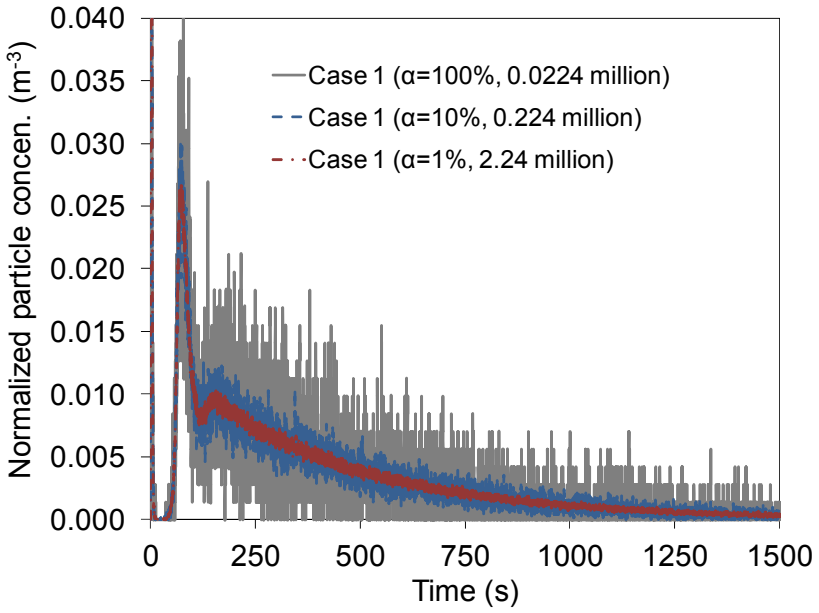

Figure 5-9. Comparison of normalized particle concentrations predicted by the Lagrangian method with particle numbers that were estimated using α values of 1%, 10%, and 100%.

5.3.2 Equations for Other Particle Sources

In order to demonstrate the proposed methods, the analysis above used an example in which particles were emitted from the inlet. Another typical scenario is the emission of particles from a location inside the room, such as from the cough of an occupant. In this case, the boundary condition of Eq. (5.1) is:

$$S(t)=\begin{cases}\dfrac{N}{t_s} & 0\le t\le t_s\\ 0 & t>t_s\end{cases} \quad \text{and} \quad C_{in}(t)=0 \tag{5.20}$$

Using the approach described in Section 5.1.1, the equation for calculating the necessary particle number can be obtained. One finds that the equation for a particle source inside the room is identical to that for a particle source from the inlet (Eq. (5.11)).

For some particle sources, Eq. (5.1) cannot be solved analytically with the corresponding boundary condition. One such case is that studied by Zhang et al. (2009), as described in Section 5.2.4. In this case, the inlet particle concentrations were time-varying, as shown in Figure 4-7. The study solved the equation numerically for this case by simply using Microsoft Excel. Therefore, even if the equation cannot be solved analytically, the proposed methods can be used to accelerate the Lagrangian method by numerically solving the ordinary differential equation.

5.3.3 Limitations

There are a number of limitations to the present work, beginning with the assumption of a steady-state airflow field, which may be a problem in some cases. For instance, transient particle transport in a building with natural ventilation is likely to have an unsteady-state airflow field. In such cases, the time-averaging method can still be used; however, the

superimposition method may not be suitable. In addition, this study neglected particle deposition onto surfaces because the modeled particle size was 1 μm. However, for ultrafine or coarse particles in a room with a low air change rate, the impact of particle deposition may be considerable. Therefore, to model the transient transport of ultrafine or coarse particles, the influence of deposition should be taken into account. Although the transient airflow and particle deposition could affect the necessary particle number in the Lagrangian method, it should be noted that the proposed method is to estimate a reasonable magnitude of the necessary particle number rather than determining a precise value. Therefore, the proposed method can still be used for these scenarios.

5.4 Conclusions

This chapter developed a method for estimating and reducing the necessary particle number in order to accelerate the Lagrangian method for predicting transient particle transport in indoor environments. The investigation has led to the following conclusions:

(1) The proposed method can estimate the necessary particle number and thus reduce the effort that is normally required for evaluating different numbers of particles in order to achieve statistically meaningful results.

(2) The superimposition and time-averaging method can reduce the necessary particle number, and, as a result, the computing cost can be further reduced.

(3) The combined Lagrangian, superimposition, and time-averaging method can predict transient particle transport in indoor environments with reasonable accuracy.

CHAPTER 6. DEVELOPING A MARKOV CHAIN MODEL

Both the Eulerian and Lagrangian models can provide detailed information about transient particle concentration distributions. However, even with the Eulerian method, the unsteady-state calculation with iterations in each time step is considerably time-consuming. Several studies have demonstrated the ability of the Markov chain technique to quickly predict spatial and temporal particle concentrations. However, these models can only work for an extremely coarse grid. Therefore, a new model that not only works on a fine grid, as do the Eulerian and Lagrangian methods, but also runs faster than these two methods, is desirable. This chapter aims to develop a Markov chain model, which is much faster than the traditional models, for predicting detailed transient particle concentration distributions in enclosed environments.

6.1 Model Development

6.1.1 Markov Chain Model for Transient Particle Transport

This study used the first-order homogeneous Markov chain technique (Ross, 1996) to calculate transient particle transport. This Markov chain technique is effective for particles with a diameter smaller than 3 μm, which have negligible inertial effects (Chen et al., 2012). Assuming that the CFD grid has n-1 cells, the additional cell n can be assigned to represent the space to which the particles are removed. Then the probabilities of the state's changing of a particle can form an n×n transition probability matrix, p_{ij}:

$$P = (p_{i,j})_{(n\times n)} = \begin{pmatrix} p_{1,1} & p_{1,2} & \cdots & p_{1,n} \\ p_{2,1} & p_{2,2} & \cdots & p_{2,n} \\ \vdots & \vdots & & \vdots \\ p_{n,1} & p_{n,2} & \cdots & p_{n,n} \end{pmatrix} \tag{6.1}$$

where $p_{i,j}$ is the probability of a particle's moving from cell i to cell j in a certain time step, Δt. The transition probability matrix has the following property:

$$\sum_{j=1}^{n} p_{i,j} = 1 \quad , \quad p_{i,j} \geq 0 \tag{6.2}$$

This property can be regarded as the constraint of mass balance for the whole domain. Since the movement of the particles normally does not have a major impact on the airflow field, the transition probability matrix is fixed.

The particle number vector at the present time (state k) is assumed to be:

$$N_k = \begin{pmatrix} N_{k,1} & N_{k,2} & \cdots & N_{k,n} \end{pmatrix} \tag{6.3}$$

where $N_{k,i}$ represents the number of particles in cell i at time k. Then, after one time step (time k+1), the number of particles in cell i can be calculated by:

$$N_{k+1,i} = N_{k,1} p_{1,i} + N_{k,2} p_{2,i} + \cdots + N_{k,n} p_{n,i} \tag{6.4}$$

Thus, the particle number vector at time k+1 can be calculated by:

$$N_{k+1} = N_k P \tag{6.5}$$

If one calculates the particle transport from time zero, the particle number vector at time k can be calculated by:

$$N_k = N_{\text{int}} P^k \tag{6.6}$$

where N_{int} is the initial particle number vector. The particle number concentration in cell i at time k can be calculated by:

$$C_{k,i} = \frac{N_{k,i}}{V_i} \tag{6.7}$$

where V_i is the volume of the cell.

The transition probability matrix can require a considerably large storage memory for a normal CFD grid. To reduce the size of the matrix, Eq. (6.4) was rewritten as:

$$N_{k+1,i} = N_{k,i} p_{i,i} + \sum_{nb} N_{k,nb} p_{nb,i} \tag{6.8}$$

where the subscript nb represents the neighboring cells or boundaries. Eq. (6.8) shows that the Markov chain model does not require iterations in each time step. Therefore, this model has the potential to reduce the computing cost.

6.1.2 Transition Probabilities

The key operation in applying the Markov chain technique to the calculation of transient particle transport is to obtain the transition probabilities, p_{ij}. Again, p_{ij} is the probability of a particle's moving from cell i to cell j in a certain time step, Δt. The first step is to calculate the probability of a particle's remaining in the current cell in Δt, p_{ii}. It is assumed that there are N_0 particles present in cell i at time zero and that these particles can be removed only by the flow of air. The particle mass balance equation for this cell is (Nicas, 2000):

$$\frac{dN(t)}{dt} = -\frac{N(t)}{V_i}\sum_{nb} Q_{i,nb} \tag{6.9}$$

where $Q_{i,nb}$ is the airflow rate from cell i to the neighboring cell. Solving Eq. (6.9) leads to the following equation (Nicas, 2000):

$$N(\Delta t) = N_0 \exp(-\sum_{nb}\frac{Q_{i,nb}}{V_i}\Delta t) \tag{6.10}$$

Therefore, after a certain time step, Δt, $N(\Delta t)$ particles remain in this cell. Thus, the probability of a particle's remaining in the current cell in Δt can be expressed as (Nicas, 2000):

$$p_{i,i} = \exp(-\sum_{nb}\frac{Q_{i,nb}}{V_i}\Delta t) \tag{6.11}$$

If cell j is one of the neighboring cells, the probability of a particle's moving from cell i to cell j in Δt can be calculated by (Nicas, 2000):

$$p_{i,j} = \frac{Q_{i,j}}{\sum_{nb} Q_{i,nb}}(1 - p_{i,i}) \tag{6.12}$$

where $Q_{i,nb}$ consists of the mean airflow rate ($Q_{mean,i,nb}$) and the turbulent fluctuating airflow rate ($Q_{fluctuating,i,nb}$) from cell i to the neighboring cell:

$$Q_{i,nb} = Q_{mean,i,nb} + Q_{fluctuating,i,nb} \tag{6.13}$$

The mean airflow rate from cell i to the neighboring cell can be obtained from the CFD simulation results. The turbulent fluctuating airflow rate from cell i to the neighboring cell is determined on the basis of the discrete random walk (DRW) model (ANSYS, 2010). The turbulent fluctuating velocity in cell i can be calculated by:

$$u'_i = \xi\sqrt{2k_i / 3} \tag{6.14}$$

where ξ is a standard normal random number and k_i is the turbulent kinetic energy in cell i. This study estimated the turbulent fluctuating airflow rate from cell i to the neighboring cell as:

$$Q_{fluctuating,i,nb} = \alpha_{i,nb}\sqrt{2k_i / 3} \cdot A_{i,nb} \tag{6.15}$$

where $A_{i,nb}$ is the area of the connecting face between cell i and the neighboring cell The coefficient $\alpha_{i,nb}$ is calculated by:

$$\alpha_{i,nb} = 2 \cdot (1 - \Phi(\frac{\Delta s_{i,nb} / \Delta t}{\sqrt{2k_i / 3}})) \tag{6.16}$$

where $\Delta s_{i,nb}$ is the distance between the centroid of cell i and that of the neighboring cell. The function $\Phi()$ is the cumulative distribution function for a standard normal distribution:

$$\Phi(x) = \frac{1}{2}(1 + erf(\frac{x}{\sqrt{2}})) \tag{6.17}$$

where erf() is the error function. The coefficient $\alpha_{i,nb}$ considers the effects of the distance between the cell centroids and the time step on the turbulent dispersion of particles. For instance, when the distance between the cell centroids, $\Delta s_{i,nb}$, is extremely small, its effect is negligible, and the coefficient $\alpha_{i,nb}$ should be equal to 1. However, when the distance between the cell centroids is extremely large, a particle originally at the center of the cell has almost no chance of moving to the neighboring cell in one time step, and the coefficient should be equal to 0.

This investigation used the CFD code ANSYS Fluent 12.1 (ANSYS, 2010) to calculate the airflow field. A user-defined function (UDF) was implemented in order to realize the Markov chain model.

6.2 Validation of the Markov Chain Model

This investigation used two cases, transient particle transport in an isothermal ventilated chamber (Zhang et al., 2009) and a chamber with displacement ventilation (Bolster and Linden, 2009), to validate the Markov chain model. This section discusses the validation results.

6.2.1 Particle Transport in an Isothermal Ventilated Chamber

The first study was the case of transient particle transport in an isothermal ventilated chamber as addressed by Zhang et al. (2009). The configuration of the chamber is shown in Figure 5-1. The spatial dimensions were 4 m in length, 2.1 m in width, and 2.4 m in height. The size of both the supply inlet and exhaust was 0.3 m × 0.3 m. The supply inlet was located 0.3 m from the ceiling, while the exhaust was located 0.3 m from the floor. The averaged supply-air velocity magnitude and turbulence intensity were 0.84 m/s and 20%, respectively. The incident angle of the supply air was 10° downward. Particles with a size of 1 μm were injected through the inlet into the chamber. Transient particle concentrations were measured at two locations on a vertical line in the z-directional center-cutting plane and 1 m away from the inlet. The measurement locations were 0.9 and 1.8 m from the floor. Two optical particle counters were used to measure the transient particle concentrations at the inlet and one of the measurement locations simultaneously. Therefore, the experiment was conducted twice in order to obtain the results at the two locations.

Note that the current Markov chain model can only calculate transient particle transport from a pulse source. However, the measurement results show that there was an initial peak in the particle concentration, and then the concentration decreased significantly to a stable level. Thus, this study first divided the inlet concentration into various pulse sources with duration of one time step (Δt). The Markov chain model was then used to calculate the transient particle concentrations from a pulse source, C_{MC}, with an inlet

particle number concentration of 1 per m^3. The total particle concentration can be calculated using the superimposition method (Gupta et al., 2011):

$$C(t) = C(m \cdot \Delta t) = \sum_{n=0}^{m} C_{in}(n \cdot \Delta t) \cdot C_{MC}((m - n + 1) \cdot \Delta t) \tag{6.18}$$

where Δt is the time step, m is the number of calculation steps, $C_{in}(n \cdot \Delta t)$ is the inlet particle concentration at time $n \cdot \Delta t$, and $C_{MC}((m\text{-}n+1) \cdot \Delta t)$ is the particle concentration from a pulse source with an inlet particle number concentration of 1 per m^3 at time $(m\text{-}n+1) \cdot \Delta t$.

Three grid resolutions (4,934, 18,009, and 134,090) were tested for CFD grid independence. The resolution of 18,009 was sufficiently fine to capture the turbulent flow in the chamber. The time step size was set at 0.01 s. The independence test showed that this time step size was sufficiently fine to capture the transient features. Particle deposition and resuspension are negligible at a particle size of 1 μm (Zhao et al., 2009, Zhu et al., 2012). Figure 6-1 compares the numerical results for transient particle concentration with the experimental data. Note that two sets of simulations were performed on the basis of the corresponding inlet particle concentrations, as shown in Figure 5 of Zhang et al. (2009). In Figure 6-1(a), both the Markov chain model and the experimental data exhibit an initial peak in particle concentration. In Figure 6-1(b), the model and the experimental data both display smaller peaks in particle concentration than those in Figure 6-1(a). Furthermore, the Markov chain model can capture the fact that the peak at this location was delayed in time. In general, the trends in transient particle transport predicted by the Markov chain model agree well with the experimental data.

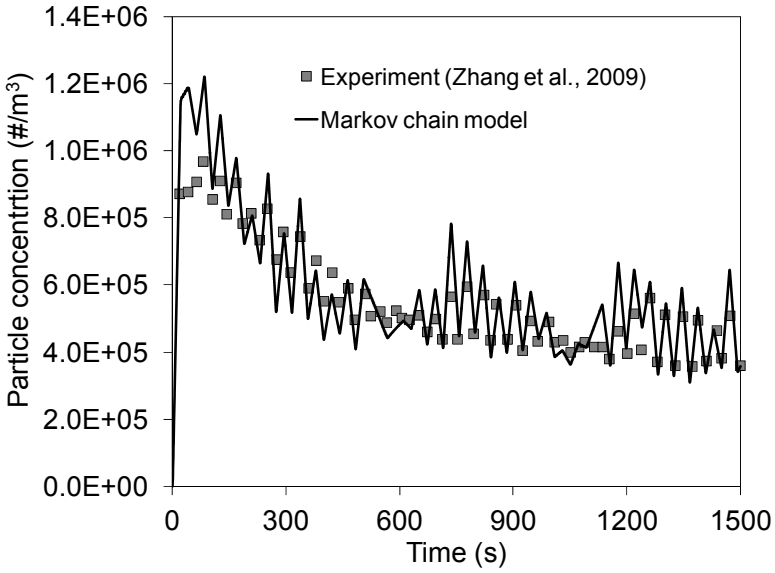

(a)

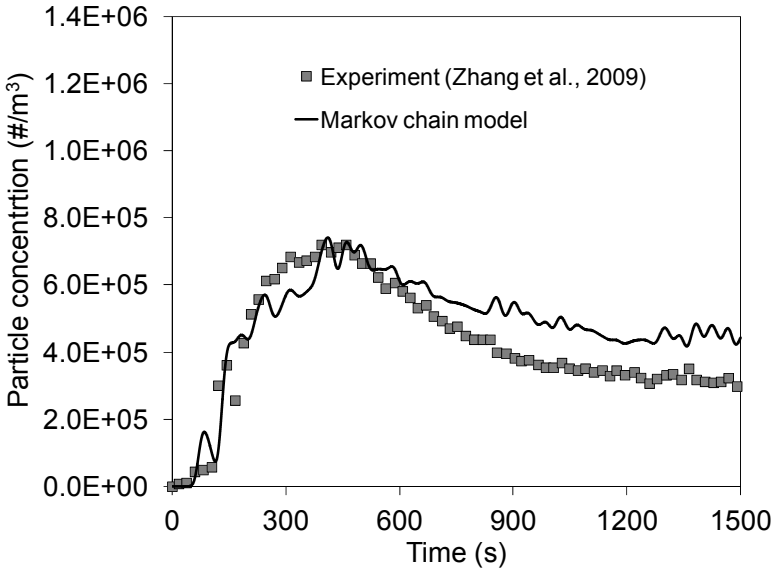

(b)

Figure 6-1. Comparison of the numerical results for transient particle concentration with the corresponding experimental data: (a) y = 1.8 m, (b) y = 0.9 m.

6.2.2 Particle Transport in a Chamber with Displacement Ventilation

The second case was a chamber with displacement ventilation, as shown in Figure 6-2 and used by Bolster and Linden (2009) for measuring transient particle transport. The

chamber had dimensions of 2.6 m in length, 1.3 m in width, and 1.8 m in height. The air was supplied through four linear slot diffusers, each with a width of 2.5 cm, that were installed at the edges of the floor. The exhausts were located at ceiling level according to the schematic in Figure 1 of Bolster and Linden (2009). A heated box with a power of 65 W was located at the center of the floor. The box had dimensions of 0.2 m in length, 0.2 m in width, and 0.22 m in height. The supply-air velocity was 0.08 m/s. Particles with a size of 2 μm were injected from a point above the heated box for 328 s. Transient particle concentrations were measured at four locations on a vertical line in the x-directional center-cutting plane and 0.65 m away from the heated box. The measurement locations were 0.2, 0.6, 1.1, 1.4, and 1.7 m from the floor.

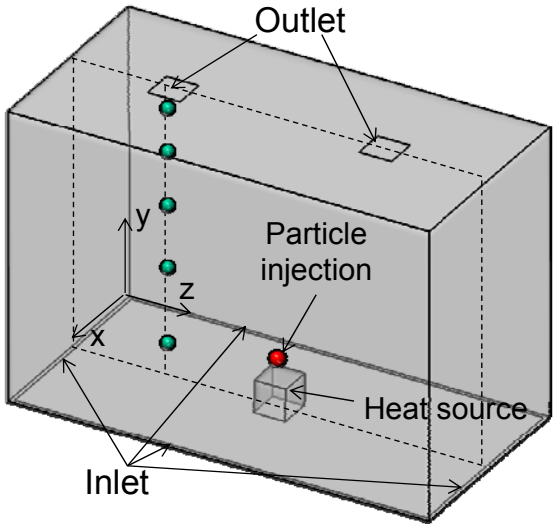

Figure 6-2. Configuration of the chamber studied by Bolster and Linden (2009).

This study first used the Markov chain model to calculate C_{MC} and then applied the superimposition method (Eq. (6.18)) to calculate the total particle concentration. This investigation tested three grid resolutions (19,100, 53,740, and 383,120) for CFD grid independence. The resolution of 53,740 was sufficiently fine to capture the turbulent flow in the chamber. The time step size was set at 0.01 s. The independence test showed that this time step size was sufficiently fine to capture the transient features. Particle

deposition and resuspension at a particle size of 2 μm were neglected (Zhao et al., 2009, Zhu et al., 2012). Figure 6-3 compares the numerical results for transient particle concentration with the experimental data. All the particle concentrations were normalized by the concentration at the source. The Markov chain model and experimental data display similar particle concentration profiles at the locations with heights of 1.7 and 1.4 m. At the location with a height of 1.1 m, the peak in the particle concentration was delayed in comparison with the peaks at the 1.7 and 1.4 m locations, and this delay was correctly captured by the Markov chain model. Furthermore, the model correctly predicted lower particle concentrations at the location with a height of 0.2 and 0.6 m than at the other locations, which are not shown here. Generally speaking, the trends in the normalized particle concentration distributions predicted by the Markov chain model again agreed reasonably well with the experimental data.

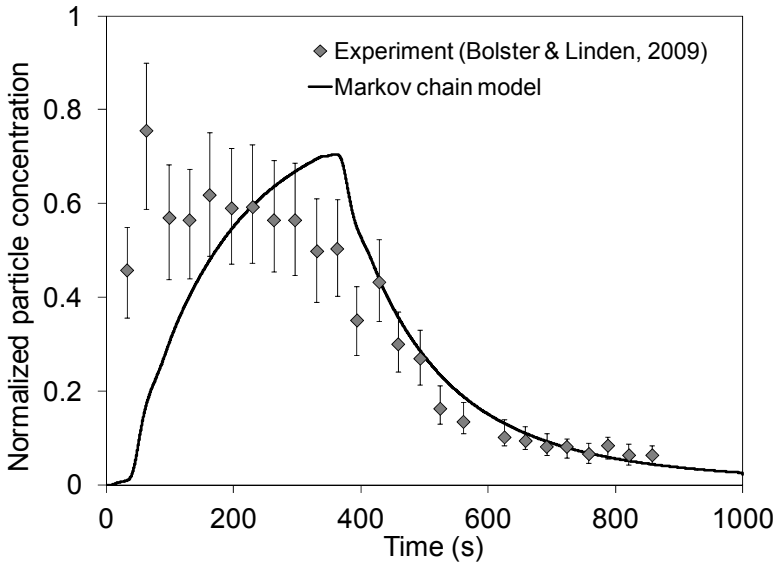

(a)

Figure 6-3. Comparison of the numerical results for transient particle concentration with the corresponding experimental data: (a) y = 1.7 m, (b) y = 1.4 m, and (c) y = 1.1 m.

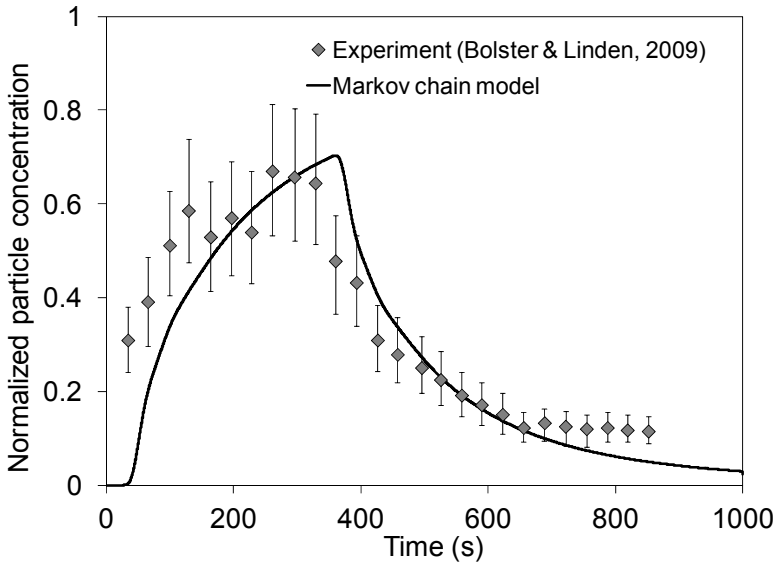

(b)

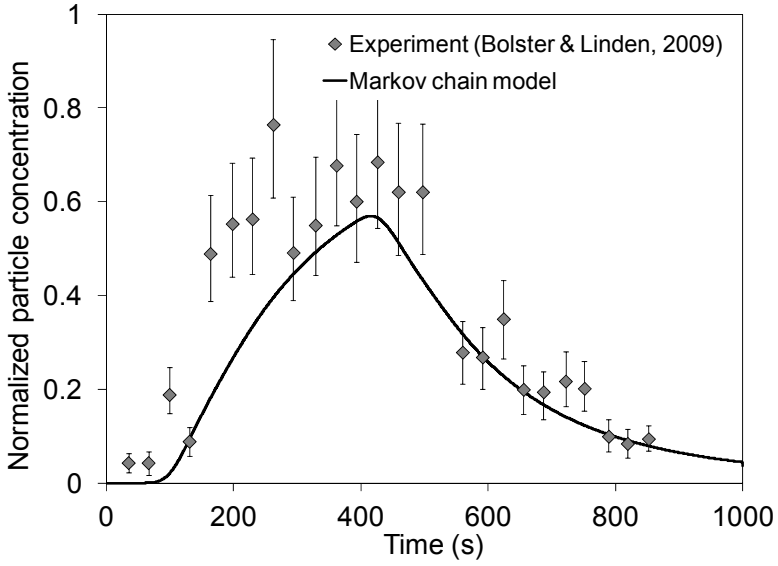

(c)

Figure 6-3. continued.

6.2.3 Particle Transport in an Aircraft Cabin

This study then used the experimental data of transient particle transport in the first-class cabin of the MD-82 aircraft to further validate the Markov chain model. Figure 6-4 compares the transient particle distributions predicted by the Markov chain model with the corresponding experimental data. Chapter 3 showed that the particle concentrations at

Seat 1B, 1C were relatively high, while that at the other seats were relatively low. Figures 6-4(a) and 6-4(b) shows that the combined method accurately predicted relatively high peak concentrations at Seats 1B and 1C when compared with the experimental data. For the other seats where the concentrations were relatively low, only the comparison results at Seats 2B and 3B are shown here in Figures 6-4(c) and 6-4 (d) to keep the main body of thesis concise. Seat 3B was a representative location where the agreement between simulation and experiment was very good, while Seat 2B was a representative location where the agreement was worse. Generally speaking, the Markov chain model can predict the general trends of person-to-person particle transport in the aircraft cabin with reasonable accuracy.

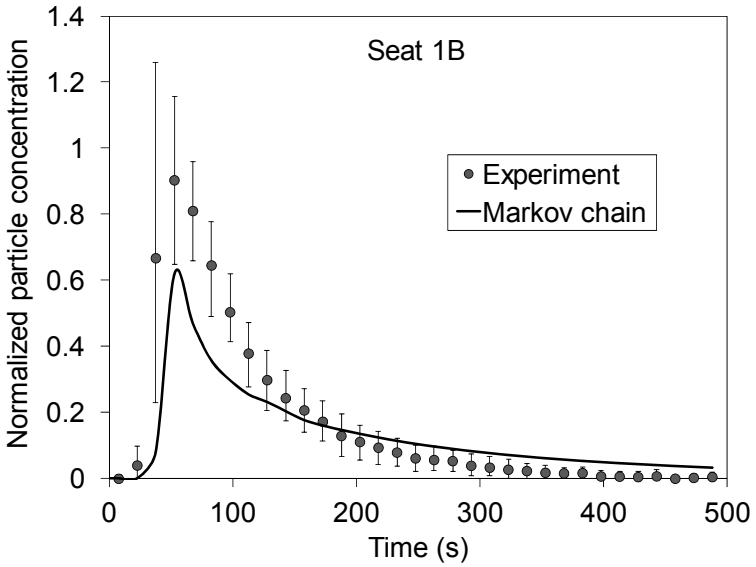

(a)

Figure 6-4. Comparison of the numerical results of transient particle concentrations predicted by the Markov chain model with the corresponding experimental data at seats: (a) 1B, (b) 1C, (c) 2B, and (d) 3B.

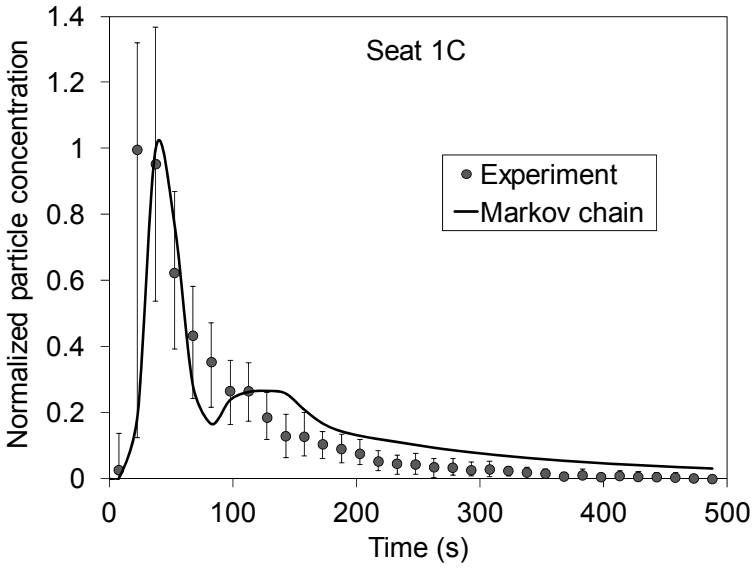

(b)

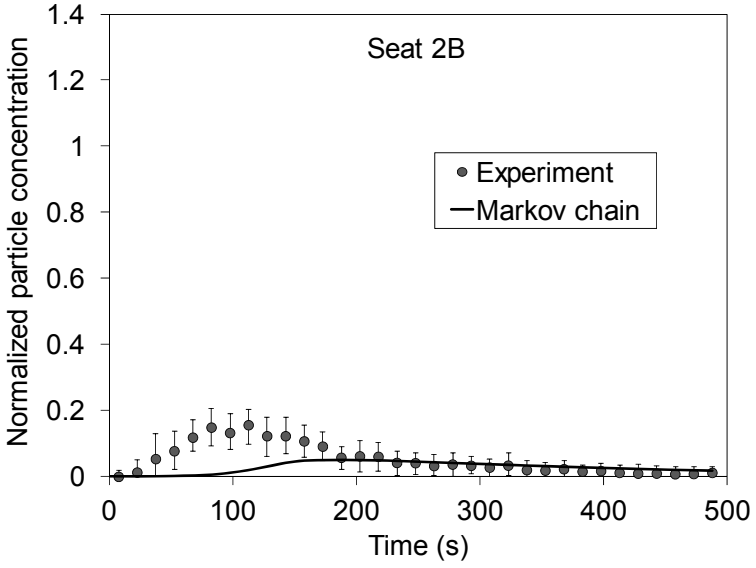

(c)

Figure 6-4. continued.

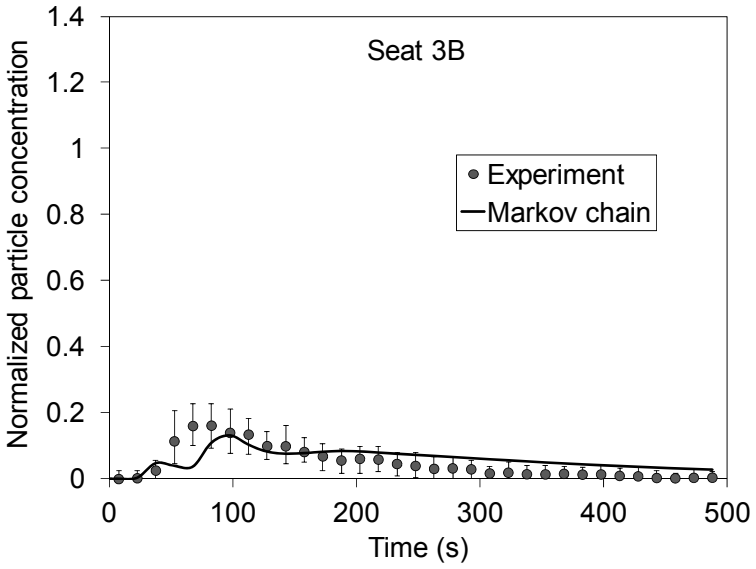

(d)

Figure 6-4. continued.

6.3 Application of the Markov Chain Model

This study used the validated Markov chain model to predict person-to-person particle transport in a ventilated room. Figure 4-11 illustrates the configuration of the room used in this study. Detailed description of the study is provided in section 4.3.1. Two persons, represented by heated manikins, were seated face to face in the room, with a distance of about 1.0 m between their noses. The person on the left was assumed to be the index person, while the one on the right was the receptor. The room was ventilated by a mixing ventilation system with an air change rate of 3 ACH. The forced air and thermal plumes generated by the heated manikins formed a mixed convection airflow pattern. The index person was assumed to have a release of particles with zero velocity at time zero. The particle release duration was 0.15 s. A particle size of 1 μm was assumed in order to represent fine particles.

Since no experimental data was available for this case, this study used the Lagrangian and Eulerian models as benchmarks to assess the performance of the Markov chain model. Three grid resolutions (669,109, 1,446,790, and 2,937,128) were tested for CFD

grid independence. This investigation used a grid resolution of 1,446,790 in the simulation, which was sufficiently fine to capture the turbulent flow in the room. The evaporative process is almost instantaneous for droplets with a diameter of 1 μm (Chen and Zhao, 2010). The time step size was 0.1 s. The independence test showed that this time step size was sufficiently fine to capture the transient features. The calculations for this case were performed over a time period of 5 room time constants. For the Lagrangian model, the particle number injected from the source was 2.29×10^{6}, which was calculated using the method proposed in Chapter 4.

Figure 6-5 compares the time-varying particle concentration distributions predicted by the Markov chain model with those predicted by the Lagrangian and Eulerian models in the first 100 seconds. All three models show that the exhaled particles initially moved upward with the thermal plume generated by the index person. The particles then dispersed throughout the room and reached the receptor. It can be seen in Figure 6-5 that the Markov chain and Lagrangian models both predicted slower particle dispersion than did the Eulerian model. Note that both the Markov chain and Lagrangian models use the principle of the random walk model (Eq. 6.14) to calculate the turbulent diffusion, while the Eulerian model includes the turbulent diffusion term in the particle governing equation. The numerical diffusion introduced by the Eulerian model may be an important reason for its more dispersive characteristics. Generally speaking, the trends in transient particle transport predicted by the Markov chain model agree well with both the Largangian and Eulerian models. For the calculation as a whole in this case, the Markov chain model was 8.0 times faster than the Lagrangian model and 6.3 times faster than the Eulerian model.

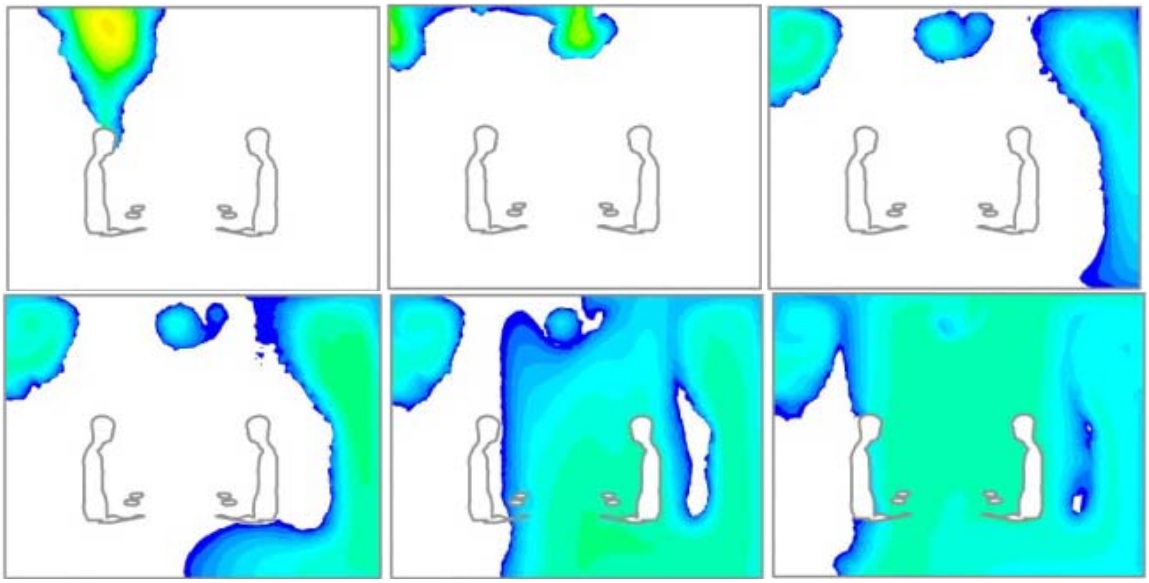

(a)

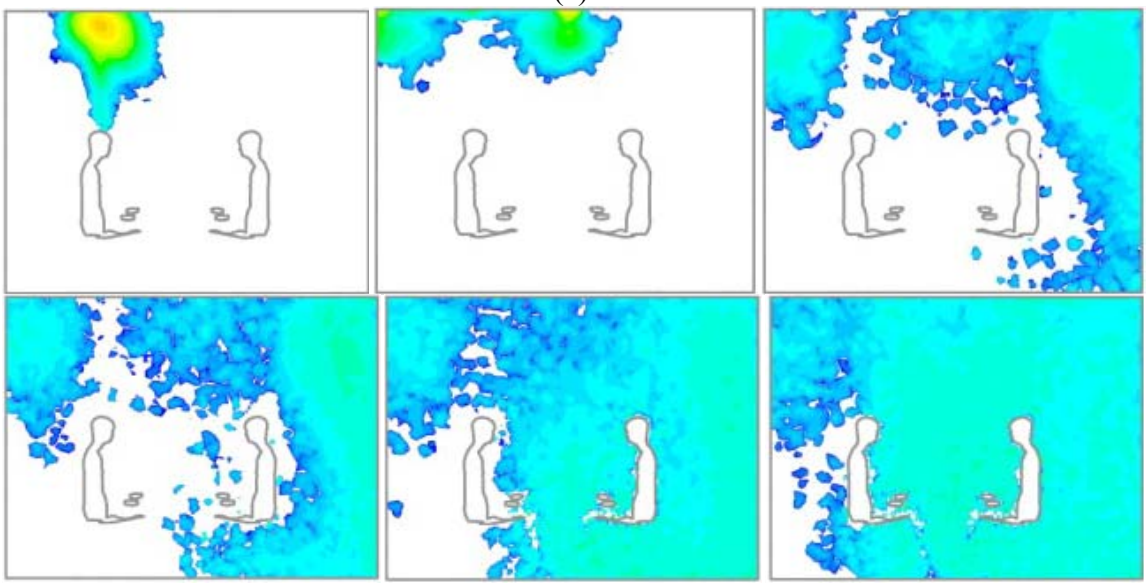

(b)

Figure 6-5. Comparison of particle concentration distributions at 5, 15, 50, 60, 80, and 100 s predicted by (a) the Markov chain model, (b) the Lagrangian model, and (c) the Eulerian model.

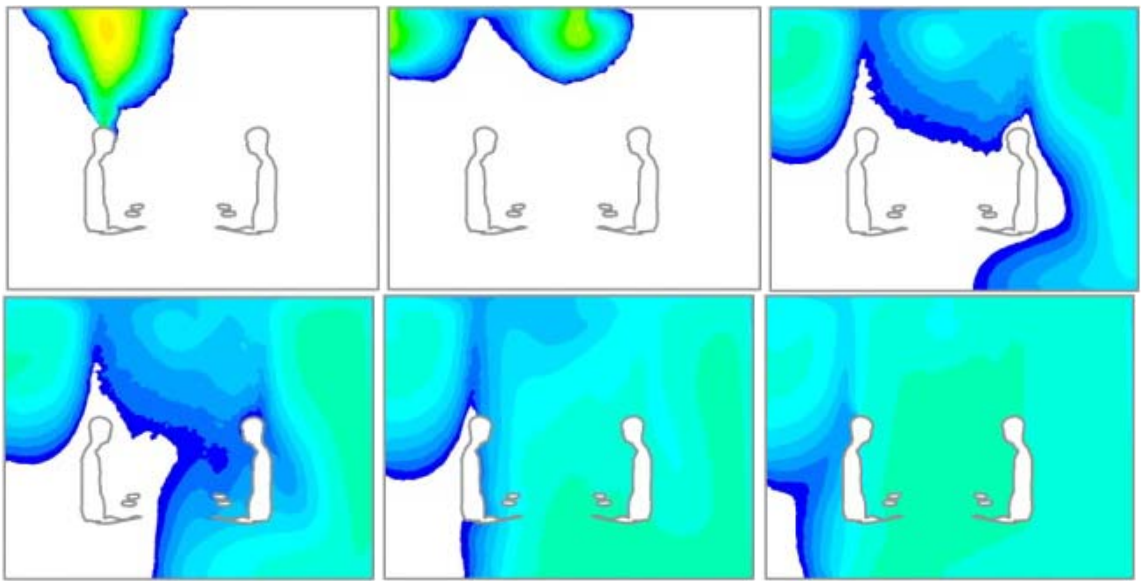

(c)

Figure 6-5. continued.

6.4 Discussion

There are a number of limitations to the present study, beginning with the assumption of a steady-state airflow field. For instance, some sources could change the airflow pattern, such as a powerful cough or sneeze from an uncovered mouth. In these cases, the probability transition matrix would also change. Therefore, the Markov chain model developed in this study is suitable only for those scenarios in which the mouth is effectively covered or the influence of the exhaled air is negligible. In the future, we intend to develop an improved Markov chain model for transient particle transport under unsteady-state airflow conditions. Note that, when combining with the superimposition method, the Markov chain model can also be used for predicting steady-state particle concentrations with a continuous source. However, when compared with the steady-state Eulerian model, the Markov chain model is more time-consuming because it needs to be performed under a transient condition. Therefore, the Markov chain model is not superior for steady-state particle concentration predictions. The Markov chain technique can also be applied in a zonal model so that the calculation speed can be further increased while

the results would be less informative. This study also developed an improved zonal Markov chain model for predicting faster-than-real-time information about transient particle transport in enclosed environments. Details please see Appendix B.

The Markov chain model that was developed considers the dispersion of particles by the mechanisms of advection and turbulence diffusion. For particles with a diameter smaller than 3 μm, as were used in this study, these are the only important mechanisms in typical indoor environments (Zhao et al., 2009). If only these two mechanisms are considered, this model can also be used for tracer gas simulations. However, for particle transport, there are other mechanisms, such as gravitational settling, thermophoresis, particle fluctuation due to turbulence, and particle acceleration. Zhao et al. (2009) indicated that gravitational settling could significantly affect the particle concentration distribution for particles with a diameter larger than 5 μm. Thus, to model the transient transport of coarse particles, the effect of gravitational settling should be further considered. Furthermore, for coarse and ultrafine particles in a room with a low air change rate, the influence of particle deposition on the particle concentration distribution may be considerable. Therefore, the implementation of particle deposition into the current Markov chain model deserves further study.

6.5 Conclusions

This chapter developed a Markov chain model for quickly predicting transient particle transport in enclosed environments. Within the scope of this research, the following conclusions can be drawn:

(1) The proposed Markov chain model can be used for predicting detailed information about transient particle transport in enclosed environments.

(2) The Markov chain model increased the speed of calculation by 8.0 and 6.3 times in comparison with the Lagrangian and Eulerian models, respectively, for the case that was studied.

CHAPTER 7. COMPARISON OF THREE PARTICLE MODELS

This chapter reports our effort in comparing the performance, computing cost, and robustness of the Eulerian, Lagrangian, and Markov chain models for indoor transient particle transport simulations. On the basis of this comparison, suitable models can be identified for the study of transient particle transport indoors and for use by engineers in the design of air distributions.

7.1 Comparison of the Performance

This study used four cases of particle transport to assess the performance of the Eulerian, Lagrangian, and Markov chain models. The first case was that of particle transport from a single pulsed source in an empty chamber, from Wang and Chen (2009). The present investigation used the first case to qualitatively compare the transient particle concentration distributions predicted by the three models. The second case was particle transport in an isothermal ventilated chamber with a source at the inlet, from Zhang et al. (2009). The third case was particle transport from a source located inside a chamber with displacement ventilation, from Bolster and Linden (2009). The present study used the second and third cases to quantitatively assess the performance of the three models by comparing their results with experimental data. The fourth case was person-to-person particle transport in the first-class cabin of an MD-82 aircraft cabin with heated manikins from Chapter 3. Experimental data was used to assess the performance of the three models in a realistic scenario of airborne infectious disease transmission.

7.1.1 Case 1: Particle Transport from a Single Pulsed Source

The first case was that of particle transport from a single pulsed source in an empty chamber. Figure 7-1 shows the configuration of the chamber studied by Wang and Chen (2009). The dimensions of the chamber were 2.44 × 2.44 × 2.44 m. An isothermal jet from an inlet at the upper edge of the chamber developed along the ceiling and then moved downward, forming a circulation pattern in the chamber. This is a basic forced convection airflow pattern in a mechanically ventilated room. The air change rate was 22.6 ACH. The thermo-fluid boundary conditions were measured by Wang and Chen (2009). Our study modeled a scenario with a pulsed source near the inlet, and another scenario with a pulsed source in the circulation zone. Particle transport in the first scenario was dominated by convection, while turbulent diffusion also served as an important driven force in the second scenario. In the scenario with the pulsed source, the duration of the particle source was one time step.

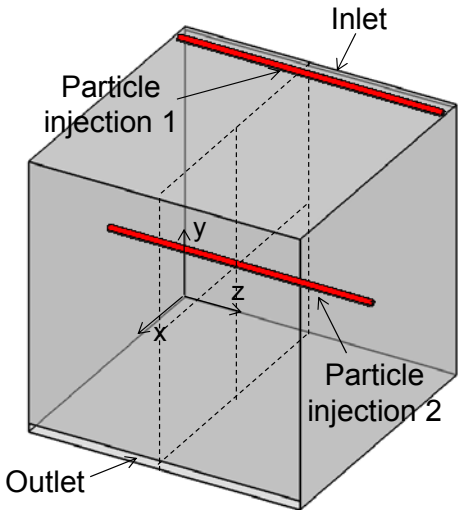

Figure 7-1. Configuration of the empty chamber studied by Wang and Chen (2009).

Three structured grid resolutions (8,000, 51,840, and 414,720) were tested for CFD grid independence. The resolution of 51,840 was sufficiently fine to produce accurate results

for the airflow in the chamber. The Eulerian, Lagrangian, and Markov chain models were used to calculate transient particle transport. The particle diameter used was 1 μm. Particle deposition and resuspension were neglected because of their limited effects (Zhao et al., 2009, Zhu et al., 2012). The time step size was set at 0.01 s. For the Lagrangian model, the necessary particle number injected from the source was 1.61 million.

Figure 7-2 compares the transient particle concentration distributions predicted by the Eulerian, Lagrangian, and Markov chain models for the scenario with a pulsed source near the inlet. All three models predicted that the particles moved along the ceiling, traveled downward along the right wall, moved to the floor, and finally were dispersed throughout the whole chamber by means of recirculation. Figure 7-3 compares the three models for the scenario with a pulsed source in the circulation zone. For these two scenarios, the three models agreed well with one another in terms of the general trend of transient particle transport in the chamber.

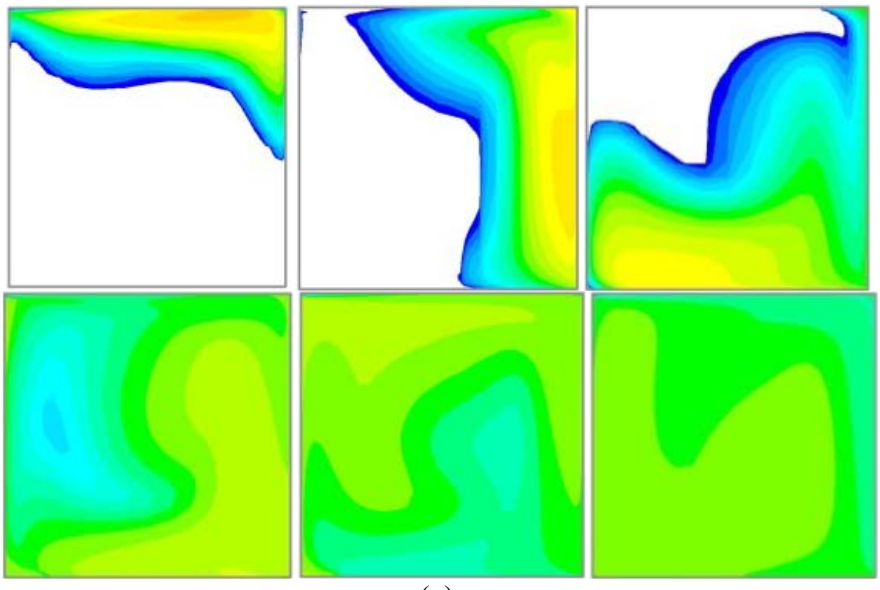

(a)

Figure 7-2. Comparison of particle concentration distribution with a pulsed source near the inlet at 5, 10, 20, 50, 75, and 100 s predicted by (a) Eulerian model, (b) Lagrangianmodel, and (c) Markov chain model.

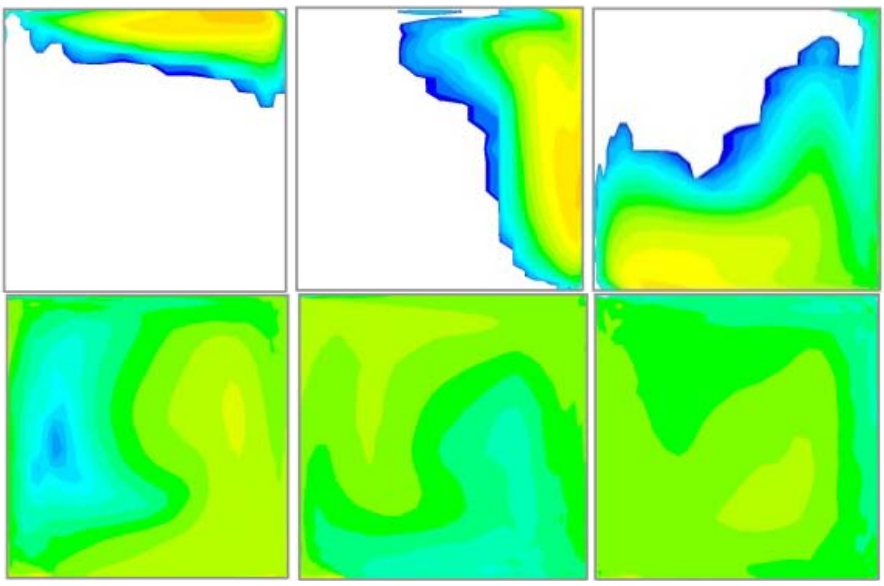

(b)

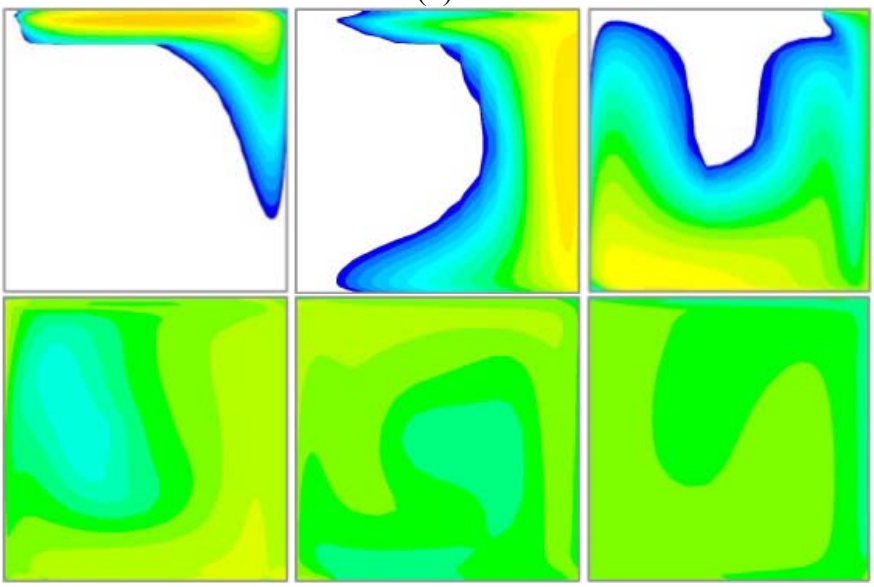

(c)

Figure 7-2. continued.

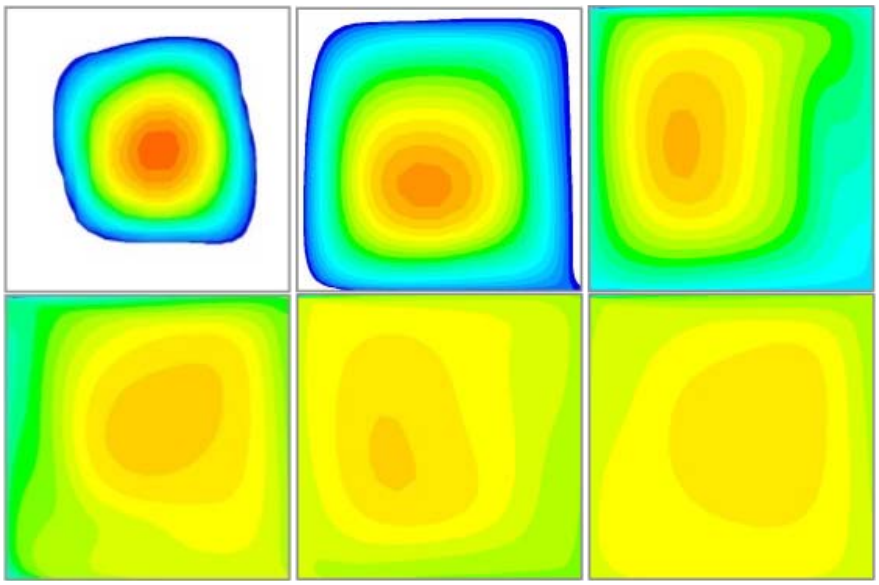

(a)

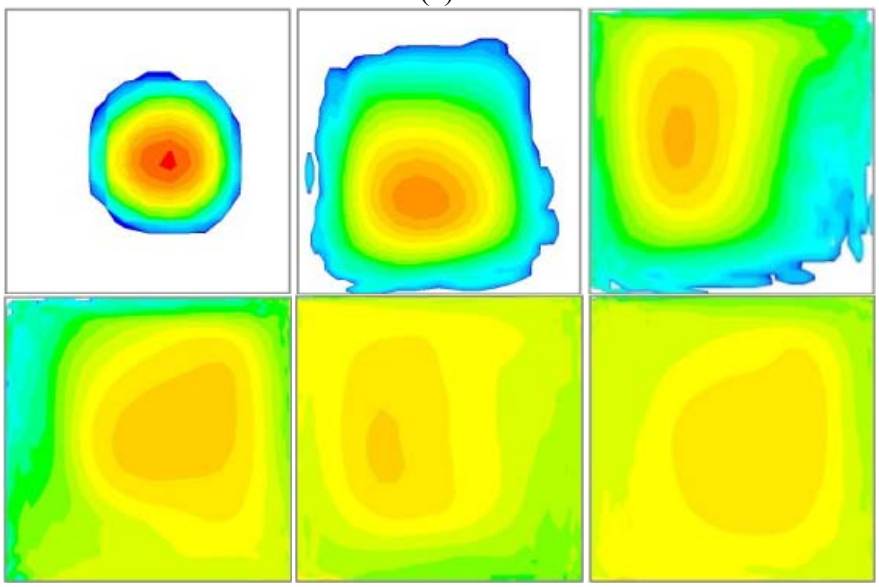

(b)

Figure 7-3. Comparison of particle concentration distribution with a pulsed source in the circulation zone at 5, 15, 30, 50, 75, and 100 s predicted by (a) Eulerian model, (b) Lagrangian model, and (c) Markov chain model.

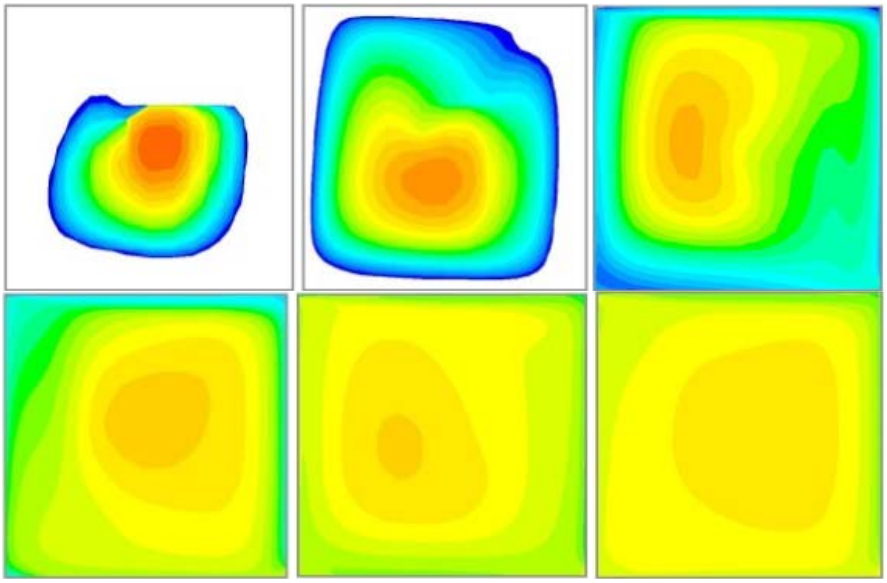

(c)

Figure 7-3. continued.

7.1.2 Case 2: Particle Transport from a Source at the Inlet

The second case was that of transient particle transport from a source at the inlet in an isothermal ventilated chamber, as studied by Zhang et al. (2009). The dimensions of the chamber were 4 m in length, 2.1 m in width, and 2.4 m in height, as shown in Figure 5-1. Particles with a size of 1 μm were injected through the inlet into the chamber. Particle concentrations as a function of time were measured at two locations. The two measurement locations (Point 1 and Point 2) were 1.8 and 0.9 m, respectively, from the floor, as shown in Figure 5-1.

This study used a grid resolution of 18,009, which was sufficiently fine to produce accurate results for the airflow in the chamber. The Eulerian, Lagrangian, and Markov chain models were used to calculate the transient particle concentration distributions. The time step size was set at 0.01 s. Particle deposition and resuspension were negligible at a particle size of 1 μm (Zhao et al., 2009, Zhu et al., 2012). It should be noted that two sets of simulations were performed on the basis of the corresponding inlet particle

concentrations, as shown in Figure 5 of Zhang et al. (2009). For the Lagrangian model, the necessary particle number injected from the source was 2.24 million.

Figure 7-4 compares the numerical results for transient particle concentration as predicted by the Eulerian, Lagrangian, and Markov chain models and as measured experimentally. Figure 7-4(a) compares the results at the location with a height of 1.8 m, which was near the inlet. All three models correctly predicted the peak in particle concentration in the initial stage that was observed in the experimental data. However, as shown in Figure 7-4(b), both the simulations and the experiment exhibited a smaller peak than that in Figure 7-4(a). Furthermore, all three models captured the fact that the peak was delayed in time at this location. This weaker response was due to the greater distance between this location and the source. Generally speaking, the trends in transient particle concentration predicted by the Eulerian, Lagrangian, and Markov chain models agreed reasonably well with the experimental data.

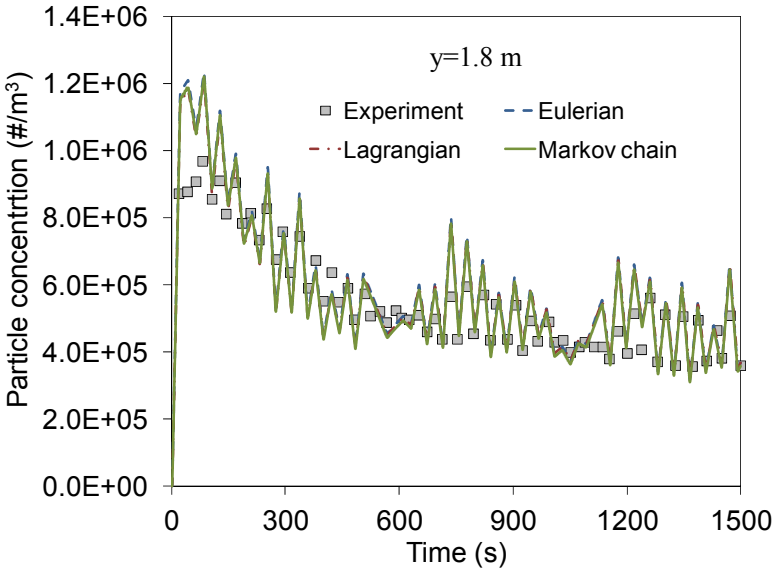

(a)

Figure 7-4. Comparison of the numerical results of transient particle concentrations predicted by Eulerian, Lagrangian, and Markov chain models with the corresponding experimental data at positions (a) y=1.8 m and (b) y=0.9 m.

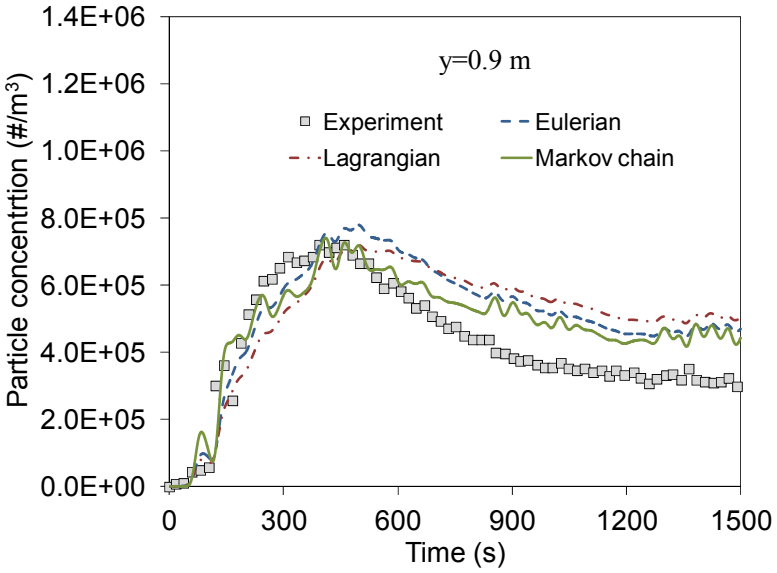

(b)

Figure 7-4. continued.

7.1.3 Case 3: Particle Transport from a Source Inside the Chamber

The third case was that of particle transport from a source inside a chamber with displacement ventilation, as shown in Figure 5-2 (Bolster and Linden, 2009). The chamber dimensions were 2.6 m in length, 1.3 m in width, and 1.8 m in height. The air was supplied through four linear slot diffusers around the floor, and the exhausts were located at ceiling level. The air velocity at the supply inlet was 0.08 m/s. There was a heated box with a power of 65 W on the floor. The particle source was located above the box. The particle size was 2 μm, and the duration of particle release was 328 s. Transient particle concentrations were measured at five locations, which were 0.2, 0.6, 1.1, 1.4, and 1.7 m above the floor, respectively, as shown in Figure 5-2.

Our study used a grid resolution of 53,740, which was sufficiently fine. The Eulerian, Lagrangian, and Markov chain models were used to calculate the particle concentration as a function of time. The time step size was set at 0.01 s. This study neglected particle deposition and resuspension for this case (Zhao et al., 2009, Zhu et al., 2012). For the

Lagrangian model, the necessary particle number injected from the source was 0.68 million.

Figure 6-5 compares the numerical results for transient particle concentration as predicted by the Eulerian, Lagrangian, and Markov chain models and as measured experimentally. This investigation normalized all the particle concentrations by the maximum concentration at the location with a height of 1.7 m. At the locations with heights of 1.7 and 1.4 m, the three models obtained particle concentration profiles that were similar to the experimental data. At the location with a height of 1.1 m, the peak in particle concentration in the experimental data was delayed as compared with the peak at the 1.7 and 1.4 m locations, and this delay was correctly captured by all the models. In addition, all three models correctly predicted extremely low particle concentrations at the locations with heights of 0.6 and 0.2 m. To keep this paper concise, the results at these two locations are not presented here. In general, the trends in transient particle transport calculated by the three models again agreed reasonably well with the experimental data.

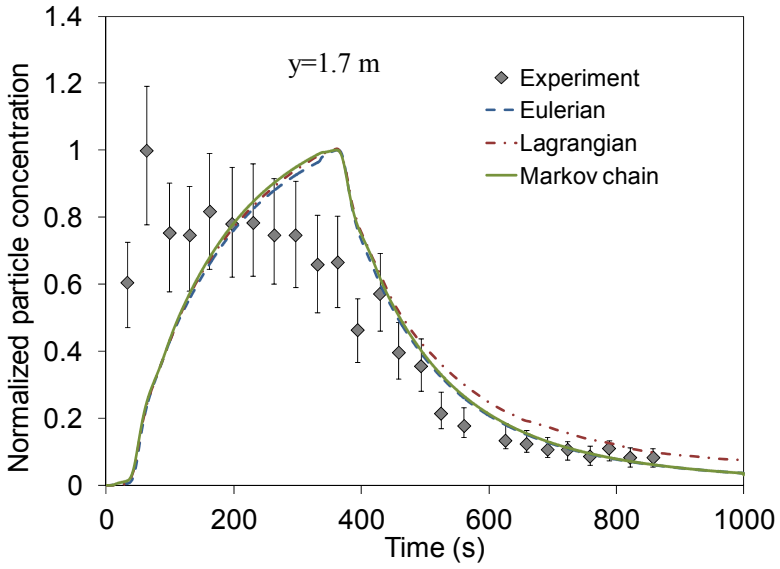

(a)

Figure 7-5. Comparison of the numerical results of transient particle concentrations predicted by Eulerian, Lagrangian, and Markov chain models with the corresponding experimental data at positions: (a) y=1.7 m, (b) y=1.4 m, and (c) y=1.1 m.

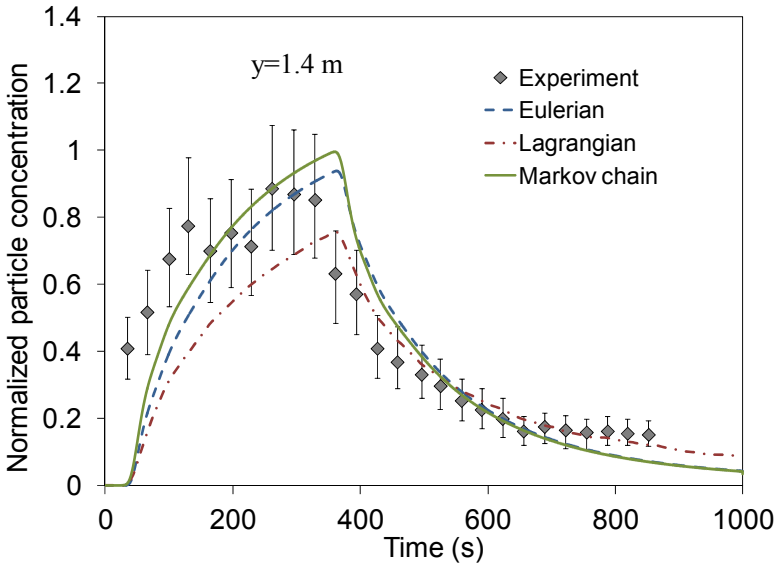

(b)

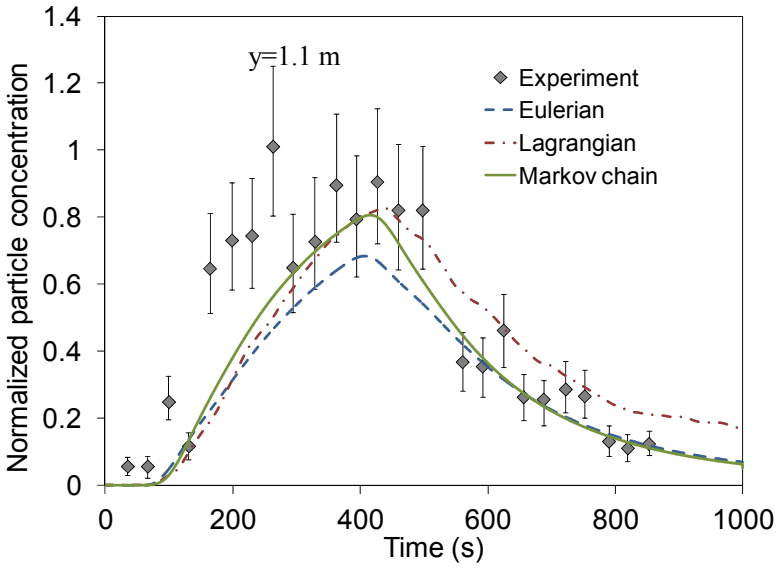

(c)

Figure 7-5. continued.

7.1.4 Case 4: Person-To-Person Particle Transport in an Airplane

The fourth case was the person-to-person particle transport in the first-class cabin of an MD-82 airplane, as shown in Figure 3-6. Liu et al. (2012) has described the aircraft cabin and measured the thermo-fluid boundary conditions in details. The cabin contained three

rows with a total of 12 seats as numbered in Figure 3-6. The cabin was fully-occupied by heated manikins. Particles with a diameter of 3 μm were released from the mouth of the manikin at Seat 2C into the cabin for duration of 20 s. The particle concentrations as a function of time were measured at the breathing zones of each passenger. Detailed information about the experiment is provided in Chapter 3.

In the simulation, this investigation used a resolution of 6.4 million, which has been proven to be sufficiently fine. The Eulerian, Lagrangian, and Markov chain models were used to calculate the transient particle concentration distributions. The time step was set at 0.01 s. Particle deposition and resuspension at a particle size of 3 μm were negligible. For the Lagrangian model, the necessary particle number injected from the source was 1.76 million.

Figure 7-6 compares the normalized particle concentration distribution as a function of time as predicted by the Eulerian, Lagrangian, and Markov chain models and as measured experimentally. Chapter 3 showed that the particle concentrations at Seats 1B and 1C were relatively high, while those at the other seats were relatively low. Figures 7-6(a) and 7-6(b) show that all three models accurately predicted the relatively high peak concentrations at Seats 1B and 1C that were observed in the experimental data. For the other seats, where the concentrations were relatively low, the comparison results are shown only for Seats 2B and 3B in Figures 7-6(c) and 7-6(d), respectively, in order to keep the paper concise. Seat 3B is representative of the locations at which the agreement between the simulation and experiment was very good, while Seat 2B is representative of those locations at which the agreement was worse. Generally speaking, the Eulerian, Lagrangian, and Markov chain models can all provide the transient particle concentration distribution with reasonable accuracy for such a complex case.

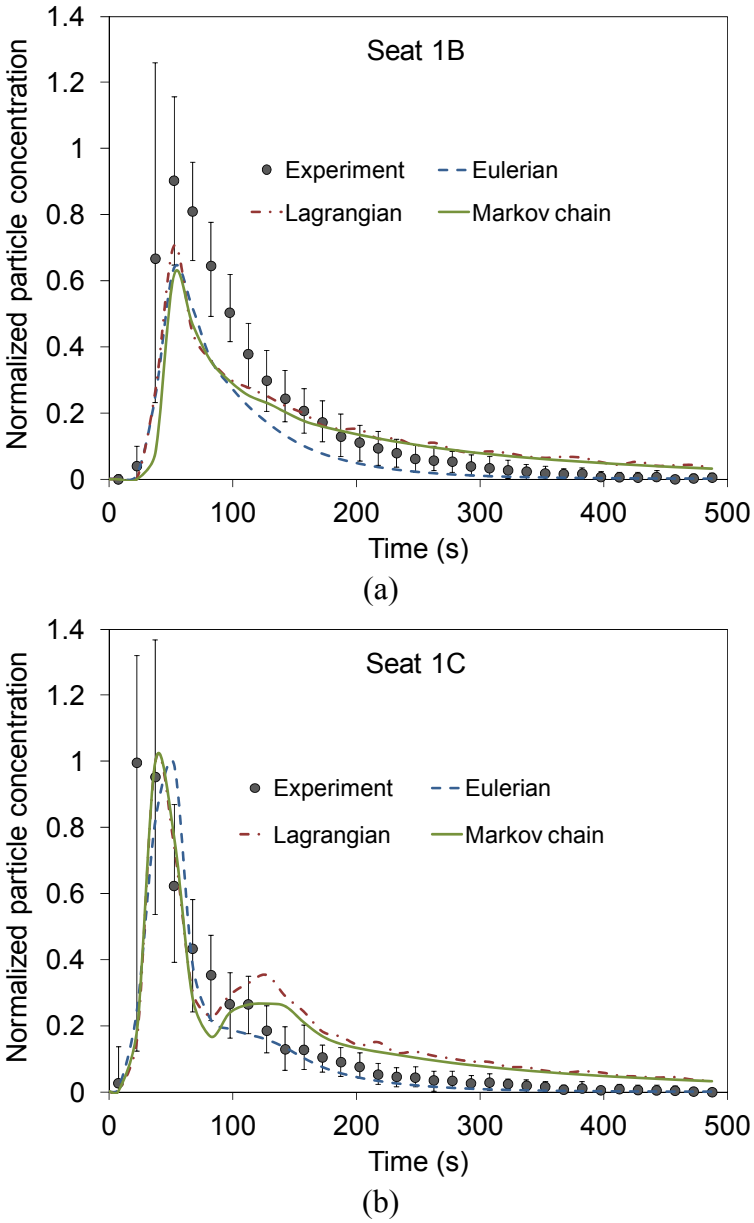

Figure 7-6. Comparison of the numerical results of transient particle concentrations predicted by Eulerian, Lagrangian, and Markov chain models with the corresponding experimental data at seats: (a) 1B, (b) 1C, (c) 2B, and (d) 3B.

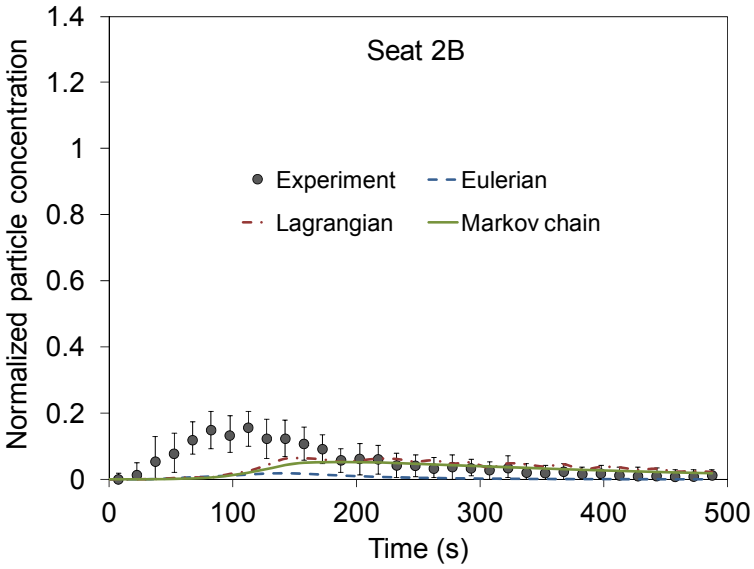

(c)

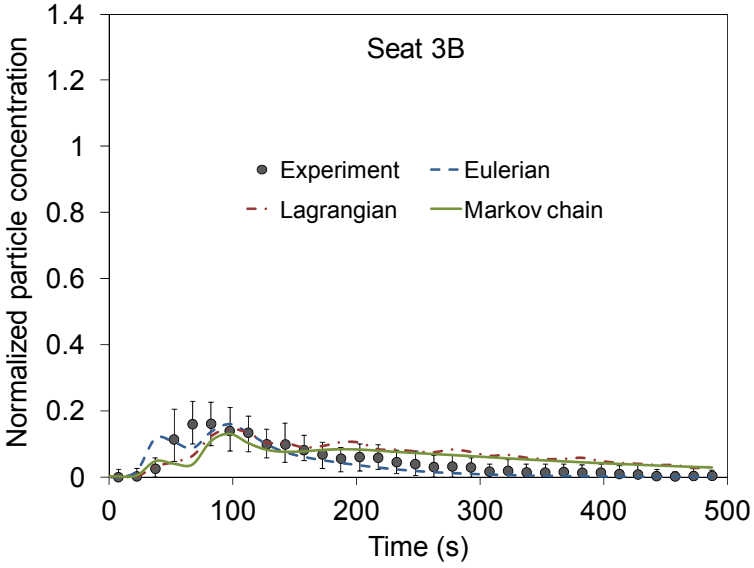

(d)

Figure 7-6. continued.

7.2 Comparison of the Computing Cost

The comparisons above show that the Eulerian, Lagrangian, and Markov chain models can provide information about transient particle transport with similar accuracy.

Computing cost is another important factor in the identification of an efficient model. This section evaluates the computing costs of the three models.

Theoretically, the computing cost of the Eulerian model is related to the grid number and the number of iterations in each time step. For the Markov chain model, which does not require any iterations, the computing cost is related only to the grid number. For the Lagrangian model, the cost factors include the grid number and the number of particles being tracked. The necessary particle number for the Lagrangian model can be calculated by Eq. (5.11). It can be seen that the particle source duration can influence the necessary particle number and therefore the computing time. To isolate the impact of source duration, this study substituted the combined Lagrangian and superimposition method for the pure Lagrangian method. With the combined method, the necessary particle number can be calculated by Eq. (5.13), which is independent from the source duration. For the purpose of a fair comparison among the cases, the ratio of V_{room} to V_{target} was set at a consistent value of 1000, so that the number of particles being tracked was the same for all cases. A ratio of 1000 ensured that the volumes of the target zones were of the same magnitude in all three cases, and that they were smaller than the volumes of the breathing zones. This investigation first used these assumptions to fairly compare the computing costs and to develop empirical equations for determining the relative computing times of the three models. Next, the empirical equations were modified to account for the effects of source duration and the ratio of V_{room} to V_{target} with the Lagrangian model. Furthermore, for the purpose of a fair comparison, all the cases were calculated over a period of five time constants of the room, 5τ, and the time step size was set at the same value for all models.

To quantitatively investigate the speed of calculation, this study determined the relative computing times of the three models. For each case, the computing time of the Eulerian model relative to that of the Markov chain model was defined as:

$$\eta_{E/M,i} = \frac{t_{Eulerian,i}}{t_{Markov,i}} \tag{7.1}$$

where $t_{Eulerian,i}$ and $t_{Markov,i}$ is the computing time of Eulerian and Markov chain model for Case i, respectively. Similarly, the relative computing time of Lagarngian to Markov chain model was defined as:

$$\eta_{L/M,i} = \frac{t_{Lagrangian,i}}{t_{Markov,i}} \tag{7.2}$$

where $t_{Lagrangian,i}$ is the computing time of Lagrangian model for Case i.

Figure 7-7 shows the relative computing times for the four cases as a function of grid number. The linear regression shows that the computing time of the Eulerian model relative to that of the Markov chain model was independent of the grid number (the slope was zero). This occurred because the only difference between the Eulerian and Markov chain models in regard to computing time was the number of iterations in each time step. Normally, the Eulerian model requires several iterations in each time step, while the Markov chain model does not require any iterations. For a given grid number, the computing time of the Eulerian model for a single iteration is comparable to that of the Markov chain model for a single time step. Therefore, the computing time of the Eulerian model relative to that of the Markov chain model depends only on the number of iterations required by the Eulerian model in each time step. For the studied cases, on average, the Eulerian model required five to six iterations in each time step, where the simulations were assumed to have converged when the residual for the particle equation was less than 1×10^{-5}. Therefore, according to regression analysis, the computing time of the Eulerian model relative to that of the Markov chain model is:

$$\eta_{E/M,i} = \frac{t_{Eulerian,i}}{t_{Markov,i}} = 5.59 \tag{7.3}$$

The factor of reduction in computing time may be different if the iteration number is different.

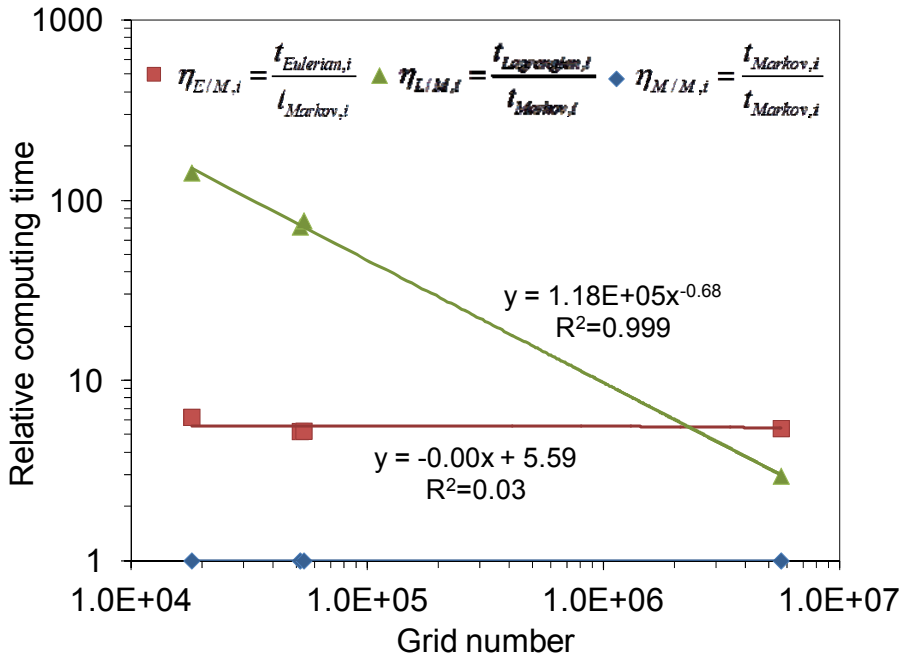

Figure 7-7. Relative computing time as a function of grid number for the Eulerian, Lagrangian, and Makov chain model.

Figure 7-7 also shows that the computing time of the Lagrangian model relative to that of the Markov chain model was negatively associated with the grid number. When the grid number was relatively small, the Lagrangian model required a much longer computing time than did the Eulerian and Markov chain models. However, when the grid number was relatively large, the Lagrangian model required less computing time than the other two models. As indicated in the Lagrangian equations, the calculation of particle trajectory is independent of the grid number. Therefore, the influence of grid number on the computing time of the Lagrangian model tends to be weaker than its influence on the other two models. As shown in the figure, a power function could satisfyingly describe

the relationship between the relative computing time of the Lagrangian to Markov chain model and the grid number:

$$\eta_{L/M,i} = \frac{t_{Lagrangian,i}}{t_{Markov,i}} = 1.18 \times 10^5 \cdot n^{-0.68} \tag{7.4}$$

where n is the grid number. Note that this equation was derived based on the assumptions that the ratio of V_{room} to V_{target} was equal to 1000. To account for the impact of this ratio, Eq. (7.4) should be modified as:

$$\eta_{L/M,i} = \frac{t_{Lagrangian,i}}{t_{Markov,i}} = 1.18 \times 10^5 \cdot n^{-0.68} \cdot \frac{V_{\text{room}}}{1000 \cdot V_{\text{target}}} = 118 \cdot n^{-0.68} \cdot \frac{V_{\text{room}}}{V_{\text{target}}} \tag{7.5}$$

Moreover, the above equation was developed based on the combined Lagrangian and superimposition method in order to isolate the impact of source duration. If the pure Lagrangian method is used, the necessary particle number would be increased by a factor which can be calculated by Eq. (5.15). Therefore, to account for the impact of source duration, Eq. (7.5) should be further modified as:

$$\eta_{L/M,i} = \frac{t_{Lagrangian,i}}{t_{Markov,i}} = 118 \cdot n^{-0.68} \cdot \frac{V_{\text{room}}}{V_{\text{target}}} \cdot \frac{\frac{t_s}{\tau}}{1 - \exp(-\frac{t_s}{\tau})} \tag{7.6}$$

Empirical equations (7.3) and (7.6) can be used to evaluate the relative computing time of the Eulerian, Lagrangain, and Markov chain models. They can together serve as a general

guideline for selecting an efficient model to calculate transient particle transport in indoor environments.

7.3 Comparison of the Robustness

7.3.1 Influence of Time Step Size

In the above comparison of the Eulerian, Lagrangian, and Markov chain models, the same time step size was used in all three models. The time step size should be small enough to capture the transient features of particle transport. Theoretically, the transient features can be fully captured if, in each time step, the particles move across a distance that is less than the width of a cell, i.e., the Courant number is less than 1 (Courant et al., 1928). Therefore, a suitable time step size can be estimated by the following equation (Courant et al., 1928):

$$\Delta t \le \min(\frac{l}{u}) \tag{7.7}$$

where l is the distance between the centroids of two adjacent cells, and u is the air velocity at the connecting face of the two cells. The time step sizes used in this study were chosen according to Eq. (7.7).

However, for engineering applications, modelers normally are concerned about the transient feature of particle transport only in certain locations, such as breathing zones. In this case, if the particle concentration does not change rapidly in these locations, the time step size may be set at a larger value in order to reduce the computing cost. This section reports our effort in exploring the influence of time step size on transient particle transport prediction with the three models.

This study conducted a sensitivity analysis of time step size using the Eulerian, Lagrangian, and Markov chain models for Case 2. The original time step size was set at 0.01 s, according to Eq. (7.7). Two larger values, 0.05 and 0.5 s, were also tested. Figure 7-8 compares the transient particle concentrations predicted by the three models with time step sizes of 0.01, 0.05, and 0.5 s. For the Eulerian and Lagrangian models, the predicted results for the different time step sizes agree very well with one another. Thus, the transient particle concentrations were relatively insensitive to time step size for the Eulerian and Lagrangian models. However, for the Markov chain model, a larger time step size resulted in lower particle concentrations. This difference occurred because the particles can move only to the adjacent cells in a time step. When the time step size was too large, the Markov chain model was not able to make the particles move beyond the adjacent cells. In this case, the transport of particles was slower than it would be in reality. Thus, the transient particle concentrations were highly sensitive to time step size for the Markov chain model.

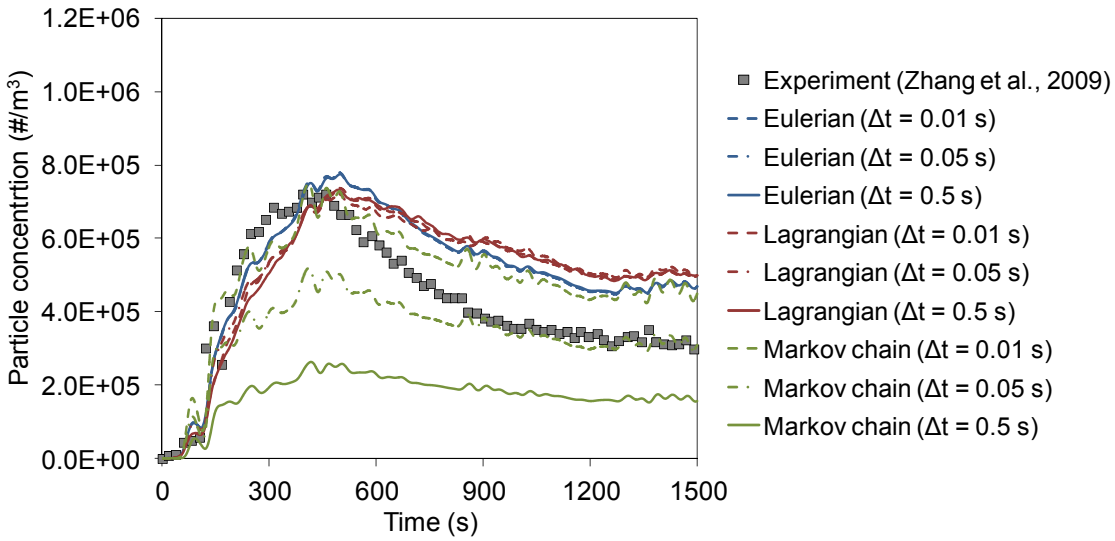

Figure 7-8. Comparison of transient particle concentrations predicted by the Eulerian, Lagrangian, and Markov chain models with a time step size of 0.01, 0.05, and 0.5 s.

Note that, when the transient features in every cell of the domain are of concern, the Courant number should be less than 1 (Courant et al., 1928). In this case, the time step size is sufficiently fine to ensure the accuracy of Markov chain model. However, in some cases, only the transient features in certain cells where particle concentration does not change rapidly are of concern. When calculating such cases, modelers may need to run the Markov model with a finer time step size when compared with the other two models, which increases the computing time. A possible solution would be merging the cells where particle concentration changes rapidly so that the time step size could be relaxed for Markov chain model, which deserves further study.

7.3.2 Other Influencing Factors

The Eulerian and Lagrangian are two mature and well-developed models for transient particle transport simulations. Although the airflow in the cases above were steady-state, the Eulerian and Lagrangian models can also be used under an unsteady-state airflow condition (Wang et al., 2012). Furthermore, the two methods can account for other mechanisms of particle dispersion such as gravitational settling and thermophoresis (Zhao et al., 2004; Zhao et al., 2009), as well as particle deposition onto the surfaces (Zhao et al., 2004; Chen et al., 2006). On the other hand, the newly developed Markov chain model cannot account for the above influencing factors and can currently only calculate the transient particle transport from a single pulsed source. Also the requirement of a small time step size is a shortcoming of the Markov chain model. Nevertheless, the Markov chain model generally uses far less computing cost compared with the other two models.

7.4 Conclusions

This chapter compares the Eulerian, Lagrangian, and Markov chain models for indoor transient particle transport simulations. The comparison discussed their accuracy, computing cost, and robustness. The following conclusions can be made:

(1) The Eulerian, Lagrangian, and Markov chain models can predict transient particle transport in enclosed environments with a similar accuracy.

(2) With the same time step size and grid number, the Markov chain model was the fastest among the three models. Unless super-find grid was used, the Eulerian model was faster than the Lagrangian model.

(3) This study developed empirical equations to quantitatively evaluate the relative computing cost among the three models.

(4) The Eulerian and Lagrangian models were more robust than the Markov chain model, because the Markov chain model was sensitive to the time step size.

CHAPTER 8. CONCLUSIONS AND FUTURE WORK

This chapter first summarizes the key conclusions from this study and then discusses the direction of future work.

8.1 Conclusions

This study first conducted experimental measurements of person-to-person particle transport in an office mockup with a UFAD system and the first-class cabin of an MD-82 airplane. The experimental data measured in the office mockup can be used in evaluating the performance of steady-state airflow and contaminant distribution models. The RNG k-ε model can be used for accurately predicting steady-state airflow and temperature distribution in enclosed environments. The steady-state Eulerian model is very fast and can be used for predicting steady-state contaminant concentration distribution indoors. The experimental data measured in the first-class cabin of the MD-82 aircraft can be used in evaluating the performance of the transient particle models.

This investigation then developed simplified models for predicting exhaled airflow from a cough with the mouth covered on the basis of the smoke visualization data. The developed models make the simulation of person-to-person particle transport more realistic. The numerical investigation found that covering a cough with a tissue, a cupped hand, or an elbow can significantly reduce the horizontal velocity and cause the exhaled particles to move upward with the thermal plumes generated by human bodies. Covering a cough or turning the head away can prevent the receptor's direct exposure.

Furthermore, this study developed a method for estimating and reducing the necessary particle number in order to accelerate the Lagrangian method for predicting transient

particle transport in indoor environments. The proposed method can estimate the necessary particle number and thus reduce the effort that is normally required for evaluating different numbers of particles in order to achieve statistically meaningful results. The superimposition and time-averaging method can reduce the necessary particle number, and, as a result, the computing cost can be further reduced. The combined Lagrangian, superimposition, and time-averaging method can predict transient particle transport in indoor environments with reasonable accuracy.

This investigation further developed a Markov chain model for quickly predicting transient particle transport in enclosed environments. The proposed Markov chain model can be used for predicting detailed information about transient particle transport in enclosed environments. The Markov chain model increased the speed of calculation by 8.0 and 6.3 times in comparison with the Lagrangian and Eulerian models, respectively, for the case that was studied.

Finally, this study compared the Eulerian, Lagrangian, and Markov chain models in terms of accuracy, computing cost, and robustness, in order to identify a suitable model for indoor transient particle transport simulations. All the three models can predict transient particle transport in enclosed environments with a similar accuracy.With the same time step size and grid number, the Markov chain model was the fastest among the three models. Unless super-find grid was used, the Eulerian model was faster than the Lagrangian model. The Eulerian and Lagrangian models were more robust than the Markov chain model, because the Markov chain model was sensitive to the time step size.

8.2 Future Work

This investigation performed numerical simulations to assess the influence of mouth coverings on the receptor’s exposure to exhaled particles. It was found that covering a cough with a tissue, a cupped hand, or an elbow can significantly reduce the horizontal velocity and cause the particles to move upward with the thermal plumes generated by a

human body. However, mouth covering not only can re-direct the exhaled airflow but also can remove a portion of the coughed droplets. The removal of coughed droplets by the mouth covering is attributed by the mechanism of particle deposition (Lai, 2002), which deserves further experimental and detailed numerical study. In addition, this study only considered the coughing scenarios, while the sneezing scenarios are equally important, which deserves further investigation.

For the Markov chain model developed in this study, a major limitation is the assumption of a steady-state airflow field. For instance, some sources could change the airflow pattern, such as a powerful cough or sneeze from an uncovered mouth. In these cases, the probability transition matrix would also change. Therefore, in the future, it is worthwhile to develop an improved Markov chain model for transient particle transport under unsteady-state airflow conditions.

Furthermore, the newly developed Markov chain model can only account for the mechanisms of advection and turbulence diffusion. It cannot account for other mechanisms of particle dispersion such as gravitational settling and thermophoresis, as well as particle deposition onto the surfaces. On the other hand, the Markov chain model can currently only calculate the transient particle transport from a single pulsed source. Also the requirement of a small time step size is a shortcoming of the Markov chain model. Nevertheless, the Markov chain model generally uses far less computing cost compared with the other two models. Therefore, it is worthwhile to develop an improved Markov chain model for transient particle transport which can account for these influencing factors.

In addition, this investigation did not consider the effect of virus survival on the receptor's exposure. There are several environmental parameters affecting the survival of virus, such as humidity, temperature, ultraviolet (UV) radiation and ozone reaction (Weber and Stilianakis, 2008). For instance, given the first-order inactivation rate reported by Hemmes et al. (1960), in an environment with a relative humidity at 15 to 40%, 21.9% of the influenza A virus would be inactivated after 30 minutes in the air. This implies that, although covering a cough cannot avoid the indirect exposure, it can

delay the exposure so that a portion of virus could be inactivated. Thus, this characteristic further enhances the effectiveness of covering a cough on the receptor's exposure to virus particles, which deserves further detailed study.

LIST OF REFERENCES

LIST OF REFERENCES

ANSYS. 2010. Fluent 12.1 Documentation. Fluent Inc., Lebanon, NH.

ASHRAE/ASHE Standard, 170-2008. 2008. Ventilation of Health Care Facilities. Atlanta: American Society of Heating, Refrigerating, and Air-conditioning Engineers.

Axley, J. 2007. Multizone airflow modeling in buildings: History and theory. HVAC&R Research 13, 907-928.

Bolster, D.T. and Linden, P.F. 2009. Particle transport in low-energy ventilation systems. Part 2: Transients and experiments, Indoor Air 19, 130-144.

Center for Disease Control and Prevention (CDC). 2005. Guidelines for preventing the transmission of mycobacterium tuberculosis in health-care settings, 2005. Morbidity and Mortality Weekly Report (MMWR) 54 (17): 1-141.

Center for Disease Control and Prevention (CDC). 2009. Cover your cough. (website available: http://www.cdc.gov/flu/protect/covercough.htm)

Chao, C.Y.H. and Wan, M.P. 2006. A study of the dispersion of expiratory aerosols in unidirectional downward and ceiling-return type airflows using a multiphase approach. Indoor Air 16, 296-312.

Chao, C.Y.H., Wan, M.P., Morawska, L., Johnson, G.R., Ristovski, Z.D., Hargreaves, M., Mengersen, K., Corbett, S., Li, Y., Xie, X. and Katoshevski, D. 2009. Characterization of expiration air jets and droplet size distributions immediately at the mouth opening. Journal of Aerosol Science 40, 122-133.

Chen, C. and Zhao, B. 2010. Some questions on dispersion of human exhaled droplets in ventilation room: Answers from numerical investigation. Indoor Air 20, 95-111.

Chen, C., Zhao, B., Cui, W., Dong, L., An, N. and Ouyang, X. 2010. The effectiveness of an air cleaner in controlling droplet/aerosol particle dispersion emitted from a patient's mouth in the indoor environment of dental clinics. Journal of the Royal Society Interface 7, 1105-1118.

Chen, C., Zhao, B., Yang, X. and Li, Y. 2011. Role of two-way airflow owing to temperature difference in severe acute respiratory syndrome transmission: revisiting the largest nosocomial severe acute respiratory syndrome outbreak in Hong Kong. Journal of the Royal Society Interface 8, 699-710.

Chen, C., Zhao, B., Zhou, W., Jiang, X. and Tan, Z. 2012. A methodology for predicting particle penetration factor through cracks of windows and doors for actual engineering application. Building and Environment 47, 339-348.

Chen, F., Yu, S.C.M. and Lai, A.C.K., 2006. Modeling particle distribution and deposition in indoor environments with a new drift-flux model. Atmospheric Environment 40, 357–367.

Chen, Q. 1996. Prediction of room air motion by Reynolds-stress models. Building and Environment 31, 233-244.

Chen, Q. 2009. Ventilation performance prediction for buildings: A method overview and recent applications. Building and Environment 44, 848-858.

Chen, Q. and Glicksman, L. 2003. System Performance Evaluation and Design Guidelines for Displacement Ventilation. Atlanta: ASHRAE.

Chen, Q. and Xu, W. 1998. A zero-equation turbulence model for indoor airflow simulation. Energy and Buildings 28, 137-144.

Ching, W. H., Leung, M. K. H., Leung, D. Y. C., Li, Y. and Yuen, P. L. 2008. Reducing risk of airborne transmitted infection in hospitals by use of hospital curtains. Indoor and Built Environment 17: 252–259.

Choudhury D. 1993. Introduction to the renormalization group method and turbulence modeling, Canonsburg, Fluent Inc. Technical Memorandum TM-107.

Cole, E.C. and Cook, C.E. 1998. Characterization of infectious aerosols in health care facilities: An aid to effective engineering controls and preventive strategies. American Journal of Infection Control 26, 453–464.

Courant, R., Friedrichs, K. and Lewy, H. 1928. On the partial difference equations of mathematical physics. IBM Journal of Research and Development 11, 215–234.

Davidson, L., Nielsen, P.V. and Sveningsson, A. 2003. Modification of the v2f model for computing the flow in a 3D wall jet. Turbulence, Heat and Mass Transfer 4, 577-84.

Davies, A., Thompson, K.A., Giri, K., Kafatos, G., Walker, J. and Bennett, A. 2013. Testing the efficacy of homemade masks: would they protect in an influenza pandemic? Disaster Medicine and Public Health Preparedness 7, 413-418.

Decramer, M., Janssens, W. and Miravitlles, M. 2012. Chronic obstructive pulmonary disease. Lancet 379, 1341-1351.

Diaz, K.T. and Smaldone, G.C. 2010. Quantifying exposure risk: surgical masks and respirators. American Journal of Infection Control 38, 501-508.

Duguid, J.F. 1945. The numbers and the sites of origin of the droplets expelled during expiratory activities. Edinburgh Medicine Journal 52, 335-340.

Durrett, R. 2010. Probability: Theory and Examples, 4th Edition. Cambridge University Press, New York.

Dye, C., Scheele, S., Dolin, P., Pathania, V. and Raviglione, M.C. 1999. Global burden of tuberculosis: estimated incidence, prevalence, and mortality by country. Journal of American Medicine Association 282, 677-68.

Fairchild, C.I. and Stamper, J.F. 1987. Particle Concentration in Exhaled Breath. American Industrial Hygiene Association Journal 48, 948–949.

Gao, N. and Niu, J. 2007. Modeling particle dispersion and deposition in indoor environments. Atmospheric Environment 41, 3862-3876.

Gao, N., He, Q. and Niu, J. 2012a. Numerical study of the lock-up phenomenon of human exhaled droplets under a displacement ventilated room. Building Simulation 5, 51–60.

Gao, X., Li, Y., Xu, P. and Cowling, B.J. 2012b. Evaluation of intervention strategies in schools including ventilation for influenza transmission control. Building Simulation 5: 29–37.

Germano, M., Piomelli, U., Moin, P. and Cabot, W.H. 1996. Dynamic subgrid-scale eddy viscosity model. In Summer Workshop, Center for Turbulence Research, Stanford, CA.

Gibson, M.M. and Launder, B.E. 1978. Ground effects on pressure fluctuations in the atmospheric boundary layer. Journal of Fluid Mechanics 86, 491-511.

Green, C.F., Davidson, D.S., Panlilio, A.L., Jensen, P.A., Jin, Y., Gibbs, S.G. and Scarpino, P.V. 2012. Effectiveness of selected surgical masks in arresting vegetative cells and endospores when worn by simulated contagious patients. Infection Control and Hospital Epidemiology 33, 487-494.

Gupta, J.K. 2010. Respiratory exhalation/inhalation models and prediction of airborne infection risk in an aircraft cabin. PhD Thesis, School of Mechanical Engineering, Purdue University.

Gupta, J.K., Lin, C.-H. Chen, Q. 2009. Flow dynamics and characterization of a cough. Indoor Air 19, 517-525.

Gupta, J.K., Lin, C.-H. and Chen, Q. 2010. Characterizing exhaled airflow from breathing and talking. Indoor Air 20, 31-39.

Gupta, J.K., Lin, C.-H. and Chen, Q. 2011a. Transport of expiratory droplets in an aircraft cabin. Indoor Air 21, 3-11.

Gupta, J.K., Lin, C.-H. and Chen, Q. 2011b. Inhalation of expiratory droplets in aircraft cabin, Indoor Air 21, 341–350.

Gupta, J.K., Lin, C.-H. and Chen, Q. 2012. Risk assessment for airborne infectious diseases in aircraft cabins, Indoor Air 22:388-395.

Hang, J., Li, Y. and Jin, R. 2014. The influence of human walking on the flow and airborne transmission in a six-bed isolation room: Tracer gas simulation. Building and Environment 77, 119-134.

He, Q., Niu, J., Gao, N., Zhu, T. and Wu, J. 2011. CFD study of exhaled droplet transmission between occupants under different ventilation strategies in a typical office room. Building and Environment 46, 397-408.

Hemmes, J.H., Winkler, K.C. and Kool, S.M. 1960. Virus survival as a seasonal factor in influenza and poliomyelitis. Nature 188, 430-431.

Hinds, W.C. 1999. Aerosol Technology: Properties, Behavior, and Measurement of Airborne Particles, 2nd edition. New York: Wiley.

ISO. 2007. Respiratory protective devices—human factors. Part 1. Metabolic rates and respiratory flow rates. Geneva: ISO/TS, 16976-1.

Jones, R.M., Masago, Y., Bartrand, T., Nicas, M. and Rose J.B. 2009. Characterizing the risk of infection from mycobacterium tuberculosis in commercial passenger aircraft using quantitative microbial risk assessment. Risk Analysis 29, 355 – 365.

Jones, R.M. and Nicas, M. 2014. Benchmarking of a Markov multizone model of contaminant transport, Annals of Occupational Hygiene 58, 1018-1031.

Jones, R.M. and Nicas, M. 2014. Experimental evaluation of a Markov multizone model of particulate contaminant transport, Annals of Occupational Hygiene 58, 1032-1045.

Khan, K., Arino, J., Hu, W., Raposo, P., Sears, J., Calderon, F., Heidebrecht, C., Macdonald, M., Liauw, J., Chan, A. and Gardam, M. 2009. Spread of a Novel Influenza A (H1N1) Virus via Global Airline Transportation. New Englnd Journal of Medicine 361, 212-214.

Kenyon, TA., Valway, SE., Ihle, WW., Onorato, IM., and Castro, KG. 1996. Transmission of multidrug resistant mycobacterium tuberculosis during a long airplane flight. New England Journal of Medicine 334, 933-938.

Klepeis, N.E., Nelson, W.C., Ott, W.R., Robinson, J.P., Tsang, A.M., Switzer, P., Behar, J.V., Hern, S.C. and Engelmann, W.H. 2001. The National Human Activity Pattern Survey (NHAPS): a resource for assessing exposure to environmental pollutants. Journal of Exposure Analysis and Environmental Epidemiology 11, 231–252.

Klepeis, N.E. and Nazaroff, W.W. 2002. Characterizing size-specific ETS particle emissions Indoor Air 2, 162-167.

Kirking, H.L., Cortes, J., Sherry, B., Hall, A.J., Cohen, N.J., Lipman, H., Kim, C., Daly, E.R. and Fishbein, D.B. 2010. Likely Transmission of Norovirus on an Airplane, October 2008. Clinical Infectious Diseases 50, 1216-1221.

Ko, G., Thompson, K.M. and Nardell, E.A. 2004. Estimation of tuberculosis risk on a commercial airliner. Risk Analysis 24, 379–88.

Launder, B.E., and Sharma, B.I. 1974. Application of the energy dissipation model of turbulence to the calculation of flow near a spinning disk. Letters in Heat Mass Transfer 1, 131-38.

Launder, B.E. and Spalding, D.B. 1974. The numerical computation of turbulent flows. Computer Methods in Applied Mechanics and Energy 3, 269-289.

Lai, A.C.K. 2002. Particle deposition indoors: a review. Indoor Air 12, 211-214.

Lai, A.C.K. and Wong, S.L. 2010. Experimental investigation of exhaled aerosol transport under two ventilation systems. Aerosol Science and Technology 44, 444–452.

Lai, A.C.K. and Wong, S.L. 2011. Expiratory aerosol transport in a scaled chamber under a variety of emission characteristics: an experimental study. Aerosol Science Technology 45, 899–907.

Lai, A.C.K., Poon, C.K.M. and Cheung, A.C.T. 2012. Effectiveness of facemasks to reduce exposure hazards for airborne infections among general populations. Journal of the Royal Society Interface 9, 938-948.

Lai, A.C.K., Poon, C.K.M. and Cheung, A.C.T. 2012. Effectiveness of facemasks to reduce exposure hazards for airborne infections among general populations. Journal of the Royal Society Interface 9, 938-948.

Lau, J. and Chen, Q. 2007. Floor-supply displacement ventilation for workshops. Building and Environment. 42, 1718-1730.

Li, X., Niu, J. and Gao, N. 2011. Spatial distribution of human respiratory droplet residuals and exposure risk for the co-occupant under different ventilation methods. HVAC&R Research 17, 432–445.

Li, X., Niu, J. and Gao, N. 2013. Co-occupant's exposure of expiratory droplets—Effects of mouth coverings. HVAC&R Research 18, 575–587.

Li, Y., Huang, X., Yu, I.T., Wong, T.W. and Qian, H. 2005. Role of air distribution in SARS transmission during the largest nosocomial outbreak in Hong Kong. Indoor Air 15, 83–95.

Li, Y., Leung, G.M., Tang, J.W., Yang, X., Chao, C., Lin, J.H., Lu, J.W., Nielsen, P.V., Niu, J.L., Qian, H., Sleigh, A.C., Su, H.J., Sundell, J., Wong, T.W. and Yuen, P.L. 2007. Role of ventilation in airborne transmission of infectious agents in the built environment – a multidisciplinary systematic review. Indoor Air 17, 2–18.

Lilly, D.K. 1992. A proposed modification of the Germano subgrid-scale closure model. Physics of Fluids 4, 633-635.

Liu, W., Wen, J., Chao, J., Yin, W., Shen, C., Lai, D., Lin, C.-H., Liu, J., Sun, H. and Chen, Q. 2012. Accurate and high-resolution boundary conditions and flow fields in the first-class cabin of an MD-82 commercial airliner. Atmospheric Environment 56, 33-44.

Liu, W., Wen, J., Lin, C.-H., Liu, J., Long, Z. and Chen, Q. 2013. Evaluation of various categories of turbulence models for predicting air distribution in an airliner cabin. Building and Environment 65, 118-131.

Loudon, R.G. and Roberts, R.M. 1967. Relation between the airborne diameter of respiratory droplets and the diameter of the stains left after recovery. Nature 213, 95–96.

Mangili, A., Gendreau, M.A., 2005. Transmission of infectious disease during commercial air travel. Lancet 365, 989-996.

Mansour, M.M. and Smaldone, G.C. 2013. Respiratory source control versus receiver protection: impact of facemask fit. Journal of Aerosol Medicine and Pulmonary Drug Delivery 26, 131-137.

Marple, V.A. and Liu, B.Y.H. 1974. Characteristics of laminar jet impactors, Environmental Science and Technology 8, 648-654.

Megri, A.C. and Haghighat, F. 2007. Zonal modeling for simulating indoor environment of buildings: review, recent developments, and applications. HVAC&R Research 13, 887-905.

Memarzadeh, F. and Xu, W. 2012. Role of air changes per hour (ACH) in possible transmission of airborne infections. Building Simulation 5, 15–28.

Menter, F.R. 1992. Improved two-equation k-w turbulence model for aerodynamic flows. ASA TM-103975.

Menter, F.R. 1994. Two-equation eddy-viscosity turbulence models for engineering applications. AIAA Journal 32, 1598-1605.

Milton, D.K., Fabian, M.P., Cowling, B.J., Grantham, M.L. and McDevitt, J.J. 2013. Influenza virus aerosols in human exhaled breath: particle size, culturability, and effect of surgical masks. PLoS Pathogens 9, e1003205.

Morawska, L. 2006. Droplet fate in indoor environments, or can we prevent the spread of infection? Indoor Air 16, 335–347.

Morawska, L., Johnson, G.R., Ristovski, Z.D., Hargreaves, M., Mengersen, K., Corbett, S., Chao, C.Y.H., Li, Y. and Katoshevski, D. 2009. Size distribution and sites of origin of droplets expelled from the human respiratory tract during expiratory activities. Journal of Aerosol Science 40, 256-269.

Morsi, S.A. and Alexander, A.J. 1972. An investigation of particle trajectories in two-phase flow systems. Journal of Fluid Mechanics 55, 193-208.

Moser, M.R., Bender, T.R., Margolis, H.S., Noble, G.R., Kendal, A.P. and Ritter, D.G. 1979. An outbreak of influenza aboard a commercial airliner. American Journal of Epidemiology 110, 1-6.

Murakami, S., Kato, S. and Kondo, Y. 1990. Examining k-e EVM by means of ASM for a 3-D horizontal buoyant jet in enclosed space. International Symposium on Engineering Turbulence Modelling and Measurements, Dubrovnik: ICHMT.

Murakami, S., Kato, S., Nagano, S. and Tanaka, S. 1992. Diffusion characteristics of airborne particles with gravitational settling in a convection-dominant indoor flow field, ASHRAE Transaction 98, 82–97.

Nicas, M., 2000. Markov modeling of contaminant concentrations in indoor air. American Industrial Hygiene Association Journal 61, 484–491.

Nicas, M., Nazaroff, W.W., Hubbard, A. 2005. Toward understanding the risk of secondary airborne infection: Emission of respirable pathogens. Journal of Occupational and Environmental Hygiene 2, 143–154.

Nielsen, P.V., Li, Y., Buus, M. and Winther, F.V. 2010. Risk of cross-infection in a hospital ward with downward ventilation. Building and Environment 45, 2008–2014.

Olmedo, I., Nielsen, P.V., Ruiz de Adana, M., Jensen, R.L. and Grzelecki, P. 2012. Distribution of exhaled contaminants and personal exposure in a room using three different air distribution strategies. Indoor Air 22, 64–76.

Olsen, S.J., Chang, H., Cheung, T.Y., Tang, A.F., Fisk, T.L., Ooi, S.P., Kuo, H., Jiang, D.D., Chen, K., Lando, J., Hsu, K., Chen, T. and Dowell, S.F. 2003 Transmission of the severe acute respiratory syndrome on aircraft. New England Journal of Medicine 349, 2416-2422.

Papineni R.S. and Rosenthal F.S. 1997. The size distribution of droplets in the exhaled breath of healthy human subjects. Journal of Aerosol Medicine 10, 105–116.

Qian, H., Li, Y., Nielsen, P.V., Hyldgaard, C.E., Wong, T.W. and Chwang, A.T.Y. 2006. Dispersion of exhaled droplet nuclei in a two-bed hospital ward with three different ventilation systems. Indoor Air 16, 111–128.

Renz, U. and Terhaag, U. 1990. Predictions of air flow pattern in a room ventilated by an air jet, the effect of turbulence model and wall function formulation. Proceeding of Roomvent '90: 18.1-18.15, Oslo.

Ross, S.M. 1996. Stochastic Processes, 2nd Edn. John Wiley & Sons, Inc.

Seepana, S. and Lai, A.C.K. 2012. Experimental and numerical investigation of interpersonal exposure of sneezing in full-scale chamber. Aerosol Science and Technology 46, 485–493.

Shih, T., Liou, W., Shabbir, A., Yang, Z. and Zhu, J. 1995. A new k–e eddy viscosity model for high Reynolds number turbulent flows. Journal Computer Fluids 24, 227-238.

Shur, M., Spalart, P. R., Strelets, M. and Travin, A. 1999. Detached-eddy simulation of an airfoil at high angle of attack. In 4th International Symposium on Engineering Turbulence Modeling and Experiments, Corsica, France.

Smagorinsky, J. 1963. General circulation experiments with the primitive equations I: the basic experiment. Monthly Weather Review 91, 99-164.

Song, F., Zhao, B., Yang, X., Jiang, Y., Gopal, V., Dobbs, G. and Sahm, M. 2008. A new approach on zonal modeling of indoor environment with mechanical ventilation. Building and Environment 43, 278-286.

Spalart, P. and Allmaras, S. 1992. A one-equation turbulence model for aerodynamic flows. Technical Report AIAA-92-0439, AIAA.

Student. 1908. The probable error of a mean. Biometrika 6, 1-25.

Sze To, G.N. and Chao, C.Y.H. 2010. Review and comparison between the Wells–Riley and dose-response approaches to risk assessment of infectious respiratory diseases. Indoor Air 20, 2–16.

Tang, J.W., Path, F.R.C. and Settles, G.S. 2008. Coughing and aerosols. New England Journal of Medicine 359, E19-E19.

Tang, J.W. and Settles, G.S. 2009. Coughing and Masks. New England Journal of Medicine 361, E62-E62.

Tang, J.W., Liebner, T.J., Craven, B.A. and Settles, G.S. 2009. A schlieren optical study of the human cough with and without wearing masks for aerosol infection control. Journal of Royal Society Interface 6, S727-736.

Tang, J.W., Nicolle, A.D., Pantelic, J., Jiang, M., Sekhr, C., Cheong, D.K. and Tham, K.W. 2011. Qualitative real-time schlieren and shadowgraph imaging of human exhaled airflows: an aid to aerosol infection control. PLoS One 6, e21392.

Tang, J.W., Nicolle, A.D., Pantelic, J., Koh, G.C., Wang, L.D., Amin, M., Klettner, C.A., Cheong, D.K., Sekhar, C. and Tham, K.W. 2012. Airflow dynamics of coughing in healthy human volunteers by shadowgraph imaging: an aid to aerosol infection control. PLoS One 7, e34818.

US DOT (United States Department of Transportation), 2011. 2010 Traffic Data for U.S Airlines and Foreign Airlines U.S. Flights: Total Passengers up from 2009, Still Below 2008, Washington DC.

Viboud, C., Boelle, P.Y. and Pakdaman, K. 2004. Influenza epidemics in the United States, France, and Australia, 1972–1997. Emergence Infectious Diseases 10, 32–39.

Walkinshaw, D.S., 2010. Germs, flying and the truth. ASHRAE Journal 52, 70-73.

Wang, M. and Chen, Q. 2009. Assessment of various turbulence models for transitional flows in enclosed environment. HVAC&R Research 15, 1099-1119.

Wang, M., Lin, C.-H. and Chen, Q. 2012. Advanced turbulence models for predicting particle transport in enclosed environment. Building and Environment 47, 40-49.

Weber, T.P. and Stilianakis, N.L. 2008. Inactivation of influenza A viruses in the environment and modes of transmission: A critical review. Journal of Infection 57, 361-373.

WHO, 2002. Bulletin of the World Health Organization; 80 (3): 261.

World Bank 2005. http://web.worldbank.org/WBSITE/EXTERNAL/NEWS/0,,contentMDK :20715408~pagePK:64257043~piPK:437376~theSitePK:4607,00.html

Wilcox, D.C. 1988. Reassessment of the scale-determining equation for advanced turbulence models. AIAA Journal 26, 1299-1310.

Yang, S., Lee, G.W.M., Chen, C.M., Wu, C.C. and Yu, K.P. 2007. The size and concentration of droplets generated by coughing in human subjects. Journal of Aerosol Medicine 20, 484–494.

Yang, Y., Chan, W.Y., Wu, C.L., Kong, R.Y.C. and Lai, A.C.K. 2012. Minimizing the exposure of airborne pathogens by upper-room ultraviolet germicidal irradiation: an experimental and numerical study. Journal of the Royal Society Interface 9, 3184-3195.

Yakhot, V. and Orszag, S.A. 1986. Renormalization group analysis of turbulence. Journal of Scientific Computing 1, 3-51.

Yin, Y., Gupta, J.K., Zhang, X., Liu, J. and Chen, Q., 2011. Distributions of respiratory contaminants from a patient with different postures and exhaling modes in a single-bed inpatient room. Building and Environment 46, 75-81.

You, R. and Zhao, B. 2013. A simplified method for assessing particle deposition rate in aircraft cabins, Atmospheric Environment 67, 80-84.

Zhang, L. and Li, Y. 2012. Dispersion of coughed droplets in a fully-occupied high-speed rail cabin. Building and Environment 47, 58-66.

Zhang, N., Zheng, Z., Eckels, S., Nadella, V.B. and Sun, X. 2009. Transient response of particle distribution in a chamber to transient particle injection, Particle & Particle Systems Characterization 26, 199-209.

Zhang, Z. and Chen, Q. 2006. Experimental measurements and numerical simulations of particle transport and distribution in ventilated rooms. Atmospheric Environment, 40, 3396-3408.

Zhang, Z., Zhai, Z.Q., Zhang, W. and Chen, Q. 2007. Evaluation of various turbulence models in predicting airflow and turbulence in enclosed environments by CFD: part 2 - comparison with experimental data from literature. HVAC&R Research 13, 871-886.

Zhang, Z., Chen, X., Mazumdar, S., Zhang, T. and Chen, Q. 2009. Experimental and numerical investigation of airflow and contaminant transport in an airliner cabin mockup. Building and Environment 44, 85-94.

Zhao,B., Chen,C. and Tan, Z. 2009. Modeling of ultrafine particle dispersion in indoor environments with an improved drift flux model. Journal of Aerosol Science 40, 29–43.

Zhao, B., Zhang, Y., Li, X., Yang, X. and Huang, D. 2004. Comparison of indoor aerosol particle concentration and deposition in different ventilated rooms by numerical method. Building and Environment 39, 1-8.

Zhu, S., Kato, S., and Yang, J.H. 2006. Study on transport characteristics of saliva droplets produced by coughing in a calm indoor environment. Building and Environment 41, 1691-1702.

Zhu, Y., Zhao, B., Zhou, B. and Tan, Z. 2012. A particle resuspension model in ventilation ducts. Aerosol Science and Technology 46, 222-235.

APPENDICES

Appendix A. Steady-State Particle Transport Simulations

A1 Introduction

Ventilation mode, ventilation rate, and person-to-person distance are among the factors that may influence person-to-person contaminant transport in enclosed spaces. A number of studies have focused on these influencing factors. The first factor, ventilation mode, was investigated by Qian et al. (2006) and Yin et al. (2011); they compared the effectiveness of mixing and displacement ventilation in controlling person-to-person contaminant transport in hospital wards. Lai and Wong (2010, 2011) and Olmedo et al. (2012) experimentally investigated person-to-person contaminant transport in laboratory chambers with mixing and displacement ventilation. There are more than 30 cases comparing the effect of mixing and displacement ventilation on person-to-person contaminant transport available in these studies. However, fewer studies are available in the literature for another commonly used ventilation mode, the Under-Floor Air-Distribution (UFAD) system (He et al., 2011; Li et al., 2011).

In regard to the second factor, ventilation rate, Qian et al. (2006) experimentally investigated its effect on person-to-person contaminant transport in a hospital ward with a displacement ventilation system. Nielsen et al. (2010) compared the person-to-person contaminant exposure in a hospital ward with ventilation rates of 6, 9, and 10 ACH. In addition, Yin et al. (2011) compared the person-to-person contaminant exposure in an inpatient room with ventilation rates of 4 and 6 ACH. However, in most of these cases, the patients were lying in beds, which may not be representative of normal scenarios such as working in an office.

The third factor, person-to-person distance, was investigated by Qian et al. (2006); they assessed its effect on person-to-person contaminant transport in a hospital ward with a ventilation rate of 4 ACH. Recently, Olmedo et al. (2012) experimentally investigated the effect of person-to-person distance on exhaled contaminant transport in a room with a

ventilation rate of 5.6 ACH. However, the effect of person-to-person distance on exhaled contaminant transport under high ventilation rates has not been well understood.

The review of existing studies shows that additional cases of person-to-person contaminant transport are needed to in order to address the limitations discussed above. Thus, this study aims to develop a database and systematically investigate the general effect of ventilation mode, ventilation rate, and person-to-person distance on person-to-person contaminant transport in mechanically ventilated spaces.

A2 Methods

A2.1 Developing a Database from the Literature

This study first collected the cases available in the literature to create a database. Note that different studies used different units or normalization methods for the exposure data. Thus, the selected studies must be comparative so that the relative effects of the target factors on person-to-person contaminant transport can be calculated for each individual study. In this investigation, the relative effect of ventilation mode on exposure was calculated for each study by:

$$E^*_{\text{mod}} = \frac{E}{E_{mixing}} \tag{A1}$$

where E is the exposure for a particular case, and E_{mixing} is the average exposure for mixing ventilation in that study. Thus, the relative effects of ventilation mode on exposure could be compared among different studies. The database from the literature included 32, 34, and 4 cases for mixing ventilation, displacement ventilation, and UFAD systems, respectively.

Because all the collected studies included at least one case with a ventilation rate of 6 ACH, the relative effect of ventilation rate was calculated by:

$$E^*_{ACR} = \frac{E}{E_{6ACH}} \tag{A2}$$

where E_{6ACH} is the average exposure at a ventilation rate of 6 ACH for each study. The database from the literature contained 23, 20, 15, and 15 cases for 4, 6, 9, and 10 ACH, respectively.

Because all the collected studies included at least one case with a person-to-person distance of 1.1 m, the relative effect of person-to-person distance was calculated by:

$$E^*_{dis} = \frac{E}{E_{1.1m}} \tag{A3}$$

where $E_{1.1m}$ is the average exposure of the cases with a person-to-person distance of 1.1 m for each study. There are 40 cases for different person-to-person distances available in the literature.

A2.2 Adding Necessary Cases to the Database

As discussed in the introduction, the effect of the UFAD system on controlling person-to-person contaminant transport has not been thoroughly studied. Thus, this study added 24 UFAD system cases with different ventilation rates and person-to-person distances to the database. The ventilation rate varied from 3 to 9 ACH, which is a reasonable range for common indoor environments. The person-to-person distance varied from 0.5 to 1.8 m,

which corresponds to common scenarios in a two-person office. Because only comparative data could be used for the database, 12 mixing ventilation and 12 displacement ventilation cases were also set up for comparison with the UFAD systems. Table A1 lists detailed information about ventilation mode, ventilation rate, and person-to-person distance for the cases added to the database.

Table A1. Case setup for this study.

Case	Mode	ACR (ACH)	Dis. (m)	Exp.	CFD
1	UFAD	3	0.5	√	√
2	UFAD	3	0.8		√
3	UFAD	3	1.1	√	√
4	UFAD	3	1.8		√
5	UFAD	5	0.5		√
6	UFAD	5	0.8		√
7	UFAD	5	1.1		√
8	UFAD	5	1.8		√
9	UFAD	6	0.5	√	√
10	UFAD	6	0.8		√
11	UFAD	6	1.1	√	√
12	UFAD	6	1.8		√
13	UFAD	7	0.5		√
14	UFAD	7	0.8		√
15	UFAD	7	1.1		√
16	UFAD	7	1.8		√
17	UFAD	8	0.5		√
18	UFAD	8	0.8		√
19	UFAD	8	1.1		√
20	UFAD	8	1.8		√
21	UFAD	9	0.5	√	√
22	UFAD	9	0.8		√
23	UFAD	9	1.1	√	√
24	UFAD	9	1.8		√
25	Mixing	3	0.5		√
26	Mixing	3	1.1		√
27	Mixing	5	0.5		√
28	Mixing	5	1.1		√
29	Mixing	6	0.5		√

Table A1. continued.

30	Mixing	6	1.1		√
31	Mixing	7	0.5		√
32	Mixing	7	1.1		√
33	Mixing	8	0.5		√
34	Mixing	8	1.1		√
35	Mixing	9	0.5		√
36	Mixing	9	1.1		√
37	Displace	3	0.5		√
38	Displace	3	1.1		√
39	Displace	5	0.5		√
40	Displace	5	1.1		√
41	Displace	6	0.5		√
42	Displace	6	1.1		√
43	Displace	7	0.5		√
44	Displace	7	1.1		√
45	Displace	8	0.5		√
46	Displace	8	1.1		√
47	Displace	9	0.5		√
48	Displace	9	1.1		√

In addition, the literature assessed the effect of ventilation rate on the transport of contaminants exhaled only by reclining patients, which may not be representative of normal scenarios such as working in an office. Although the patient room settings are more likely to a concern for infectious disease transmission, numerous studies have focused on the contaminant transport in hospital environments (Chen et al., 2010; Chen et al., 2011; Ching et al., 2008; Nielsen et al., 2010; Qian et al., 2006; Yin et al., 2011). The office settings where people spend considerable time are also important, since the cross infections occurring in the offices are strongly related to working efficiency and productivity. Therefore, this study investigated person-to-person contaminant transport in an office with different ventilation rates to extend the knowledge in this area. The schematic of the office is depicted in Figure 3-1(a). There were two seated persons with a height of 1.2 m, two personal computers, and two desks in the office. The following section details the strategy for obtaining person-to-person contaminant exposure data.

A2.3 Obtaining Person-to-Person Contaminant Exposure Data

Compared with experimental measurements, Computational Fluid Dynamics (CFD) modeling is more cost-effective for obtaining person-to-person contaminant exposure data. However, the reliability of the CFD modeling should be verified. Thus, this study first conducted experimental measurements in the office to validate the model (Chapter 3), and then applied the model to obtain the exposure data for all the cases listed in Table A1.

Because the UFAD system has not been well studied, the experiment was conducted for this system. Furthermore, because ventilation rate and person-to-person distance are the target parameters in this study, different ventilation rates and person-to-person distances were included in the experiment. Ventilation rates of 3, 6, and 9 ACH correspond to low, medium, and high ventilation, respectively, in normal indoor environments. Person-to-person distances of 0.5 and 1.1 m correspond to close and normal distances, respectively, for common scenarios. Table A1 also illustrates the measurement cases identified.

A3 Results

A3.1 Effect of Ventilation Mode

Using the 118 cases in the database that address ventilation mode, it is possible to study the effect of ventilation mode on person-to-person contaminant transport. Figure A1 compares the median value of the relative effect of mixing ventilation, displacement ventilation, and the UFAD system on person-to-person contaminant exposure. The lower and upper bounds of the error bars represent the 10^{th} and 90^{th} percentiles of the data from the database, respectively.

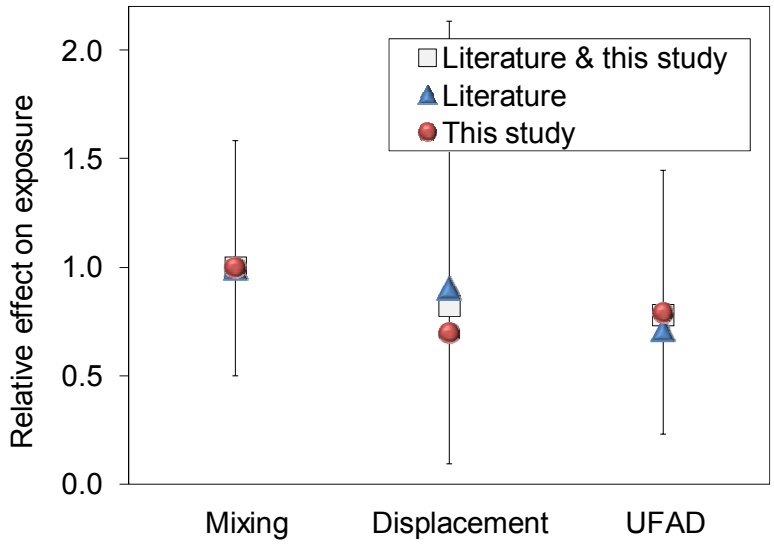

Figure A1. Relationship between ventilation mode and person-to-person contaminant exposure.

The median value of the relative effect from the literature and from this study is also shown separately in the figure. Because the reference for the relative effect was the person-to-person contaminant exposure under mixing ventilation, the median values of the relative effect for mixing ventilation from the literature and from this study were both close to 1.0. The median value of the relative effect for displacement ventilation from the literature was 0.91, while the median value from this study was 0.70. The difference may be attributed to the differences in scenarios. For instance, some cases from the literature were for the scenario of contaminant transport between reclining patients (Qian et al., 2006; Yin et al., 2011). The thermal plumes from the reclining patients tended to be weaker than those from the standing or seated persons in our study. Thermal plumes from the human body play an important role in the distribution of exhaled contaminants (Gao et al., 2012a). Weaker thermal plumes may reduce the chance of removal of exhaled contaminants by fresh air. When the relative effects from the literature and this study were combined, the median value of the relative effect for displacement ventilation was 0.82. The median values of the relative effect for the UFAD system from the literature and from this study were in good agreement. The median value from the combination of

the literature and this study for the UFAD system was 0.78. It can be seen that the deviation in the performance of displacement ventilation was larger than in that of mixing ventilation. The high exposure cases of displacement ventilation were the measurement cases by Olmedo et al. (2012) when the person-to-person distance was 0.35 m. Their measurements showed that, when the person-to-person distance was 0.35 m, the exposure under displacement ventilation was much higher than that under mixing ventilation.

Generally speaking, the performances of displacement ventilation and UFAD systems in controlling person-to-person contaminant transport were quite similar. They were about 20% better than mixing ventilation in reducing person-to-person contaminant exposure. Displacement ventilation and UFAD systems can be categorized as stratified air-distribution systems. The cool, fresh air from the inlets remains in the lower region of the room and then moves directly into the occupied zone because of thermal buoyancy. Thus, these systems have the potential to reduce person-to-person contaminant exposure and provide better indoor air quality, as compared with mixing ventilation. This finding is consistent with the results of many previous studies (Chen and Glicksman, 2003; Lau and Chen, 2006). However, Olmedo et al. (2012) pointed out that displacement ventilation may have poorer performance than mixing ventilation in controlling person-to-person exposure under certain circumstances. The large error bars shown in Figure 6 also indicate significant variations in the relative effects for different ventilation modes. The median value of the relative effect was 1.0 for mixing ventilation and around 0.8 for the displacement ventilation and UFAD systems. A factor of 1.25 may represent the general effect of ventilation mode on person-to-person contaminant transport in mechanically ventilated spaces.

A3.2 Effect of Ventilation Rate

Similarly, a total of 124 cases in the database could be used to study the effect of ventilation rate on person-to-person contaminant transport. Figure A2 shows the relationship between person-to-person contaminant exposure and ventilation rate. Each

symbol represents the median value of the relative effect for the corresponding ventilation rate. The lower and upper bounds of the error bars represent the 10th and 90th percentiles of the data, respectively. The median values of the relative effect from the literature and from this study are also shown separately in the figure. Because the reference for the relative effect was the person-to-person contaminant exposure under a ventilation rate of 6 ACH, the median values of the relative effect for 6 ACH from the literature and from this study were both close to 1.0. The trends of the relative effects on contaminant exposure versus ventilation rate in Figure 7 show that the results of this study matched well with those from the literature. However, the relative effect for 4 ACH from the literature seems to be lower than the general trend. The reason is unknown, but the difference is not significant. Combining the relative effects from the literature and from this study, a linear regression was performed for the median value of the relative effect with the corresponding ventilation rates. The correlation between ventilation rate and person-to-person contaminant transport is significant, with an R^2 of 0.87.

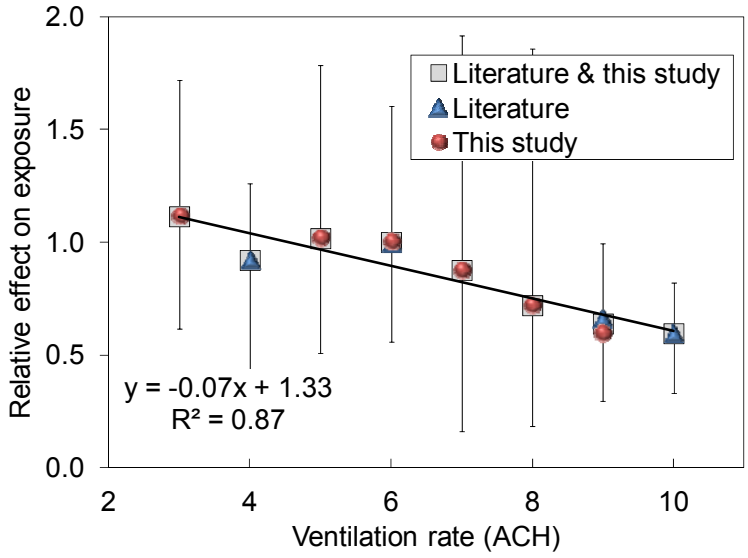

Figure A2. Relationship between ventilation rate and person-to-person contaminant exposure.

The database shows that the exposure was negatively associated with ventilation rate for all the ventilation modes. This finding makes sense because higher ventilation rate corresponds to higher dilution rate, which can reduce contaminant concentration in the breathing zone of the receptor. ASHRAE (2008) and CDC (2005) guidelines recommend a minimum ventilation rate of 12 ACH for hospital isolation rooms. These guidelines are evidence that ventilation rate is important in controlling person-to-person contaminant transport. Gao et al. (2012b) also indicated that increasing ventilation rate together with household isolation could be as effective as school closure for influenza transmission control in schools. However, the large error bars shown in Figure 7 imply significant variations in the relative effects of ventilation rate on person-to-person contaminant transport. Thus, other factors may modify the effect of ventilation rate. In addition, the median values of the relative effect on person-to-person contaminant exposure were 1.1 and 0.6 for ventilation rates of 3 and 10 ACH, respectively. This implies that an increase in ventilation rate by a factor of 3.3 resulted in a decrease of person-to-person contaminant transport by a factor of only 1.8. Memarzadeh and Xu (2012) also indicated that although increasing ventilation rate diluted concentrations more effectively when the contaminant source was constant, it did not necessarily increase the ventilation effectiveness. Thus, controlling person-to-person contaminant transport by increasing ventilation rate may have certain limitations.

A3.3 Effect of Person-to-Person Distance

Very similarly to the previous subsections, 88 cases in the database were available for studying the effect of person-to-person distance on person-to-person contaminant transport. Figure A3 shows the relationship between person-to-person contaminant exposure and person-to-person distance. Each symbol represents the median value of the cases at the corresponding person-to-person distance. The lower and upper bounds of the error bars represent the 10^{th} and 90^{th} percentiles of the data, respectively. The median values of the relative effect from the literature and from this study are also shown separately in the figure. Because the reference for the relative effects was the person-to-

person contaminant exposure at a distance of 1.1 m, the median values of the relative effect for 1.1 m from the literature and from this study should be close to 1.0, as confirmed in the figure. Most of the median values of the relative effect from the literature were close to those from this study, except at distances of 0.5 and 0.8 m. It is difficult for us to articulate the reason for these differences because there were many unknown factors. The differences are acceptable for our analysis in this investigation. Combining the relative effects from the literature and from this study, a power regression was performed for the median values of the relative effect with the corresponding person-to-person distances. An R^2 of 0.94 implies a strong correlation between person-to-person contaminant transport and person-to-person distance.

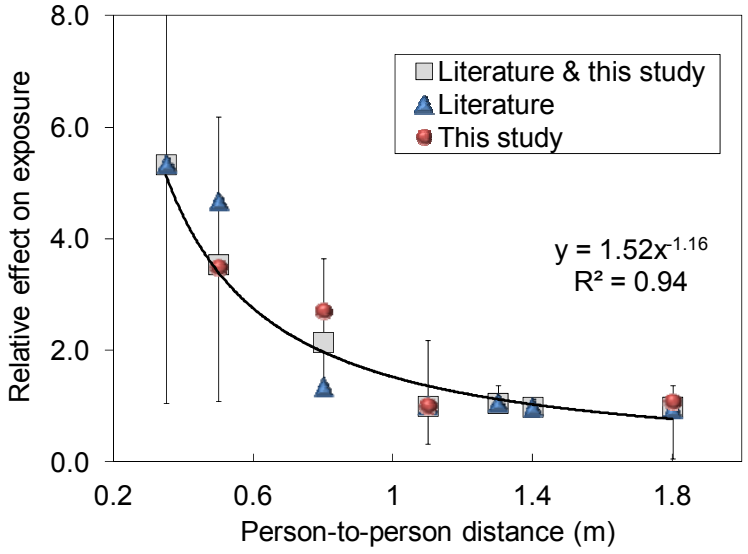

Figure A3. Relationship between person-to-person distance and person-to-person contaminant exposure.

It can be seen that when the person-to-person distance was smaller than 1.1 m, the relative effect on person-to-person contaminant exposure increased rapidly with the decrease in distance. However, when the person-to-person distance was larger than or equal to 1.1 m, the curve tended to be rather flat. This was because the contaminant

concentration gradient was larger near the source than in other locations. Thus, when the person-to-person distance increased to some extent, the influence of concentration gradient became insignificant. In this study, 1.1 m can be regarded as a cut-off person-to-person distance in terms of person-to-person contaminant transport. The median value of the relative effect on contaminant exposure was 5.3 for a distance of 0.35 m, and around 1 for a distance of 1.8 m. A factor of 5.3 indicates that person-to-person distance is a rather important parameter in terms of controlling person-to-person contaminant transport, when compared with ventilation mode and ventilation rate.

A4 Discussion

This study compared mixing, displacement, and UFAD ventilation systems, which are the most commonly used systems in residential or commercial buildings. However, other ventilation modes may also affect person-to-person contaminant transport. For instance, downward ventilation has been widely used in hospital wards or clean rooms. Qian et al. (2006) reported that downward and mixing ventilation had similar performance in a multi-bed hospital ward. Moreover, personalized ventilation has become a popular ventilation mode. He et al. (2011) concluded that personalized ventilation could increase contaminant concentration in the breathing zone of the receptor as well as provide clean personalized airflow. Whether person-to-person exposure could be reduced depends on the balance of the pros and cons of personalized ventilation.

Although the cases collected from the literature included both breathing and coughing cases, this study did not quantitatively assess the differences between breathing and coughing. The peak exhaled velocity of coughing is much higher than that of breathing. Thus, the contaminant exhaled by a cough tends to travel more quickly than by a breath. The model used in this study was for breathing cases, which can be regarded as a steady-state condition. If the transient particle transport resulting from a cough were investigated, the hybrid model developed and validated in our previous study could be used (Chen et al., 2013).

The key factor in contaminant transport is the "path" of airflow (Memarzadeh and Xu, 2012). The perfect "path" should be that the fresh air firstly goes through the receptor, then reaches to the source, and finally removes the contaminant to the exhaust. However, it is difficult to use a single parameter to describe the "path". The "path" depends on ventilation mode, ventilation rate, person-to-person distance, and other parameters. At the first stage of design, a designer needs to make a decision on what kind of ventilation mode should be used, how much ventilation is needed, and how far the person-to-person distance (e.g. desk-to-desk distance in an office) should be designed. The statistical results in this study can be a general guideline to support the designers' decisions at this stage. After that, if possible, the designer can use CFD technique to investigate the "path" in detail.

In addition to ventilation mode, ventilation rate, and person-to-person distance, which are among the ones that mostly related to HVAC design, other factors may influence person-to-person contaminant transport. Previous studies have reported that air cleaners have the potential to reduce person-to-person contaminant transport in hospital wards (Chen et al., 2010). Wearing masks has been identified as an effective method to reduce the risk of exposure to exhaled contaminants (Gupta et al., 2012; Lai et al., 2012). The use of air curtains may also reduce contaminant transport between two zones (Ching et al., 2008; Chen et al., 2011). Moreover, the use of upper-room ultraviolet germicidal irradiation (UVGI) has been proven effective in disinfecting exhaled airborne pathogens and reducing the risk of person-to-person exposure (Yang et al., 2012). Furthermore, the orientations of persons relative to one another (Olmedo et al., 2012) and the gestures of the persons can also influence person-to-person contaminant exposure.

A5 Conclusions

This appendix presents a systematic study of the effect of ventilation mode, ventilation rate, and person-to-person distance on person-to-person contaminant transport. This investigation collected a large quantity of data from the literature and used a validated

CFD model to generate additional data in order to establish a database. From this database, the following conclusions can be drawn:

(1) The overall performances of displacement ventilation and a UFAD system were similar in terms of reducing exposure to person-to-person contaminant transport, and the two systems were about 20% better than mixing ventilation.

(2) The data show that person-to-person contaminant exposure tended to be reduced with an increase in ventilation rate.

(3) When the person-to-person distance was less than 1.1 m, person-to-person contaminant exposure increased rapidly with distance. At a distance larger than 1.1 m, the effect of distance was insignificant.

(4) Person-to-person distance is more important than ventilation mode and ventilation rate in controlling person-to-person contaminant transport.

Appendix B. Developing A Zonal Markov Chain Model

B1 Introduction

In recent years, Computational Fluid Dynamics (CFD) has been widely used in modeling transient particle transport in mechanical ventilated spaces. The Eulerian and Lagrangian models have become increasingly popular for investigating interpersonal particle transport. However, when the source location is changed, even for a fixed airflow field, all of these models require recalculation of the particle equations, which requires considerable computing effort. Thus, it is worthwhile to develop an approach for quickly predicting transient particle transport in enclosed environments.

To quickly assess transient particle transport, Nicas (2000) applied the Markov chain technique in a zonal model. That study demonstrated the capability of the Markov chain technique in quickly predicting the spatial and temporal particle concentrations. However, this simple model failed to account for most of the particle dispersion mechanisms such as drag force, gravitational settling, and turbulent dispersion. Because CFD simulation can easily take these influencing factors into account, a combination of CFD with the Markov chain technique has the potential to significantly improve the zonal model. Therefore, this investigation aimed to develop and validate a zonal Markov chain model for predicting faster-than-real-time information about transient particle transport in enclosed environments.

B2 Methods

B2.1 Zonal Markov Chain Model

There are two assumptions in the first-order homogeneous Markov chain technique (Ross, 1996):

1) Any future state depends only on the present state as well as the probabilities of the state's changing;

2) These probabilities of the state's changing are time-independent (or fixed).

To satisfy these assumptions of the Markov chain technique, one should assume the inertial effect of particles to be negligible, which holds well for particles with a diameter smaller than 3 μm (Zhao et al., 2009; Yin et al., 2011). For particles with a diameter larger than 3 μm, if they are transported by an impinging jet with an extremely high velocity, the inertial impaction may significantly affect the particle transport (Chen et al., 2012). In such scenarios, the first-order homogeneous Markov chain method could have a large error. However, since most of the airflow in enclosed environment does not have strong impinging jets, this method still can be used for particles with a diameter larger than 3 μm. Since the coarse particles intend to rapidly deposit onto the floor, they may be less important in term of airborne infectious diseases transmission.

The equations of Markov chain model is the same as that described in section 6.1.1 (Eqs. (6.1)-(6.7)). The only difference is that zonal Markov chain model divides the room to only a few zones, while the Markov chain model developed in Chapter 6 works under a CFD grid. If the zones are of the same size, the resulting probability vector versus time can be regarded as the normalized particle concentrations (or normalized number of particles) versus the time in the zones. Therefore, the Markov chain technique can be used for predicting transient particle transport in enclosed environments. Moreover, for a fixed airflow, when the source location is changed, Eq. (6.6) can be used with an updated N_0 to quickly calculate the updated particle concentrations versus time. Note that the fixed airflow could be a problem if the source could change the airflow pattern, such as a powerful sneezing without covering the mouth. However, the experimental measurements and then computer simulation of airflow in an airliner cabin by Gupta et al. (2011) indicated that even a cough without covering mouth can have limited affect on the local airflow field but not the whole airflow field. If a mouth is covered when coughing or sneezing as people would usually do, the influence of coughing and sneezing on the airflow field would be minimal. Therefore, the assumption that airflow field was fixed should be valid for most of cases.

B2.2 Calculating the Transition Probability Matrix Using CFD

The key point in applying the Markov chain technique to the prediction of indoor particle transport is to obtain the transition probability matrix, p_{ij}. This study calculated the airflow field using CFD. Next, this investigation uniformly released a certain amount of particles in zone i, and used Lagrangian stochastic tracking to calculate the percentage of particles that moved from zone i to zone j in a certain time, Δt, which can be regarded as the p_{ij}. Repeating this process for all the zones, the whole transition probability matrix can be obtained. The following paragraphs detail the CFD model used in this study.

The Re-Normalization Group (RNG) k-ε model (Choudhury, 1993) was applied to calculate the airflow field. It has the best overall performance among all RANS models for enclosed environments (Zhang et al., 2007). A detailed discussion of the RNG k-ε model can be found in ANSYS (2010). The Lagrangian model was adopted to calculate the particle movements in Δt. Using the momentum equation based on Newton's law, the trajectory of each particle can be calculated. The transient process from a droplet to a droplet nucleus due to evaporation is negligible for particles with a diameter smaller than 3 μm (Chen and Zhao, 2010). The Discrete Random Walk (DRW) model (ANSYS, 2010) is used to calculate the turbulence dispersion.

Note that the time step of the Markov chain, Δt, is an important parameter that needs to be determined based on the ventilation rate of the space and the size of the divided zones. The Δt can be neither too short nor too long. If the Δt is too short, the particles may have no chance to "escape" from the current zone. If the Δt is too long, the particles may move across the adjacent zones so that the fact that they had appeared in these adjacent zones would be missed. Thus, the Δt should allow the particles to move only to the adjacent zones. In addition, to ensure the Δt to be suitable for all the zones, the sizes and dimensions of the zones should be similar. In this study, different time steps of the Zonal Markov chain model were tested for each case and the appropriate ones were then used. The specific formulas for determining the time step are not yet available. However, there may be two rules. First, the larger the air change rate is, the smaller the time step intends to be. Second, the smaller the size of the zones becomes, the smaller the time step intends

be. It would take less time for the particles to move across the adjacent zones when the size of the zones is smaller or the air change rate is larger.

B3 Validation

This study used three cases, particle transport in an isothermal clean room (Murakami et al., 1992), a room with an Under-Floor Air-Distribution (UFAD) system (Zhang and Chen, 2006), and the first-class cabin of an MD-82 airliner (Chen et al., 2013), to validate the zonal Markov chain model. This section discusses the validation results.

B3.1 Particle Transport in an Isothermal Clean Room

The first study was the case of particle transport in a ventilated clean room as addressed by Murakami et al. (1992), who conducted detailed measurements of particle distributions in a room. Figure B1(a) shows the configuration of the clean room with two ceiling supply diffusers and four exhausts located on the lower walls of the room. The total air exchange rate was 40 ACH. The thermo-fluid boundary conditions were defined according to the measurements. The details of the measured boundary conditions can be found in Murakami et al. (1992). The particle diameter used was 1 μm. The review by Lai (2002) indicated that the deposition velocity of the particles with a diameter of 1 μm ranged from 8×10^{-6} to 2×10^{-5} m/s in indoor environments. Thus, the deposition rate for such particles in this room ranged from 0.048 to 0.12 per hour. This was much lower than the air change rate in this room. Therefore, the influence of particle deposition on the results can be neglected. Furthermore, the particle resuspension was also negligible due to the low resuspension rate associated with 1 μm particles (Zhu et al., 2012). As shown in Figure B1(b), we divided the room into six zones and labeled the “removal zone” as zone 7.

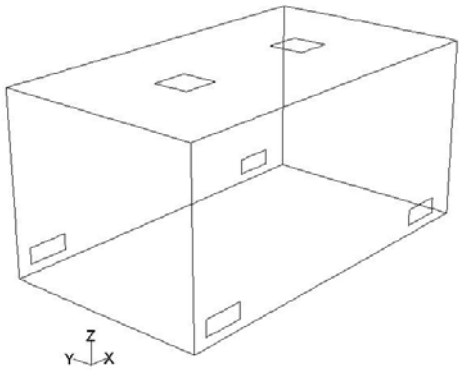

(a)

2	4	6
1	3	5

Removed: 7

(b)

Figure B1. (a) Configuration of the clean room studied by Murakami et al. (1992) and (b) the zones of the clean room on a horizontal plane.

Based on the calculated airflow field and Lagrangian particle tracking, the transition probability matrix can be obtained:

$$P = \begin{pmatrix} 0.61 & 0.01 & 0.07 & 0.00 & 0.00 & 0.00 & 0.31 \\ 0.04 & 0.63 & 0.00 & 0.01 & 0.00 & 0.00 & 0.32 \\ 0.08 & 0.00 & 0.69 & 0.10 & 0.13 & 0.00 & 0.00 \\ 0.00 & 0.15 & 0.04 & 0.70 & 0.00 & 0.10 & 0.00 \\ 0.00 & 0.00 & 0.03 & 0.00 & 0.70 & 0.02 & 0.25 \\ 0.00 & 0.00 & 0.00 & 0.03 & 0.02 & 0.67 & 0.27 \\ 0.00 & 0.00 & 0.00 & 0.00 & 0.00 & 0.00 & 1.00 \end{pmatrix} \quad \text{(B1)}$$

The time step of the Markov chain, Δt, was set as 15 s for this case, which ensures that particles move only to the adjacent zones within the Δt. Two scenarios, in which the particle source was located in zone 3 and zone 6, respectively, were used to validate the Zonal Markov chain model. The initial probability vector was:

$$\begin{aligned} \pi_0 &= (0\ 0\ 1\ 0\ 0\ 0\ 0), \quad \textit{source in zone } 3 \\ \pi_0 &= (0\ 0\ 0\ 0\ 0\ 1\ 0), \quad \textit{source in zone } 6 \end{aligned} \quad \text{(B2)}$$

Using Eq. (6.6), the probability vectors versus time of particle transport can be calculated.

The experiment measured only the steady-state airflow field and particle distributions. Validation of the Markov chain model would require transient particle distributions. However, our earlier study (Wang et al. 2012) validated the RNG k-ε – Eulerian drift flux model for this case with a good result. The model can be used to generate transient distributions of particle concentrations as the basis for validating the Markov chain model. Because steady-state and transient particle dispersion are governed by the same physics, this approach would not compromise accuracy.

Figures B2 and B3 compare the trends of the normalized particle concentrations versus time, as obtained by the Zonal Markov chain model and CFD simulations with a source in zones 3 and 6, respectively. The CFD simulation results were obtained by averaging the particle concentrations in each zone. Furthermore, all of the particle concentrations were normalized by the maximum concentration observed in the room. Figure B2 shows that both the Markov chain and CFD methods predicted higher particle concentrations in zones 1, 4, and 5 as compared with that in zones 2 and 6. This occurred because zones 1, 4, and 5 were adjacent to zone 3, where the source was located. A comparison of Figures B2 and B3 shows that both the Markov chain and CFD methods predicted higher particle concentrations with a source in zone 3 than with a source in zone 6. The results make sense because a large portion of particles were directly removed through the exhaust located in zone 6, which resulted in low concentrations in other zones for the case with source in zone 6. In general, the trends of transient particle transport predicted by the zonal Markov chain model agree well with the results of the CFD simulations.

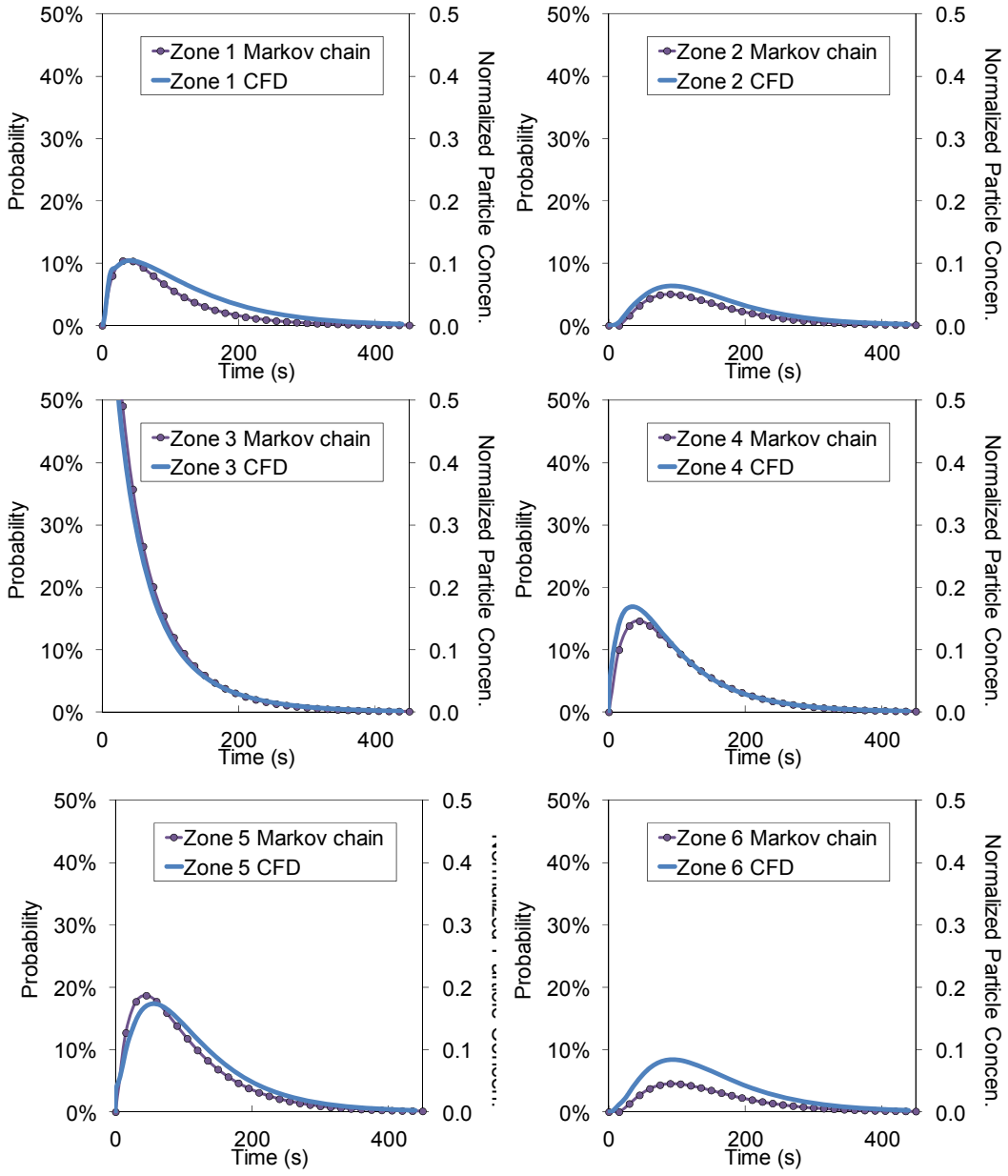

Figure B2. Comparison of the trends of the normalized particle concentrations versus time as obtained by the zonal Markov chain model and CFD simulation with a source in zone 3 for the isothermal clean room.

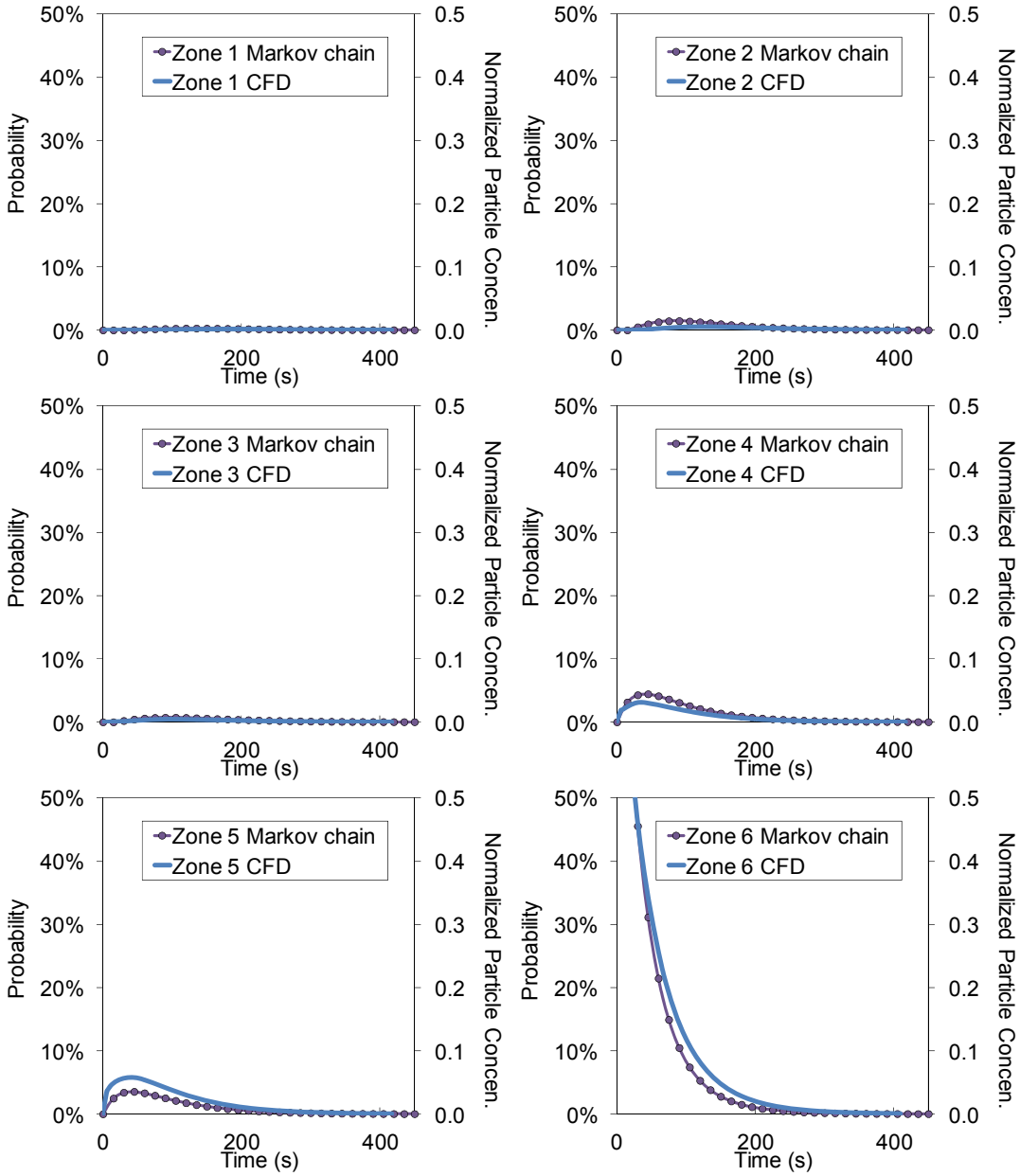

Figure B3. Comparison of the trends of the normalized particle concentrations versus time as obtained by the zonal Markov chain model and CFD simulation with a source in zone 6 for the isothermal clean room.

B3.2 Particle Transport in a Room with a UFAD System

The second case was a room with a UFAD system, as shown in Figure B4(a) and used by Zhang and Chen (2006) for measuring particle distributions. They used four heated boxes to simulate occupants in the room. The air was supplied through two floor inlets and exited through the exhaust at the ceiling. The total air exchange rate was 5.5 ACH. The thermo-fluid boundary conditions were defined according to the measurements. The detailed measured boundary conditions can be found in Zhang and Chen. (2006). The studied particle diameter was 1 μm. The deposition rate for such particles in this room ranged from 0.046 to 0.116 per hour. This was much lower than the air change rate in this room. Therefore, the influence of particle deposition was negligible. In addition, the particle resuspension was also neglected for this case. As shown in Figure B4(b), our investigation divided the room into six zones, with zone 7 as the "removal zone."

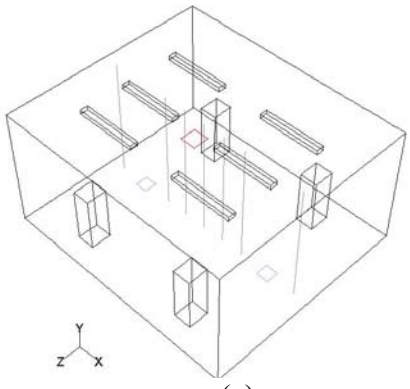

(a)

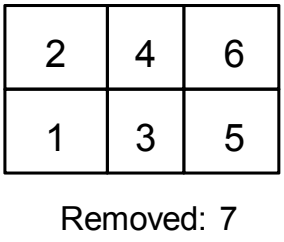

(b)

Figure B4. (a) Configuration of the room with the UFAD system studied by Zhang and Chen (2006) and (b) the zones of the room on a horizontal plane.

Based on the calculated airflow field and Lagrangian particle tracking, the transition probability matrix is:

$$P = \begin{pmatrix} 0.85 & 0.04 & 0.11 & 0.00 & 0.00 & 0.00 & 0.00 \\ 0.05 & 0.82 & 0.00 & 0.13 & 0.00 & 0.00 & 0.00 \\ 0.15 & 0.00 & 0.78 & 0.07 & 0.00 & 0.00 & 0.00 \\ 0.00 & 0.15 & 0.00 & 0.73 & 0.00 & 0.00 & 0.12 \\ 0.00 & 0.00 & 0.14 & 0.00 & 0.77 & 0.09 & 0.00 \\ 0.00 & 0.00 & 0.00 & 0.09 & 0.07 & 0.84 & 0.00 \\ 0.00 & 0.00 & 0.00 & 0.00 & 0.00 & 0.00 & 1.00 \end{pmatrix} \quad \text{(B3)}$$

The time step of the Markov chain, Δt, was set as 25 s for this case. The size of the zones of the isolation room was close to that of the room with UFAD system, while the air change rate of the isolation room was much larger than that of the room with UFAD system. Therefore, the time step used for the room with UFAD system (25 s) was larger than that for the isolation room (15 s).

Two scenarios, in which the source was located in zone 4 and zone 6, respectively, were used to validate the Zonal Markov chain model. The initial probability vector was:

$$\begin{aligned} \pi_0 &= (0\ 0\ 0\ 1\ 0\ 0\ 0), \quad \textit{source in zone } 4 \\ \pi_0 &= (0\ 0\ 0\ 0\ 0\ 1\ 0), \quad \textit{source in zone } 6 \end{aligned} \quad \text{(B4)}$$

Because of the lack of experimental data for transient particle concentrations, this study again used the CFD results as a benchmark for this study. The CFD simulation was again validated by steady-state experimental data, with good agreement between them. Figures B5 and B6 compare the trends of the normalized particle concentrations versus time as obtained by the Zonal Markov chain model and CFD simulations with a source in zone 4 and zone 6, respectively. The CFD simulation results were again obtained by averaging the particle concentrations in each zone.

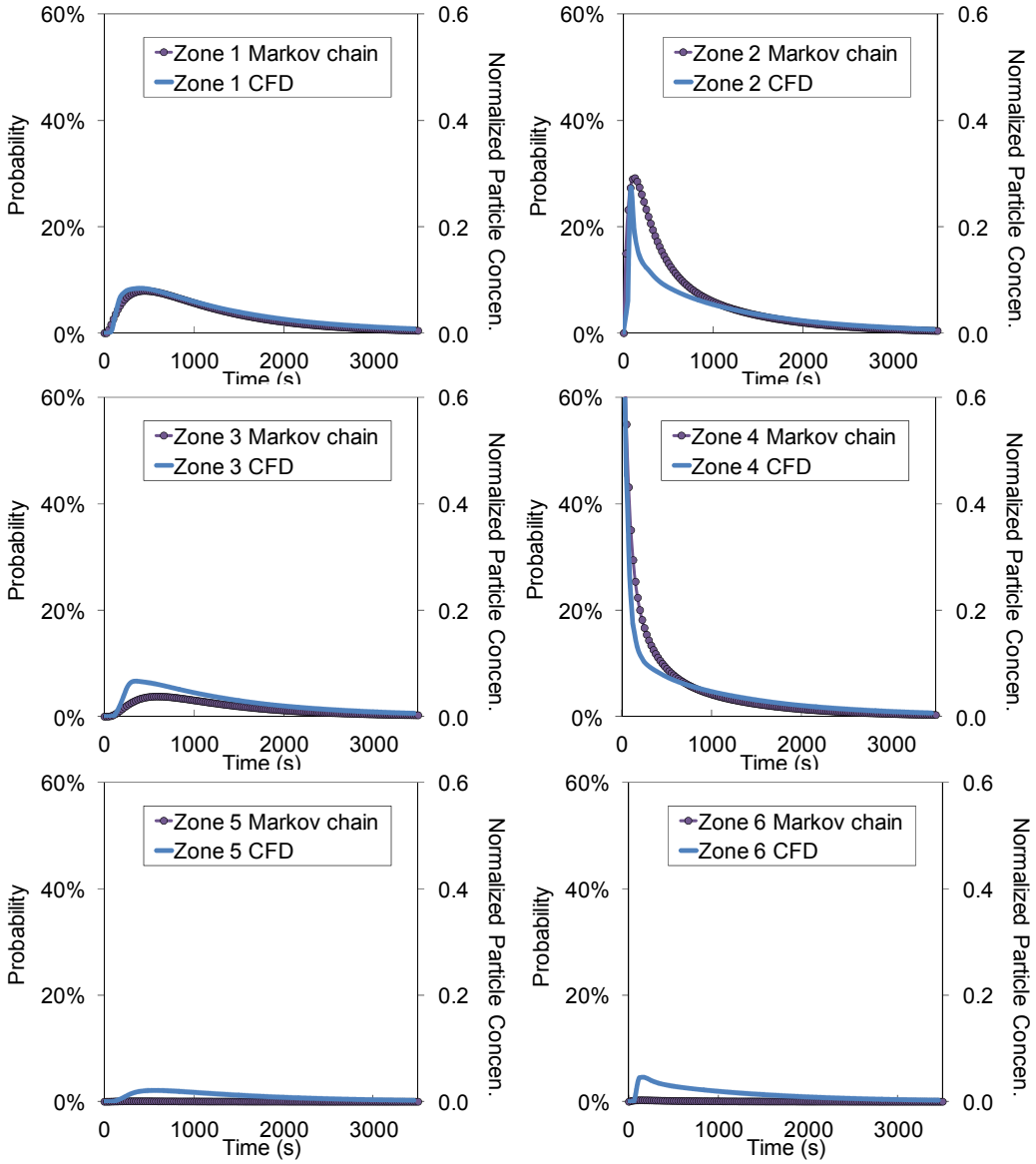

Figure B5. Comparison of the trends of the normalized particle concentration distributions versus time as obtained by the zonal Markov chain model and CFD simulation with a source in zone 4 for the room with the UFAD system.

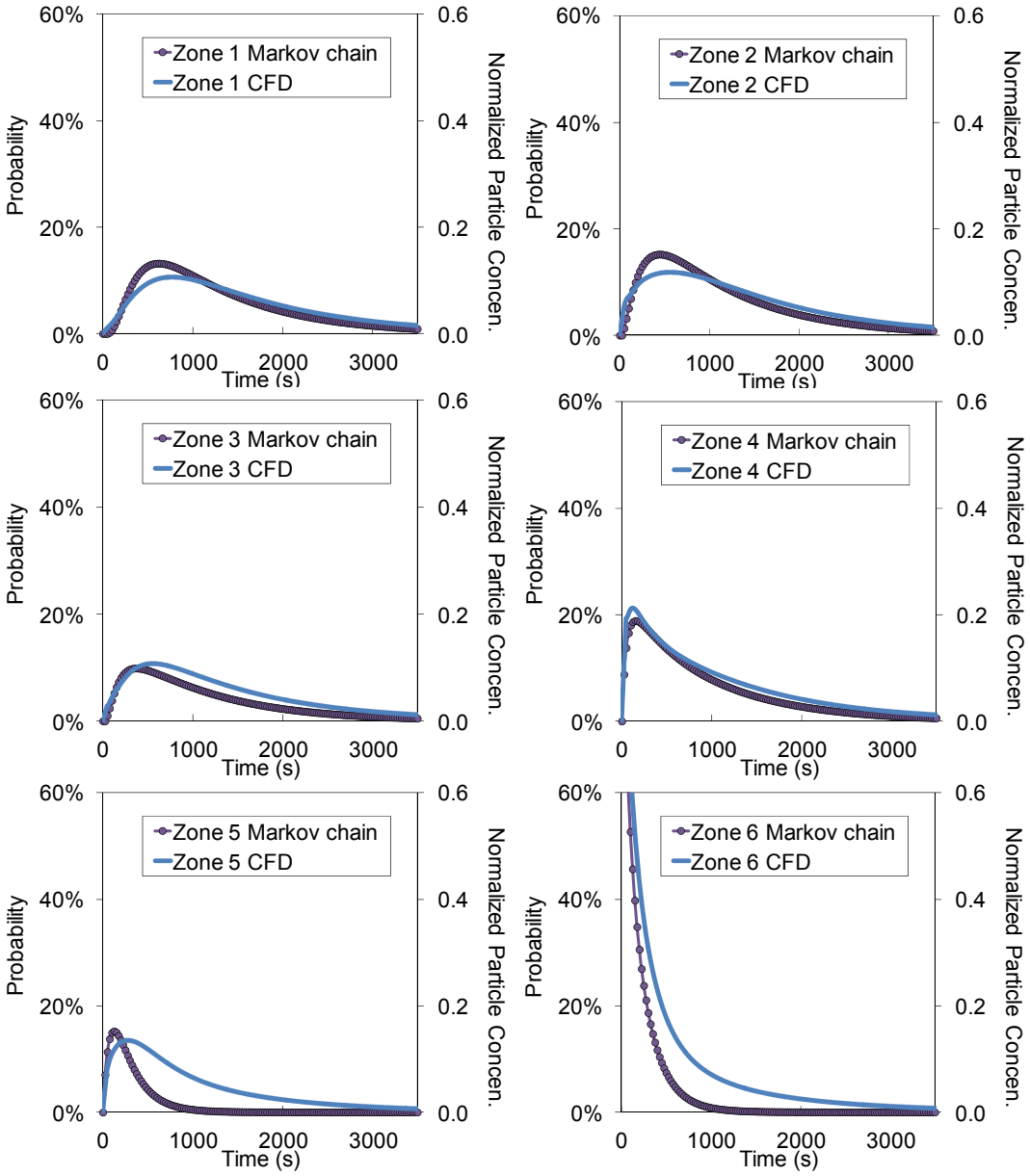

Figure B6. Comparison of the trends of the normalized particle concentration distributions versus time as obtained by the zonal Markov chain model and CFD simulation with a source in zone 6 for the room with the UFAD system.

A comparison of Figure B5 with Figure B6 shows that both methods predicted lower concentrations in the room with a source in zone 4 than that with a source in zone 6. This occurred because a considerable portion of the particles released from zone 4 tended to be

removed directly by the exhaust located in zone 4. It can be seen that the discrepancies between Markov chain and CFD method were larger in some zones than other zones. Note that the particles were uniformly released in each zone when calculating the transition probability matrix. Thus, the uniformities of the particle concentrations in the zones for a real case might influence the accuracy of the Zonal Markov chain model. Since the uniformities of the particle concentrations in the zones were different, the accuracies of the Zonal Markov chain model in different zones might be also different. Generally speaking, the trends of the normalized particle concentration distributions predicted by the zonal Markov chain model again agreed reasonably well with the CFD simulations. However, because this case is more complicated than the isothermal clean-room case, the agreement tends to be somewhat worse than that for the clean room.

B3.3 Particle Transport in an MD-82 Aircraft Cabin

The third case was the first-class cabin of a functional MD-82 commercial airliner, as shown in Figure B7. Liu et al. (2012) provided a detailed description of the cabin and aircraft and detailed measurements of the thermo-fluid boundary conditions. The cabin had three rows of seats, and each row contained four seats as numbered in Figure B7. Manikins were used to simulate passengers. The sensible heat production of each heated manikin was 75 Watt. At the mouth of the manikin in Seat 2C, we released particles with a diameter of 3 μm into the cabin air for 20 s. The particle concentrations versus time at the breathing zones were measured in front of each passenger's mouth. A detailed description of the experimental procedure and data analysis can be found in Chen et al. (2013). Both the experimental data for the transient particle concentration distributions and the CFD simulation results were used to validate the Zonal Markov chain model. You and Zhao (2013) calculated the particle deposition rates in this aircraft cabin. They found that the deposition rate of particles with a diameter of 3 μm was 1.0 per hour, which was much lower than the air change rate in the aircraft cabin (33 ACH). Therefore, the influence of particle deposition was negligible. Furthermore, the particle resuspension

was also neglected (Zhu et al., 2012). As shown in Figure 7, we divided the cabin into fifteen zones, with zone 16 as the "removal zone."

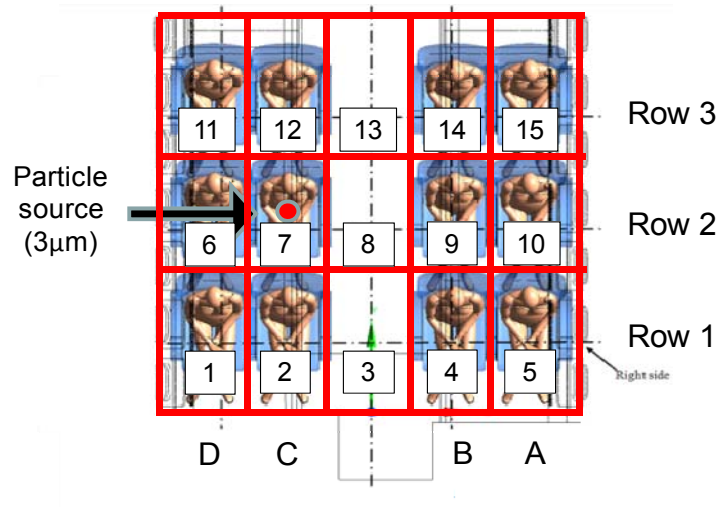

Figure B7. the zones of the cabin in a horizontal plane.

Based on the calculated airflow field and Lagrangian particle tracking, the transition probability matrix can be obtained:

$$P = \begin{pmatrix}
0.63 & 0.24 & 0.00 & 0.00 & 0.00 & 0.01 & 0.00 & 0.00 & 0.00 & 0.00 & 0.00 & 0.00 & 0.00 & 0.00 & 0.00 & 0.11 \\
0.25 & 0.63 & 0.10 & 0.00 & 0.00 & 0.00 & 0.02 & 0.00 & 0.00 & 0.00 & 0.00 & 0.00 & 0.00 & 0.00 & 0.00 & 0.00 \\
0.00 & 0.33 & 0.37 & 0.29 & 0.00 & 0.00 & 0.00 & 0.01 & 0.00 & 0.00 & 0.00 & 0.00 & 0.00 & 0.00 & 0.00 & 0.00 \\
0.00 & 0.00 & 0.11 & 0.75 & 0.14 & 0.00 & 0.00 & 0.00 & 0.00 & 0.00 & 0.00 & 0.00 & 0.00 & 0.00 & 0.00 & 0.00 \\
0.00 & 0.00 & 0.00 & 0.26 & 0.64 & 0.00 & 0.00 & 0.00 & 0.00 & 0.02 & 0.00 & 0.00 & 0.00 & 0.00 & 0.00 & 0.07 \\
0.13 & 0.00 & 0.00 & 0.00 & 0.00 & 0.39 & 0.19 & 0.00 & 0.00 & 0.00 & 0.11 & 0.00 & 0.00 & 0.00 & 0.00 & 0.17 \\
0.00 & 0.14 & 0.00 & 0.00 & 0.00 & 0.22 & 0.41 & 0.20 & 0.00 & 0.00 & 0.00 & 0.02 & 0.00 & 0.00 & 0.00 & 0.00 \\
0.00 & 0.00 & 0.56 & 0.00 & 0.00 & 0.00 & 0.11 & 0.13 & 0.09 & 0.00 & 0.00 & 0.00 & 0.11 & 0.00 & 0.00 & 0.00 \\
0.00 & 0.00 & 0.00 & 0.11 & 0.00 & 0.00 & 0.00 & 0.23 & 0.51 & 0.07 & 0.00 & 0.00 & 0.00 & 0.09 & 0.00 & 0.00 \\
0.00 & 0.00 & 0.00 & 0.00 & 0.00 & 0.00 & 0.00 & 0.00 & 0.14 & 0.59 & 0.00 & 0.00 & 0.00 & 0.00 & 0.19 & 0.08 \\
0.00 & 0.00 & 0.00 & 0.00 & 0.00 & 0.01 & 0.00 & 0.00 & 0.00 & 0.00 & 0.70 & 0.20 & 0.00 & 0.00 & 0.00 & 0.09 \\
0.00 & 0.00 & 0.00 & 0.00 & 0.00 & 0.00 & 0.19 & 0.00 & 0.00 & 0.00 & 0.03 & 0.64 & 0.14 & 0.00 & 0.00 & 0.00 \\
0.00 & 0.00 & 0.00 & 0.00 & 0.00 & 0.00 & 0.00 & 0.40 & 0.00 & 0.00 & 0.00 & 0.28 & 0.27 & 0.05 & 0.00 & 0.00 \\
0.00 & 0.00 & 0.00 & 0.00 & 0.00 & 0.00 & 0.00 & 0.00 & 0.28 & 0.00 & 0.00 & 0.00 & 0.25 & 0.30 & 0.18 & 0.00 \\
0.00 & 0.00 & 0.00 & 0.00 & 0.00 & 0.00 & 0.00 & 0.00 & 0.00 & 0.04 & 0.00 & 0.00 & 0.00 & 0.39 & 0.45 & 0.12 \\
0.00 & 0.00 & 0.00 & 0.00 & 0.00 & 0.00 & 0.00 & 0.00 & 0.00 & 0.00 & 0.00 & 0.00 & 0.00 & 0.00 & 0.00 & 1.00
\end{pmatrix} \quad \text{(B5)}$$

The time step of the Markov chain, Δt, was set as 4 s for this case. The air change rate of the aircraft cabin was close to that of the isolation room, while the size of the zones of the aircraft cabin was much smaller than that of the isolation room. Therefore, the time step used for the aircraft cabin (4 s) was smaller than that for the isolation room (15 s).

To better match the experimental setup, the particles were released only from the month of the manikin instead of the whole space of zone 7, where the source was located. The initial probability vector was:

$$\pi_0 = \left(0\ 0\ 0\ 0\ 0\ 0\ 1\ 0\ 0\ 0\ 0\ 0\ 0\ 0\ 0\ 0\right) \tag{B6}$$

Figure B8 compares the trends of the normalized particle concentration distribution versus time as obtained by the zonal Markov chain model, CFD simulation, and experimental measurement. The Zonal Markov chain model correctly predicted relatively high peak concentrations at Seats 1B and 1C and low concentrations at most of the other seats. However, the Zonal Markov chain model over-predicted the concentrations at Seats 1D and 2D. The discrepancies could be attributed to two factors. First, the differences between the simulated and measured airflow fields were significant (Chen et al., 2013), which can cause a large discrepancy in particle concentration distribution. Second, the Zonal Markov chain model calculated the average particle concentrations in each zone, while the experiment measured the particle concentration only in the breathing zones. We have further calculated the average particle concentrations in each zone by CFD as shown in Figure B8. The CFD simulation also over-predicted the concentrations at Seats 1D and 2D, which confirms the validity of the second factor above. Generally speaking, the zonal Markov chain model can predict the general trends of the particle concentrations versus time for such a complex case, and it may be used for engineering applications.

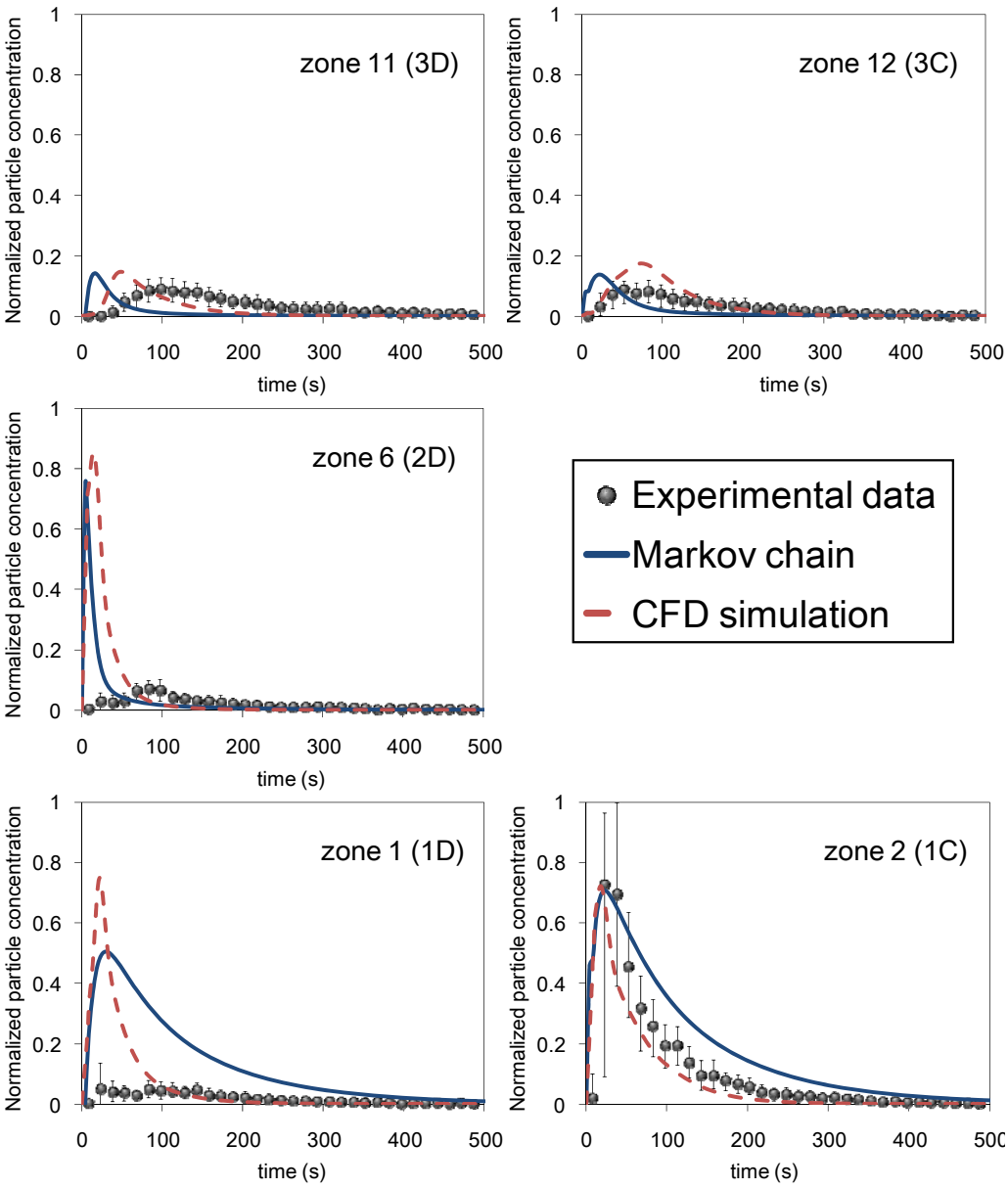

Figure B8. Comparison of the trends of the normalized particle concentration distribution versus time for the aircraft cabin as obtained by the zonal Markov chain model, CFD simulation and experimental data (Chen et al., 2013).

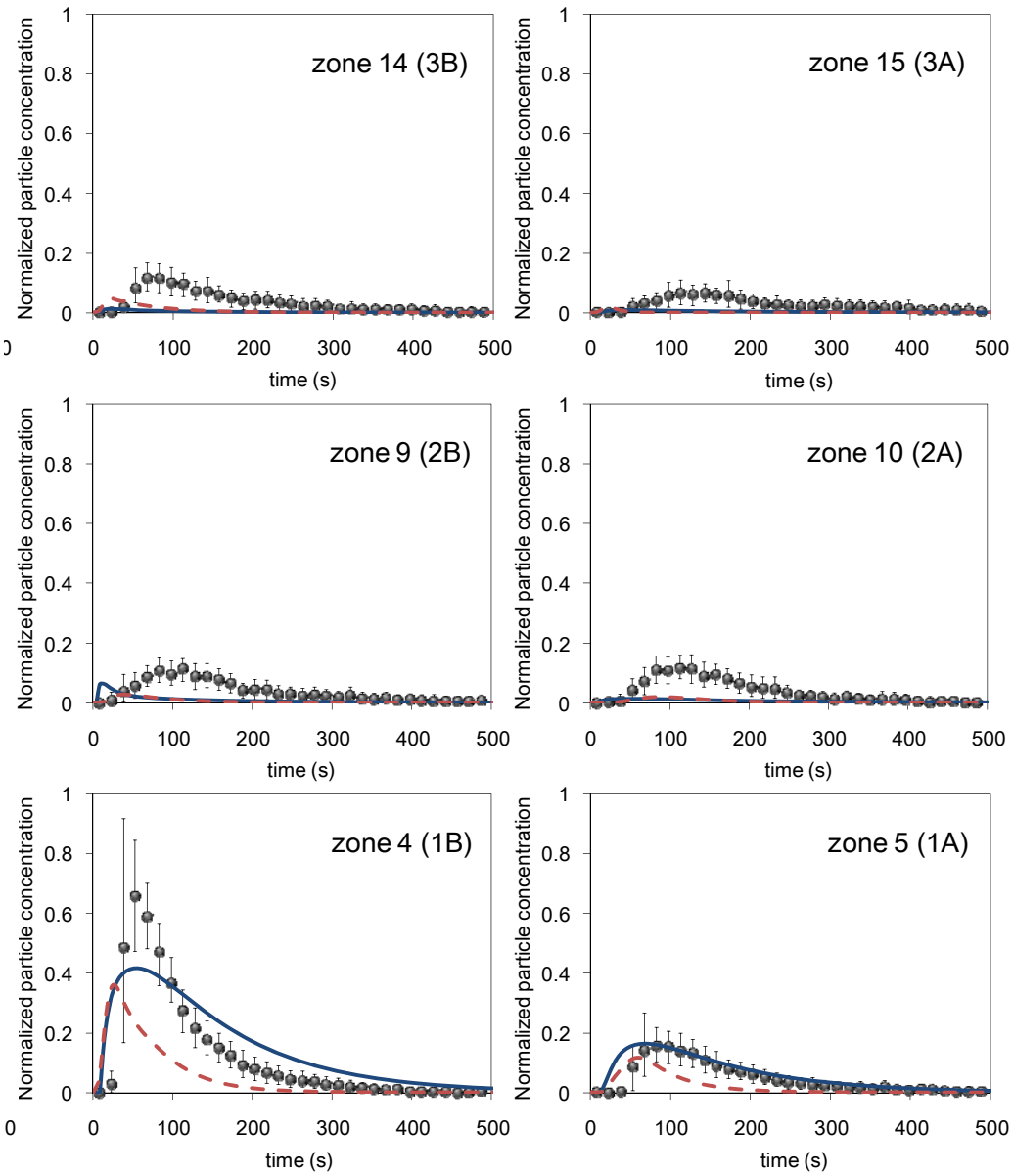

Figure B8. continued.

B4 Discussion

Quickly obtaining information about airborne infectious disease transmission in enclosed environments is crucial for reducing infection risk to the occupants. For an application of the zonal Markov chain model, the airflow field and the transition probability matrix for

an enclosed environment can be calculated in advance. For predicting infectious disease transmission, either the CFD or zonal Markov chain model can be used for calculating the transient particle transport. Table 1 compares the computing time by the CFD method using the previous calculated airflow field and zonal Markov chain model using the previous calculated transition probability matrix for the three cases. It took only seconds for the zonal Markov chain model to calculate the transient particle transport, while hours or even days were needed for the CFD simulations. This was because the zonal Markov chain model requires only simple matrix multiplications while the CFD requires a lot of numerical iteration for a large amount of grids. It can be seen that the zonal Markov chain model can provide faster-than-real-time information about particle transport in enclosed environments. In other words, for a fixed airflow field, when the index patient or the source location is changed, the zonal Markov chain model can be used to avoid recalculation of the particle transport equation and thus reduce computing costs. This capability has been validated by comparing with the CFD simulations in this study. It is meaningful since the accuracy of CFD simulations has been experimentally validated previously (e.g. Zhang and Chen, 2007; Zhao et al., 2009; Chen et al., 2013).

Table B1. Comparison of the computing time by the CFD method using the previous calculated airflow field and zonal Markov chain model using the previous calculated transition probability matrix.

Case	CFD method (hr)	Zonal Markov chain model (s)
Isolation clean room	4	<1
Room with UFAD system	15	<1
Aircraft cabin	75	5

In addition, the number of the divided zones in the Zonal Markov chain model may also affect the results. In principle, the number of the divided zones depends on the required resolution. However, as discussed above, if the size of the zones is unreasonably large, the time step also needs to be very large. Such a large time step may not be able to reflect the transient characteristics of the particle transport. To assess how the results depend on

the number of the divided zones, this study further compared the results of transient particle transport when the clean room was divided into 6 and 12 zones, as shown in Figure B9. The particle source was located in zone 3. It can be found that the differences between the results for 6 and 12 divided zones are insignificant. Thus, 6 divided zones are sufficient enough to capture the transient characteristics of the particle transport in the clean room.

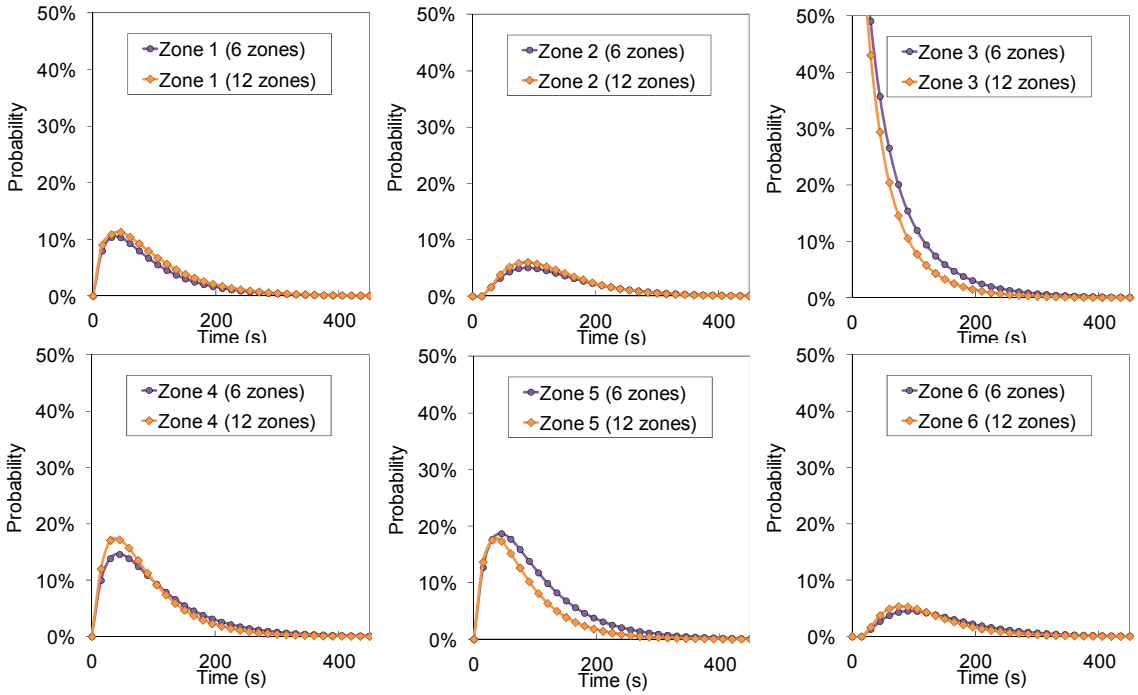

Figure B9. Comparison of the trends of the normalized particle concentrations versus time as obtained by the Zonal Markov chain model when the clean room was divided into 6 and 12 zones.

Currently, either deterministic or probabilistic approaches can be used for risk assessment of airborne infectious disease transmission (Gupta et al., 2012). In the deterministic approaches, the risk or probability of infection cannot be quantified. In the probabilistic approaches, because the quantities exhaled cannot be directly determined, their accuracy has been debated (Sze To and Chao, 2010). The Zonal Markov chain model predicts the probability of a particle's appearing in a zone at a certain point in time. Because the

movements of indoor particles tend to be independent, the calculated probabilities should be independent probabilities. Through simple calculations of the joint probability and the probability of either event's occurring, we can calculate the probability of a certain number of particles appearing in the breathing zone of the receptor. For instance, if the index patient exhales 100 particles, we can calculate the probability that 10 out of these 100 particles appear in the breathing zone. Thus, the Markov chain with probability calculations has the potential to account for both deterministic and probabilistic information.

In addition, the Zonal Markov chain model has the potential to account for other influencing factors in infectious disease transmission. For instance, compared with completely fresh-air ventilation systems assumed in this study, ventilation systems with return air are more widely used in actual engineering. In these cases, the particles can re-enter the space through the return air. To take this factor into account, we can simply modify the transition probability matrix as:

$$p_{nj} = \left(r_1 \;\; r_2 \;\cdots\; r_i \;\cdots\; r_{n-1} \;\;\; (1 - r_1 - r_2 \cdots - r_i \cdots - r_{n-1}) \right) \tag{B7}$$

where

$$r_i = f_i (1 - \eta) \beta \tag{B8}$$

where f_i is the ratio of the supply airflow rate in zone i to the total airflow rate, η is the particle removal efficiency of filter, and β is the ratio of the return airflow rate to the total airflow rate. Then the effect of contaminated return air and filter can be easily assessed using Eq. (B8) with the updated transition probability matrix. The effectiveness of wearing masks and the effects of temperature and humidity on virus survival can also be investigated using a similar approach.

B5 Conclusions

This investigation developed a zonal Markov chain model for predicting faster-than-real-time information about transient particle transport in enclosed environments. From the results presented in this paper, the following conclusions can be drawn:

(1) The proposed zonal Markov chain model can provide faster-than-real-time information about particle transport in enclosed environments.

(2) For a fixed airflow field, when the source location is changed, the zonal Zonal Markov chain model can be used to avoid recalculation of the particle transport equation and thus reduce computing costs.

VITA

VITA

Chun Chen received his B.Eng. degree in Building Science and M.Eng. degree in Civil Engineering from Tsinghua University, China in 2009 and 2012, respectively.

He joined Purdue University, USA, in 2012. His research interests include indoor air quality, healthy, energy-efficient, and sustainable buildings, computational fluid dynamics and heat/mass transfer in built environments.

During the study at Purdue University, he received the Grant-in-Aid Award from American Society of Heating, Refrigerating and Air-Conditioning Engineers (ASHRAE) in 2013, Bilsland Dissertation Fellowship from Purdue University in 2014, and Best Student Paper Award of the 13th International Conference on Indoor Air Quality and Climate in 2014.

He is a student member of the American Society of Heating, Refrigerating and Air-Conditioning Engineers (ASHRAE) and International Society of Indoor Air Quality and Climate (ISIAQ).

LIST OF PUBLICATIONS

LIST OF PUBLICATIONS

Peer Reviewed Journal Papers

Submitted

1. **Chen, C.**, Liu, W., Lin, C.-H., Chen, Q. (2015). Comparing the Markov chain models with other models for indoor transient particle transport simulations. Submitted to **Energy and Buildings**.

Published

2. **Chen, C.**, Liu, W., Lin, C.-H., Chen, Q. (2015). A Markov chain model for predicting transient particle transport in enclosed environments. Accepted by **Building and Environment**.
3. **Chen, C.**, Liu, W., Lin, C.-H., Chen, Q. (2015). Accelerating the Lagrangian method for modeling transient particle transport in indoor environments. Accepted by **Aerosol Science and Technology**.
4. Liu, W., Jin, M., **Chen, C.**, Chen, Q. (2015). Optimization of air supply location, size, and parameters in enclosed environments through using a CFD-based adjoint method. Accepted by **Journal of Building Performance Simulation**.
5. **Chen, C.**, Lin, C.-H., Jiang, Z., Chen, Q. (2014). Simplified models for exhaled airflow from a cough with the mouth covered. **Indoor Air**, 24, 580-591.
6. **Chen, C.**, Zhu, J., Qu, Z., Lin, C.-H., Jiang, Z., Chen, Q. (2014). Systematic study of person-to-person contaminant transport in mechanically ventilated spaces (RP-1458). **HVAC&R Research**, 20, 80-91.
7. **Chen, C.**, Lin, C.-H., Long, Z., Chen, Q. (2014). Predicting transient particle transport in enclosed environments with the combined computational fluid

dynamics and Markov chain method. **Indoor Air**, 24, 81-92.

8. Li, Q., You, R., **Chen, C.**, Yang, X. (2013). A field investigation and comparative study of indoor environmental quality in heritage Chinese rural buildings with thick rammed earth wall. **Energy and Buildings**, 62, 286–293.
9. You, R., Cui, W., **Chen, C.**, Zhao, B. (2013). Measuring short-term emission rate of particles in the "personal cloud" with different clothes and activity intensities in a sealed chamber. **Aerosol and Air Quality Research**, 13, 911–921.
10. **Chen, C.**, Liu, W., Li, F., Lin, C.-H., Liu, J., Pei, J., Chen, Q. (2013). A hybrid model for investigating transient particle transport in enclosed environments. **Building and Environment**, 62, 45-54.
11. **Chen, C.**, Zhao, B., Weschler, C.J. (2012). Indoor exposure to outdoor PM_{10}: assessing its influence on the relationship between PM_{10} and short-term mortality in U.S. cities. **Epidemiology**, 23, 870-878.
12. You, R., Zhao, B., **Chen, C**. (2012). Developing an empirical equation for modeling particle deposition velocity onto inclined surfaces in indoor environments. **Aerosol Science and Technology**, 46, 1090-1099.
13. Li, Q., Sun, X., **Chen, C.**, Yang, X. (2012). Characterizing the household energy consumption in heritage Nanjing Tulou buildings, China: A comparative field survey study. **Energy and Buildings**, 49, 317-326.
14. **Chen, C.**, Zhao, B., Weschler, C.J. (2012). Assessing the influence of indoor exposure to "outdoor ozone" on the relationship between ozone and short-term mortality in US communities. **Environmental Health Perspectives**, 120, 235-240.
15. **Chen, C.**, Zhao, B., Zhou, W., Jiang, X., Tan, Z. (2012). A methodology for predicting particle penetration factor through cracks of windows and doors for actual engineering application. **Building and Environment**, 47, 339-348.
16. Zhao, B., **Chen, C.**, Lai, A.C.K. (2011). Lagrangian stochastic particle tracking: further discussion. **Aerosol Science and Technology**, 45, 901-902.
17. **Chen, C.**, Zhao, B., Yang, X., Li, Y. (2011). Role of two-way airflow owing to temperature difference in severe acute respiratory syndrome transmission:

revisiting the largest nosocomial severe acute respiratory syndrome outbreak in Hong Kong. **Journal of the Royal Society Interface**, 8, 699-710.

18. **Chen, C.**, Zhao, B., Yang, X. (2011). Preventing the entry of outdoor particles with the indoor positive pressure control method: Analysis of influencing factors and cost. **Building and Environment**, 46, 1167-1173.
19. **Chen, C.**, Zhao, B., Yang, X. (2011). Impact of two-way air flow due to temperature difference on preventing the entry of outdoor particles using indoor positive pressure control method. **Journal of Hazardous Materials**, 186, 1290-1299.
20. **Chen, C.**, Zhao, B. (2011). Review of relationship between indoor and outdoor particles: I/O ratio, infiltration factor and penetration factor. **Atmospheric Environment**, 45, 275-288.
21. Wang, B., Zhao, B., **Chen, C.** (2010). A simplified methodology for the prediction of mean air velocity and particle concentration in isolation rooms with downward ventilation systems. **Building and Environment**, 45, 1847-1853.
22. **Chen, C.**, Zhao, B., Cui, W., Dong, L., An, N., Ouyang, X. (2010). The effectiveness of an air cleaner in controlling droplet/aerosol particle dispersion emitted from a patient's mouth in the indoor environment of dental clinics. **Journal of the Royal Society Interface**, 7, 1105-1118.
23. Zhao, B., **Chen, C.**, Yang, X., Lai, A.C.K. (2010). Comparison of three approaches to model particle penetration coefficient through a single straight crack in a building envelope. **Aerosol Science and Technology**, 44, 405-416.
24. **Chen, C.**, Zhao, B. (2010). Some questions on dispersion of human exhaled droplets in ventilation room: answers from numerical investigation. **Indoor Air**, 20, 95-111.
25. Zhao, B., Yang, C., **Chen, C.**, Feng, C., Yang, X., Sun, L., Gong, W., Yu, L. (2009). How many airborne particles emitted from a nurse will reach the breathing zone/body surface of the patient in ISO class-5 single-bed hospital protective environments?-a numerical analysis. **Aerosol Science and Technology**, 43, 990-1005.

26. Zhao, B., **Chen, C.**, Tan, Z. (2009). Modeling of ultrafine particle dispersion in indoor environments with an improved drift flux model. **Journal of Aerosol Science**, 40, 29-43.

Referred Conference Papers

1. **Chen, C.**, Lin, C.-H., Chen, Q. (2014). Developing simplified models for the exhaled airflow from a cough with the mouth covered. *Proceedings of the 13th International Conference on Indoor Air Quality and Climate (Indoor Air 2014)*, Hong Kong, HP0092.
2. **Chen, C.**, Lin, C.-H., Chen, Q. (2013). Predicting transient particle transport in enclosed environments based on Markov chain. *Proceedings of the 13th International Conference of the International Building Performance Simulation Association (Building Simulation 2013)*, Chambery, France, pp. 559-566.
3. **Chen, C.**, Zhao, B., Yang, X. (2011). Significance of two-way airflow effect due to temperature difference in indoor air quality. *Proceedings of the 12th International Conference on Indoor Air Quality and Climate (Indoor Air 2011)*, Austin, Texas Paper, a931-1.
4. Rai, A.C., **Chen, C.**, Lin, C.-H., Chen, Q. (2014). Numerical modeling of ozone-initiated particle generations from reactions with clothing in an environmental chamber. *Proceedings of the 13th International Conference on Indoor Air Quality and Climate (Indoor Air 2014)*, Hong Kong, HP0108.